Characterisation and gene sequencing of mussel foot proteins from indigenous marine mussel, *Perna perna* (Linnaeus, 1758): Nutrient immobilization and struvite synthesis

Thesis submitted to the
University of Calicut in partial fulfillment of the
requirements for the Degree of

DOCTOR OF PHILOSOPHY IN ZOOLOGY

By

NEETHU C. B.

Under the guidance of

Dr. Y. Shibu Vardhanan

DEPARTMENT OF ZOOLOGY
UNIVERSITY OF CALICUT
KERALA, INDIA-673635
2022

DECLARATION

I hereby declare that this dissertation work entitled **"Characterisation and gene sequencing of mussel foot proteins from indigenous marine mussel, *Perna perna* (Linnaeus, 1758): Nutrient immobilization and struvite synthesis"** is an authentic record of research work originally carried out by me under the guidance and supervision of Dr. Y. Shibu Vardhanan, Associate Professor, Department of Zoology, University of Calicut, and that no part of this has been published previously or submitted for the award of any other Degree / Diploma.

University of Calicut **Neethu C. B.**

കാലിക്കറ്റ് സർവ്വകലാശാല
ജന്തുശാസ്ത്ര പഠനവിഭാഗം
കാലിക്കറ്റ് സർവ്വകലാശാല (പി.ഒ.), മലപ്പുറം (ജില്ല),
കേരള, ഇന്ത്യ - 673 635
Dr. Y. Shibu Vardhanan
Associate Professor

UNIVERSITY OF CALICUT
DEPARTMENT OF ZOOLOGY
Calicut University (P.O.), Malappuram (Dt.),
Kerala India - 673 635
Tel: 0494 - 2407420 (Head), 0494 - 2407419 (Off.)

Re-Accredited by NAAC with "A" Grade

No:.....

Date: 24-12-2020

CERTIFICATE

This is to certify that this thesis entitled **"Characterisation and gene sequencing of mussel foot proteins from indigenous marine mussel, *Perna perna* (Linnaeus, 1758): Nutrient immobilization and struvite synthesis"** submitted by Neethu C. B. to the University of Calicut for the award of the degree of Doctor of Philosophy in Zoology, is the result of the bonafide research work carried out at the Department of Zoology, University of Calicut under my guidance and supervision. The content of the thesis has been checked for plagiarism using the software 'Ouriginal' and the similarity index fall under permissible limit. I further certify that the topic discussed in this thesis has not been previously formed the basis of the award of any degree, diploma, associate ship, fellowship or other similar title of any other University or Institute. I also hereby certify that the corrections/suggestions from the adjudicators have been incorporated in the revised thesis.

Calicut University

Dr. Y. Shibu Vardhanan

ACKNOWLEDGEMENTS

I have great pleasure to express my sincere gratitude and indebtedness to my supervising teacher Dr. Y. Shibu Vardhanan, Associate Professor, Department of Zoology, University of Calicut, for his valuable guidance and affectionate attitude which always instilled a lot of confidence in me during the course of this project. I am extremely indebted to him for the efforts taken by him for the correction of this manuscript.

I would also like to thank Herbert Waite, Distinguished Professor, University of California, Santa Barbara for his insightful comments, encouragement and guidance during my Ph.D work. He helped me a lot particularly during the most difficult times.

I also express my sincere thanks to Dr Soney Varghese, Associate professor, Department of Nano Science and Technology, NIT Calicut, Dr. Subramanyan Namboodiri Varanakkottu, Assistant Professor, Department of Physics, NIT Calicut, Mr. Anoop and Mrs. Regisha, Research Scholars, NIT Calicut for providing facilities and sharing knowledge to complete my thesis.

I am grateful to Dr. E. M. Manogem, Associate Professor and Head, Department of Zoology, University of Calicut who permitted access to the laboratory and research facilities. I am also grateful to former Heads of the Departments: Dr. E. Pushpalatha and Dr. M. Nasser.

I would like to extend my sincere gratitude to UGC Major Research Project (MRP) for providing the resources I needed to finish my project.

I am greatful to Department of Chemistry, Department of Biotechnology, and Central sophisticated instrumentation facility (CSIF), University of Calicut for providing instrumentation facilities.

Very whole hearted and warm thanks goes out to Mr. Nidhish G. for continuous support, endless help, encouragement and giving valuable suggestions during the present study.

I extend special thanks to Mrs. Bindu P.U. and Mrs. Rahila K. P. for their love, care and motivation. Thank you so much for being with me.

My heart filled thanks to Ms. Anju, Mr. Vishnu, Mr. Praveen V. P., and Mrs. Meghana for advices and extended support during the period of my work.

My thanks, which is not enough if I mention through words, goes to research scholars of my lab, Mrs. Renu V. V., Mrs. Gayathri M., Mrs. Shameema Kodassery, Mr. Sivaprasad M. S., Mrs. Seena S., Ms. Hima K. S., and Mr. Anand P. P. for their support and help they showered on me for the completion of my work.

I express my heartfelt thanks to all my teachers, nonteaching staffs and my dear friends in the department of Zoology for enthusiastic support and assistance given to me during my research.

The infinite patience and love of my mother are beyond expressions. I am grateful to my entire family, especially my grandparents, father, and brother, for their unwavering support, without which this effort would not have been possible.

Neethu C. B.

Dedicated to

My supervising teacher

CONTENTS

LIST OF TABLES

Chapter 3

cDNA Synthesis and Sequencing of Adhesive Foot Protein Genes from *Perna perna*

LIST OF FIGURES

Chapter 4
Potency Analysis of Slow-release Fertilizer Synthesised from Cow Urine and Shell Powder

ABSTRACT

Researchers are more attracted to mussels because of their magical adhesive strength on the wet substratum. This peculiar character of mussels is achieved by moisture resistant, biocompatible and biodegradable polyphenolic proteins called mussel adhesive proteins or mussel foot proteins (MAP or MFP). In mussels mainly six different adhesive proteins (mfp-1 to mfp-6) are reported and they contain unusual amino acid residues called 3,4-dihydroxyphenylalanine (DOPA), which are mainly involved in adhesion. The understanding of mussel adhesion exposes many opportunities in the area of science and medicine. Even though, mussels are considered as worst participants of biofouling, which make serious economic losses. They accumulated on ship hulls, underwater pipes and industrial equipment which lead to extensive damage. In India, two major species of mussel are present namely, *Perna perna* and *Perna viridis*. The present study focused on *P. perna* adhesive machinery, adhesive protein characterisation and also the synthesis of slow-released fertilizer by using *P. perna* shell and cow urine.

Strong adhesion of the mussel is achieved by involvement of two parts called foot and byssus thread. The structural elucidation of mussel adhesive machinery helps to develop new antifouling strategies. The first chapter of this thesis deals with the structural elucidation of *P. perna* foot and byssus thread. The byssus thread contains three regions namely proximal thread, distal thread and plaque. The proximal and distal threads are morphologically distinct, in which gradient

distribution of proteins was shown, leading to indestructible strength. Plaque is a leaf-like structure found attached to a substratum containing major polyphenolic adhesive proteins with the differential distribution. The polyphenolic protein staining of byssus thread using NBT revealed that high concentration of DOPA-rich proteins found in the adhesive region of plaque. Likewise, anatomically thread contains two parts cuticle and a core region. The cuticle is a hard protective part made up of mfp-1 and the core region contains collagens which provide elasticity and extensibility. The byssus thread's incredible thermal stability was exhibited by TGA analysis and secondary structure analysis using FTIR showed the byssus thread's strength. The elemental composition analysis indicates that mussel byssus thread can use as an excellent pollution monitoring specimen.

The adhesive proteins have high commercial value because of their non-toxic property. Natural and recombinant adhesive proteins are now commercially available. The second chapter of the present thesis concentrated on designing a new extraction protocol for the natural extraction of adhesive proteins from *P. perna*. Here, a new protocol was developed and the presence of polyphenolic foot protein 1 (fp-1) in the sample was determined by acid urea electrophoresis and UV-Visible spectroscopy. The extracted proteins pH stability was determined by UV-Visible spectroscopy, adhesive strength study was measured using AFM and hydrophobicity was determined by contact angle measurement. The third chapter of the thesis focused on gene sequencing of adhesive protein and insilico characterisation of the obtained protein. Two variants of *P. perna* foot protein 6 were

obtained and insilico characterisation results highlighted that mussel foot protein 6 two variants act as protease inhibitors and had high antioxidant activity. The mussel shells are an excellent source of minerals and mineral deficiency is one of the hurdles in the farming system. The fourth chapter of the thesis dealing the synthesis of new slow-release fertilizer by using cow urine and mussel shell powder. The combination of cow urine and shell powder leads to the formation of struvite crystals which provide a more slow-releasing property to fertilizer and also rich plants essential macro and micronutrients. *Mytilus edulis* is the most studied mussel in the field of adhesion research followed by *Mytilus californianus*, *Mytilus galloprovincialis* and *P. viridis*. The studies from *P. perna* are very basic and not much progressive. Hence, the present research work is open to new informative parts of adhesion research.

സംഗ്രഹം

സാധാരണയായി ശുദ്ധജലത്തിലും സമുദ്രത്തിലും കണ്ടുവരുന്ന ജല ജീവികളാണ് കല്ലുമ്മക്കായകൾ (Mussels). നനഞ്ഞ പ്രതലങ്ങളിൽ ശക്തമായി പറ്റിപ്പിടിച്ചിരിക്കാനുള്ള ഇവയുടെ കഴിവ് ശാസ്ത്ര ഗവേഷണ രംഗത്ത് ഏറെ ശ്രദ്ധയാകർഷിച്ചിട്ടുള്ള ഒന്നാണ്. ഇവക്ക് ഒട്ടിപ്പിടിക്കാനുള്ള കഴിവ് ലഭിക്കുന്നത് അവയുടെ ശരീരത്തിന്റെ ഭാഗമായുള്ള 'ഫൂട്ട്' (foot) പുറപ്പെടുവിക്കുന്ന പോളിഫിനോളിക് പ്രോട്ടീൻസ് മുഖേനെയാണ് ഇത്തരം . പ്രോട്ടീനുകൾ മസൽ അഡ്ഹസീവ് പ്രോട്ടീൻ (MAP) അഥവാ മസൽ ഫൂട്ട് പ്രോട്ടീൻ (MFP) എന്നാണ് അറിയപ്പെസാധരണയായി കല്ലുമ്മകായയിൽ .ആറ് വ്യത്യസ്ത തരം പോളിഫിനോളിക് പ്രോടീൻസുകളാണ് കണ്ടുവരുന്നത് വളരെ അപൂർവമായി കണ്ടു വരുന്ന3,4 ഡയ്ഹൈഡ്രോ ഓക്സിഫീനയിലലനിൻ (3.4 dihydroxyphenylalanine) അഥവാ ഡോപ്പ (DOPA) എന്ന അമിനോ ആസിഡിന്റെ സാന്നിധ്യമാണ് കല്ലുമ്മകായയിലെ പോളിഫിനോളിക് പ്രോട്ടീനുകളുടെ പ്രേത്യകത. ഡോപ്പയുടെ എണ്ണം കൂടുന്നതിനനുസരിച് പ്രൊട്ടീനിന്റെ ഒട്ടിപ്പിടിക്കാനുള്ള കഴിവും കൂടി വരുന്നതായി പഠനങ്ങൾ തെളിയിച്ചിട്ടുണ്ട്. ആയതിനാൽ ഇത്തരം പ്രോട്ടീനുകളെപറ്റിയുള്ള പഠനങ്ങൾ ശാസ്ത്ര രംഗത്ത് പുതിയ മുതൽ കൂട്ടുകളാണ്. കല്ലുമ്മക്കായയുടെ പറ്റിപ്പിടിക്കുവാനുള്ള കഴിവ് ശാസ്ത്ര ഗവേഷണ രംഗത്ത് വളരെ ആകർഷണീയമാണെങ്കിലും, ഇവയുടെ അമിതമായ പല രീതിയിലുള്ള ബുദ്ധിമുട്ടുകളും ഉണ്ടാക്കുന്നുണ്ട്. ഇവ കപ്പലുകളുടെ അടിഭാഗത്തും മറ്റു വ്യവസായിക ആവശ്യത്തിന് വേണ്ടി ഉള്ള പൈപ്പുകൾ, ഉപകരണങ്ങൾ എന്നിവയിലും അടിഞ്ഞു കൂടി അവയെ നശിപ്പിക്കുന്നത് വഴി വലിയ സാമ്പത്തിക നഷ്ടങ്ങൾ ഉണ്ടാകുന്നു. ആയതുകൊണ്ട് കല്ലുമ്മക്കായയുടെ വലിയതോതിൽ ഉള്ള ഇത്തരം ആക്രമണങ്ങൾ തടയാനുള്ള ഗവേഷണങ്ങളും നടക്കുന്നുണ്ട്. ഇന്ത്യയിൽ *പെർണ പെർണ* (*Perna perna*), *പെർണ വിരിഡിസ്* (*Perna viridis*) എന്നിങ്ങനെ പേരിലുള്ള രണ്ട് കല്ലുമ്മക്കായകൾ ആണ് വിപുലമായി കണ്ടുവരുന്നത്ഈ . പ്രബന്ധത്തിൽ നാല് അധ്യായങ്ങളിലായി ഉൾക്കൊള്ളിച്ചിരിക്കുന്നത് *പെർണ പെർണ* എന്ന കല്ലുമ്മക്കായയുടെ ഭാഗങ്ങളെ പറ്റിയും, അതിൽ കണ്ടുവരുന്ന അഡ്ഹസിവ് പ്രോട്ടീൻസിനെ പറ്റിയുള്ള പഠനങ്ങളുമാണ്അതിനു പുറമെ പെർണ . പെർണയുടെ പുറം തോടും (Shell), പശുവിന്റെ മൂത്രവും

ഉപയോഗിച്ചുകൊണ്ടുള്ള പുതിയ തരം വളപ്രയോഗത്തിന്റെ സാധ്യതയും അന്വേഷിക്കുന്നുണ്ട്.

ഫൂട്ട്, ബൈസസ്സ് ത്രെഡ് തുടങ്ങി ഭാഗങ്ങൾ ആണ് കല്ലുമ്മക്കായയുടെ പറ്റിപ്പിടിക്കാൻ ഉള്ള കഴിവിന് പിറകിൽ പ്രവർത്തിക്കുന്നത്. ഇത്തരം ഭാഗങ്ങളെ പറ്റിയുള്ള പഠനങ്ങൾ കല്ലുമ്മക്കായയുടെ ആക്രമണങ്ങൾ ഒഴിവാക്കാൻ ഉള്ള സാദ്ധ്യതകൾ അവലംബിക്കാൻ സഹായിക്കുന്നു. ഈ പ്രബന്ധത്തിന്റെ ആദ്യ അധ്യായത്തിൽ പ്രതിപാദിക്കുന്നത് *പെർണ പെർണയുടെ* ഫൂട്ടിനെയും ബൈസസ്സ് ത്രെഡിനെയും പറ്റിയുള്ള പഠനമാണ്. പ്രോക്സിമൽ ത്രെഡ്, ഡിസ്റ്റൽ ത്രെഡ്, പ്ലേഗ് തുടങ്ങി മൂന്ന് ഭാഗങ്ങൾ *പെർണ പെർണയുടെ* ബൈസസ്സ് ത്രെഡിൽ കാണാൻ സാധിക്കും .ബൈസസ്സ് ത്രെഡിന്റെ ഓരോ ഭാഗങ്ങളിലും വ്യത്യസ്തമായ പ്രോട്ടീനുകൾ ആണ് കാണപ്പെടുന്നത് ഇലയുടെ ആകൃതിയിൽ ഉള്ള ഭാഗമാണ് .പ്ലേഗ്. പ്ലേഗിൽ കാണപ്പെടുന്ന പോളിഫിനോളിക് പ്രോട്ടീൻസ് ഉപയോഗിച്ചാണ് കല്ലുമ്മക്കായ വിവിധ പ്രതലകളിൽ ഒട്ടിപ്പിടിക്കുന്നത്. പ്ലേഗിൽ, NBT ഉപയോഗിച്ചിട്ടുള്ള സ്റ്റെയിനിങ് നടത്തിയപ്പോൾ പ്രതലങ്ങളുമായി സമ്പർക്കം വരുന്ന ഭാഗത്താണ് പോളിഫീനോളിക് പ്രോട്ടീനുകൾ കേന്ദ്രീകരിച്ചിരിക്കുന്നത് എന്ന് മനസിലാക്കാൻ സാധിച്ചുയർന്ന .

താപനിലയിലും അതിജീവിക്കാനുള്ളബൈസസ്സ് ത്രെഡിന്റെ കഴിവ് തുറന്നുകാട്ടുന്നതായിരുന്ന TGA പഠനങ്ങൾ. അതിനോടൊപ്പം FTIR ഉപയോഗിച്ചുകൊണ്ടുള്ള പ്രോട്ടീൻ സെക്കന്ററി സ്ട്രക്ചർ പഠനങ്ങൾ വിരൽ ചൂണ്ടുന്നത് ബൈസസ്സ് ത്രെഡിന്റെ ശക്തിയിലേക്കാണ്.

പാർശ്വഫലങ്ങൾ ഉണ്ടാകുന്നില്ല എന്ന ഗുണമാണ് മസ്സൽ അഡ്ഹസിവ് പ്രോട്ടീനു വലിയ തോതിലുള്ള വ്യാവസായിക മൂല്യം നൽകുന്നത്നേരിട്ട് . പ്രോട്ടീനുകളുംകല്ലുമ്മകായയിൽ നിന്നും വേർതിരിച്ചെടുത്ത, റീകോമ്പിനന്റ് DNA ടെക്നോളജി വഴി നിർമ്മിച്ച പ്രോട്ടീനുകളും വിപണിയിൽ ലഭ്യമാണ്. ഈ പ്രബന്ധത്തിന്റെ രണ്ടാം അധ്യായത്തിൽ പരാമർശിക്കുന്നത് *പെർണ പെർണയിൽ* നിന്നും നേരിട്ട് പരമാവധി പ്രോട്ടീനുകളെ വേർതിരിച്ചെടുക്കാനുള്ള നൂതന മാർഗങ്ങളുടെ അന്വേഷണമാണ്ഇതിലൂടെ പെർണ . പെർണയിൽ നിന്നും നേരിട്ടു പോളിഫിനോളിക് പ്രോട്ടീനുകളെ പുതിയ .തരംതിരിക്കാനുള്ള ഒരു രീതി വികസിപ്പിച്ചെടുത്തു രീതിയിൽ വേർതിരിച്ചെടുത്ത പ്രോട്ടീൻ സാമ്പിളിൽ അടങ്ങിയിരിക്കുന്നത് *പെർണ പെർണയുടെ* ഫൂട്ട് പ്രോട്ടീൻ 1 ആണെന്ന് ആസിഡ് യൂറിയ ജെൽ

ഇലക്ട്രോഫോറെസിസ് വഴി മനസിലാക്കിപെർണ പെർണയുടെ ഫൂട്ട് . പ്രോട്ടീന്റെ ജീനുകളുടെ പഠനമാണ് മൂന്നാം അധ്യായത്തിൽ വിവരിക്കുന്നത് . ഇതുവഴി പെർണ പെർണയുടെ ഫൂട്ട് പ്രോട്ടീൻ ആറിന്റെ രണ്ടു വകഭേദങ്ങൾ കണ്ടുപിടിക്കാൻ സാധിച്ചുഇവയുടെ ഇൻസിലിക്കോ പഠനങ്ങൾ . തെളിയിക്കുന്നത് ഇവയ്ക്ക് അഡ്ഹസിവ് പ്രോട്ടീനുകളെ നശിപ്പിക്കാൻ വരുന്ന മറ്റു പ്രോട്ടീനുകളെ തടയാനുള്ള കഴിവ് ഉണ്ടെന്നാണ്അതിനുപുറമെ ഫൂ .ട്ട് പ്രോട്ടീൻ ആറ് ഒരു ആന്റിഓക്സിഡന്റ് ആയി പ്രവർത്തിക്കുന്നുഇവയുടെ . ഇത്തരം പ്രവർത്തനമികവ് മറ്റു പോളിഫിനോളിക് പ്രോട്ടീനുകളുടെ ഒട്ടിപിടിക്കാൻ ഉള്ള കഴിവിനെ സംരക്ഷിക്കാൻ സഹായിക്കുന്നു.

ഈ പഠനത്തിന്റെ നാലാം അധ്യായം കാർഷികരംഗത്തേക്കുള്ള ഒരു മുതൽക്കൂട്ടാണ് മിനറലുകളുടെ അപര്യപ്തത കാർഷികമേഖല നേരിടുന്ന ഒരു . വെല്ലുവിളിയാണ് .*പെർണ പെർണയുടെ* പുറം തോടും, പശുവിന്റെ മൂത്രവും മിനറലുകളും കൊണ്ട് സമൃഷ്ടമാണ് ആയതിനാൽ .*പെർണ പെർണയുടെ* പുറംതോടിന്റെ പൊടിയും പശുവിൻ മൂത്രവും സംയോജിപ്പിച്ചു പുതിയ ഒരു സ്ലോ .റിലീസ് വളം വികസിപ്പിച്ചെടുത്തു-ഈ വളത്തിന്റെ ഏറ്റവും വലിയ സവിശേഷത സ്ട്രൂവൈറ്റ് എന്നറിയപ്പെടുന്ന ക്രിസ്റ്റലുകളുടെ രൂപീകരണമാണ് . ഒരേ അളവിൽ മഗ്നീഷ്യം, അമോണിയം, ഫോസ്ഫറസ് എന്നിവ ക്ഷാരസ്വഭാവമുള്ള അന്തരീക്ഷത്തിൽ കൂടിചേർന്നാണ് സ്ട്രൂവൈറ്റ് ക്രിസ്റ്റലുകൾ ഉണ്ടാകുന്നത് .ഇവ വളരെ സാവധാനത്തിലാണ് വെള്ളത്തിൽ അലിയുന്നത് . റിലീസ് ഫെർട്ടിലൈസർ പെ-അതുകൊണ്ടുതന്നെ പുതിയ സ്ലോട്ടെന്ന് ചെടിയുടെ അരികിൽനിന്നും ഒഴുകിപോകാതിരിക്കുകയും, അതുവഴി തുടർച്ചയായി ആവശ്യമായ മിനറലുകൾ ലഭിക്കുകയും ചെയുന്നുവളരെ . അതിൽ .പ്രാധാന്യം അർഹിക്കുന്ന പഠനവിഭാഗമാണ് മസ്സൽ ഗവേഷണങ്ങൾ .പെർണ പെർണയെ പറ്റിയുള്ള പഠനങ്ങൾ വളരെ വിരളമാണ് അതുകൊണ്ടുതനിന്നെ ഈ പഠനത്തിലെ അറിവുകൾ പുതിയ ബയോ - അഡ്ഹസീവ്സിന്റെ ഉല്പാദനത്തിലേക്കും വിപണിയിലേക്കും വിരൽചൂണ്ടുന്നു . ഒപ്പം, പുതിയ സ്ലോറിലീസ് വളത്തിന്റെ വിളനില-ങ്ങളിലെ ഉപയോഗം കാർഷികമേഖലയിലെ ചില പ്രതിസന്ധിക്കും വിരാമമിടുന്നു.

LIST OF ABBREVIATIONS

Col-P	:	Proximal collagen
Col-D	:	Distal collagen
Col-NG	:	Non-gradient collagen
TMP	:	Thread matrix protein
mfp	:	Mussel foot protein
P. perna	:	*Perna perna*
°C	:	Degree Celsius
PSU	:	Practical Salinity Unit
FE-SEM	:	Field Emission Scanning Electron Microscopy
H&E	:	Haematoxylin and Eosin
NBT	:	Nitroblue tetrazolium
ICP-MS	:	Inductively coupled plasma mass spectrometry
FTIR	:	Fourier transform infrared spectroscopy
TGA	:	Thermogravimetric analysis
kDa	:	Kilodalton
MAP	:	Mussel adhesive protein
pH	:	Potential of hydrogen
TOPA	:	3,4,5- trihydroxyphenylalanine

DOPA	:	3,4,- dihydroxyphenylalanine
UV	:	Ultraviolet
Na_2SO_4	:	Sodium Sulfate
KCl	:	Potassium chloride
NaCl	:	Sodium chloride
HNO_3	:	Nitric acid
g	:	g-force
min.	:	Minute
mM	:	Mill molar
nm	:	Nano meter
BSA	:	Bovine serum albumin
PAGE	:	Polyacrylamide gel electrophoresis
APS	:	Ammonium persulfate
ml	:	Mili litre
M	:	Molar
g	:	Gram
µM	:	Micro molar
AFM	:	Atomic force microscopy
µl	:	Micro litre
CBBR	:	Coomassie brilliant blue
µg	:	Micro gram
RMS	:	Root mean square
Sec	:	Second

Kb	:	Kilobyte
PCR	:	Polymerase chain reaction
DNA	:	Deoxyribonucleic acid
NCBI	:	National Centre for Biotechnology Information
PTM	:	Posttranslational modifications
RNA	:	Ribonucleic acid
cDNA	:	Complementary DNA
Ppfp-6(1)	:	*Perna perna* foot protein 6 variant 1
Ppfp-6(2)	:	*Perna perna* foot protein 6 variant 2
XRF	:	X-Ray fluorescence spectroscopy
BET	:	Brunauer–Emmett–Teller

Many organisms acquire various adhesion adaptations to survive in a dynamic ocean environmment. For example, starfish use adhesion bonding for movement in the ocean, same time mussels, barnacles, and oysters produce adhesive materials for surface attachment and stability and marine worms use an adhesive composite to form protective shells for their dwellings (Burkett et al., 2009; Yuvaraj et al., 2021). Research on the biomimetic and bioinspired study has brought attention to the barnacle and mussel adhesion. Mussels are bivalves that fall under the phylum Mollusca and the majority of them belong to the families Mytilidae and Dreissenidae. Mytilidae is the largest family of mussels including 11 subfamilies, 68 genera, 519 species and 6 subspecies. Mussels from the genera *Mytilus* and *Perna* are common in temperate to polar and subtropical to tropical marine zones, respectively, are quite well suited for consumption and are actively cultivated (Inoue et al., 2021). The most studied mussel genus is *Mytilus*, followed by *Perna*. A total of nine species of *Perna* were identified, and Indian coastal regions are predominated with two *Perna* species namely *Perna perna* and *Perna viridis*.

Mussels are sessile animals, dominant species of shallow-sea, freshwater, and deep-sea chemosynthetic ecosystems. Mussels live predominantly in intertidal zones; as a result, they must be very tolerant to environmental changes since they are constantly exposed to changing ambient factors, such as temperature and salt (Inoue et al., 2021). In addition, the mussel exhibited strong osmoregulatory abilities; since they can change the osmolality of their bodily fluids to match the environment, they are referred to be osmoconformers (Rola

et al., 2017). Mussels play a significant role in the food web, because they are filter feeders, and actively capture plankton and small organic particles in the water. As a result of their capacity to filter feed, mussels have become a popular subject of research on environmental pollution since their body composition reflects the state of their surroundings (de Fouw et al., 2020). Due to this attraction, Goldberg (1975) suggested the "mussel watch" concept to track worldwide aquatic contamination.

Mussels have two unique calcareous valves linked by a leathery hinge that make up the complete shell, represent major part of the body (Chakraborty et al., 2020). The shape, size, colour, and biomass of mussel shells vary widely, and the calcium carbonate mineral constitutes the great majority (about 94%) of the shell's material. The two most common types of $CaCO_3$ crystal called calcite and aragonite, are used to make mussel shells. The entire shell formation is regarded as a typical biomineralization process, that is physically and genetically regulated at the cellular level (Chakraborty et al., 2020; Mititelu et al., 2021). Usually, mussel shells are dumped as waste, which severely pollutes the environment. Nevertheless, waste shells are a valuable resource that may be utilized for a variety of applications. Calcination for calcium oxide would be one of the recovery strategies of mussel shell waste; however the amount of energy needed to do so severely restrict the commercial feasibility. The use of whole mussel shell in sulfate-reducing bioreactors for acid mine drainage treatment allows the reduction of pollution load and the use of the calcined mussel shell in the waste water treatment is also

encouraged. Modified mussel shell powder is also used to immobilise microalgae and for removal of nutrients. Mussel shell can also act as a catalyst in the production of biodiesel and can be incorporated in polypropylene or in reinforced composites (Hu et al., 2011; Jones et al., 2011; Uster et al., 2015; Mititelu et al., 2021).

Mussels are notoriously invasive and major biofoulers due to their unique ability to adhere to submerged surfaces via the proteinaceous holdfast known as the byssus. Mussels may group together in vast collections known as "mussel beds" by adhering to one another with their byssi (Engel et al., 2017). The invasion of mussels results in a sharp decline in phytoplankton biomass, changes in water quality, and the extinction of native mussel species due to direct competition for food and habitat. They may also obstruct cooling systems on power boats, clog pipelines and water supplies, sink navigation buoys as a result of their weight, and dock pilings can become dangerously weakened (Rolla et al., 2020). The researchers were more attracted to mussels because of their incredible adhesion capacity. In essence, the byssus is formed of radially spaced threads that aids in mussel attachment to a substrate and adhesion achieved by the activity of collection of proteins. The *Mytilus edulis* is the most studied mussel for the understanding the adhesion mechanism (Bandara et al., 2013).

The studies of the adhesion mechanism of mussels are helpful in design new synthetic materials as well as concepts for the creation of antifouling strategies. The biofouling issue is a persistent concern for the marine shipping industry since it may drive up annual vessel

operating costs by several millions of dollars due to a gradient of operational drag induced by coating roughness, biofilms, algal biofouling, and animal biofouling. Therefore, a deep understanding of the structure and factors affecting the strength of the mussel adhesion may help to develop suitable antifouling materials. One of the significant mussel species found in the Indian coastal region is the brown mussel called *P. perna*, a good source of adhesive proteins and less explored. Hence, the present study mainly targeted understanding the adhesive mechanism of the *P. perna*.

Objectives of the study

- ✓ Structural and chemical characterization of *Perna perna* foot and thread.
- ✓ Biochemical analysis of mussel foot proteins from *Perna perna*.
- ✓ Molecular identification and characterization of foot protein genes.
- ✓ Immobilization of nutrients and struvite synthesis using maritime waste of *Perna perna* (Mussel shell)

Various organisms, including bacteria, spiders, marine tubeworms, sea cucumbers, barnacles, and mussels, may naturally manufacture specialised adhesives, but their strength and durability are incomparable to those of synthetic adhesives. Barnacles, mussels, and other marine organisms have developed adhesive strategies for dealing with the fluctuating ocean environment, particularly at the tidal interface (Silverman & Roberto, 2007). The natural adhesive proteins that used marine and freshwater mussels to attach to a variety of surfaces in an aqueous environment are very strong and long-lasting, and they contain repeating amino acid motifs, high DOPA content and different chemical modifications (hydroxylations) to specific amino acids. Similar to mussel adhesives, there are no synthetic adhesives that may be used in an aquatic environment that are resistant to water and turbulence (Brazee & Carrington, 2006). Mussel biofouling is the most notorious issue makes a huge economical loss. Hence, research in the area of antifouling and foul release are most desirable. Chemical or physical approaches are the two main categories of antifouling and bivalve control strategies. Chemical control is the most accepted method but heavy metal-based and organotin coatings are prohibited because of their toxic effect on aquatic organisms. Imides, terpenoids, proteases, and phloroglucinol are biodegradable compounds used to inhibit mussel attachments (Hellio et al., 2001; Zentz et al., 2002).

The structure involved in mussel adhesion is termed byssus; it consists of a bundle of threads called byssus threads. The entire byssus contains three parts namely, root, stem and byssus threads. The root is attached to the byssal retractor muscle found at the base of the foot organ and

the stem is the extension of the root, from which individual byssal threads originated. Byssus threads were generated from the mussel's foot organ; here adhesive proteins were synthesized from a separate gland and released into the foot's longitudinal groove that serves as a thread template (Brazee & Carrington, 2006). The effectiveness and strength of mussels' attachment are influenced by several physiological and environmental parameters, including salinity, temperature, pH, season, substratum preference, age, and metabolic condition (Carrington, 2002). DOPA is the principal component found in polyphenolic foot proteins formed from the hydroxylation of tyrosine residues by a polyphenol oxidase (tyrosinase) and is actively involved in adhesion.

Mussel adhesive proteins

A byssus thread mainly consists of three collagen proteins namely Col-D, Col-P and Col-NG and six different polyphenolic adhesive proteins designated foot proteins 1 to 6 synthesised from foot tissue.

Mussel foot protein 1 (mfp-1 or fp-1)

The first identified polyphenolic mussel adhesive protein was *Mytilus edulis* mussel foot protein 1 (Mefp-1). Fp-1 is the most abundant adhesive protein, primarily found in the cuticle of the byssus thread but the plaque area contains only around 5% of it. The foot proteins decapeptide repeat frequency, residue composition, molecular mass and non-repetitive regions are varies with species. Foot protein 1 is the largest polyphenolic protein, has a molecular mass of around 115 kDa

and comprises about 897 amino acid residues. It is a simple hydrophilic protein with 10–15% DOPA residues and has relatively little secondary structure (Filpula et al., 1990). The fp-1 contains numerous hexapeptide and decapeptide repeats which help to improve strength. The *Mytilus edulis* foot protein 1 contains 71 decapeptides and 12 hexapeptides. In these repetitive peptides, approximately 60 to 70 % of the amino acid residues are hydroxylated. DOPA (dihydroxyphenylalanine), diHYP (dihydroxy proline) and HYP (hydroxy proline) are the major hydroxylated residues found in mfp-1(Haemers et al., 2005). Many studies were conducted for the structural confirmation of foot protein 1. According to Haemers et al., (2005) conclusion *Mytilus edulis* foot protein 1 has a random coil conformation but a helical or turned appearance was found at the decapeptide region.

Mussel foot protein 2 (mfp-2 or fp-2)

Fp-2 is a small adhesive protein with approximately 42-47 kDa molecular mass, located in byssus plaques and is the second most abundant polyphenolic protein (Rzepecki et al., 1992). Fp-2 contains a large amount of cysteine residue and 11 tandem repeats resemble epidermal growth factor (EGF) like motifs. EGF had a knot-like structure that stabilized by the Disulfied Bridge and exhibited the stabilization role of mfp-2 in plaque. Fp-2 contains very low DOPA content and it is mainly concentrated in N- and C- terminal regions of the protein and in every EGF motif. Mainly, fp-2 maintains the integrity of byssus plaque and is more resistant to proteases (Inoue et

al., 1995). Hwang et al. (2010) studied the interaction of fp-2 with metal ions and other polyphenolic proteins. Their results concluded that mfp-2 does not act as an adhesive protein; instead, it maintains plaque cohesiveness by interacting with metal ions, particularly Fe^{3+}. The team also noticed that mfp-2 only interacts with mfp-5, not with mfp-3 at the plaque-substratum interface.

Mussel foot protein 3 (mfp-3 or fp-3)

Fp-3 is mainly located in plaque and is actively involved in adhesion with substratum, which is the smallest, non-repetitive protein with a molecular mass of around 5 to 7 kDa. Fp-3 is rich in DOPA, 4-hydroxyarginine and tryptophan residues involved in adhesion with substratum (Papov et al., 1995). Since fp-3 is small and contains a glycine residue, it is structurally flexible and may rapidly change conformation. This key property of fp-3 aids in develops cross-links with DOPA and hydrogen bonds with 4-hydroxy-L-arginine, which together promote greater adhesion strength. The study of even et al. (2008) confirmed the ability of fp-3 to change its conformation by using frequency generation (SFG) vibrational spectroscopy. They confirmed that depending on the hydrophobicity of the contact medium and specific chemical group interactions, the conformation of mfp-3 varies in different interfaces. Warner and Waite (1999) published 20 gene variants of foot protein 3 from *Mytilus edulis*. Similarly, 12 gene variants of foot protein 3 from *Mytilus californianus,* 2 variants from *M. galloprovincialis*, 15 variants from *Mytilus coruscus* and a single variant from *Perna viridis* were reported (Zhao & Waite, 2006b; Anand & Vardhanan, 2020).

Mussel foot protein 4 (mfp-4 or fp-4)

Foot protein 4 is a highly repetitive and asymmetric plaque protein with a molecular mass of around 79 kDa and acts as a coupling agent in the thread-plaque junction. It is found between collagen-D and mfp-2 and functions as a macromolecular bifunctional linker (Silverman & Roberto, 2007). The histidine-rich sequence in the N-terminal region of foot protein 4 binds with the histidine-rich metal-binding domain of collagen through metal binding. Transition metal ion Cu^{+}, act as a coupling agent between two proteins. Similarly, the Asp/Asn-rich C terminal of fp-4 joined to the calcium-binding domain of fp-2 by calcium ions (Cha et al., 2008). Foot protein 4 contains a unique tyrosine-rich octapeptide as well as an increased number of glycine, arginine, and histidine but DOPA content is restricted to 4% ((Zhao & Waite, 2006b).

Mussel foot protein 5 (mfp-5 or fp-5)

Foot protein 5 is another small plaque protein with a molecular mass of 9.5 kDa and high DOPA content. In mfp-5, 65 mol % of amino acids are composed of aromatic amino acids, lysine, and glycine and more than one-third of the protein's residues undergo posttranslational modifications such as hydroxylation or phosphorylation (Waite and Qin, 2001). In foot protein 5, two-thirds of the DOPA residues are found in clusters with flanking Lys or Arg on one or both sides, while the remaining third is flanked by small neutral residues like Gly, Pro, Asn, or Ala. The presence of phosphoserine is the unique feature of fp-5, that helps to bind with calcareous surfaces (Waite & Qin, 2001).

Mussel foot protein 6 (mfp-6 or fp-6)

Foot protein 6 is a small protein with a molecular mass of around 11.6 kDa and is found at the plaque interface. It contains high tyrosine and cysteine concentrations but DOPA content is low (Bandara et al., 2013).

Mussel adhesion mechanisms

The mussel adhesion mechanism has yet to be fully understood, but it depends on the structure of mussel adhesive proteins and their interactions. There are many factors that affect mussel adhesion mechanism (Bandara et al., 2013). The key features of protein in the adhesive surface of plaque are their very low molecular weight and high DOPA content. Here, DOPA cross-linking is the principal mechanism that occurs during adhesion. Because of low molecular weight, fp-3 and fp-5 can easily make conformational changes that lead to the formation of hydrogen bonds by 4-hydroxy-L-arginine and also DOPA-mediated cross-linking, which ultimately leads to strong adhesion on surfaces (Burzio & Waite, 2000). Similarly, Adhesion strength is increased by the open conformation of adhesive proteins, which promotes the availability of functional groups for cross-linking and hydrogen bonding (Haemers et al., 2005). There are many chemical bonds involved in mussel adhesion including, strong hydrogen bonding between DOPA and hydrophilic surfaces, DOPA forms strong noncovalent interactions with silicon dioxide, metal ions, and metal oxides found on mineral surfaces, π–π interactions between DOPA and other aromatic groups, and positively charged adhesive

proteins makes strong electrostatic interactions with negatively charged mineral surfaces (Baty et al., 1997; Wiegemann, 2005; Cha et al, 2009).

The presence of L-DOPA is the key characteristic of adhesive proteins but its role is not completely understood and it is considered an important element in the adhesion mechanism (Lee et al., 2006). Many studies revealed that high DOPA content included proteins like fp-3 and fp-5 actively involved in adhesion (Yu, 1999; Akemi & Garrell, 2000). In the presence of oxidizing agents, catechol oxidase enzyme oxidizes DOPA into DOPA-quinone or DOPA-semiquinone which participate in MAP cross-linking processes through aryl-aryl coupling (creation of di-DOPA) or Michael additions in the presence of amine-containing protein residues (Haemers et al., 2003; Monahan & Wilker, 2003). The mussel can bind to both organic and inorganic surfaces. The study of Lee et al. (2006) revealed that the binding of mussels to inorganic surfaces is achieved through strong and reversible bonds created by unoxidized DOPA and oxidized form of DOPA help to make adhesion on organic surfaces through covalent bonds. The study of Guvendiren et al. (2009) substantiates the results of Lee et al. (2006). Their studies observed that oxidized DOPA residues make strong adhesion to soft tissue. Like DOPA residue, lysine and glycine residues are involved in the adhesion mechanism. Lysine makes ionic bonds during the adhesion of MAP with negatively charged surfaces like collagen and acidic polysaccharides (Suci & Geesey, 2000). Similarly, open-confirmation glycine facilitates adhesive proteins

binding with surface groups of the substrate (Silverman & Roberto, 2007).

MAP-crosslinking is the most important step that occurs in plaque formation, which is accomplished either by aromatic nucleophiles or by autooxidation of quinone by adjacent hydroquinone. Redox potential and pH are the two main factors that affect cross-linking (Hight & Wilker, 2007). Metal ions are cross-linking agents and they contribute an important role in mussel adhesion. Sever et al. (2004) reported that metals are involved in protein cross-linking. For example, Fe^{3+} bind with three adhesive protein molecule to form tricomplexes (Fe(DOPA)3), which react with oxygen to create reactive radical species that aid in the curing of proteins by connecting with other proteins or by forming interactions with the surface of the substrate. According to research by Hwang et al. (2010) and Zeng et al. (2010), Fe^{3+} ions can strengthen adhesion by forming strong, completely reversible bridge interactions. Plaque contains large amounts of Ca^{2+} ions, which can interact with the catecholate portion of DOPA to create mono- and bis-catecholate-Ca^{2+} complexes (Holten-Andersen et al., 2009b). Similar to this, interprotein chelation causes DOPA-containing proteins to cluster in the presence of Cu^{2+}, which decreases the plaque's viscoelasticity (Hedlund et al., 2009).

Recombinant expression of mussel foot proteins

The challenges associated with extracting adhesive proteins from mussels prevent its practical application. The natural extraction of mussel adhesive protein is laborious and not economically feasible.

The current method for extracting MAPs from mussels involves removing the byssal structure and extracting proteins under acidic conditions (Cha et al., 2008). Recombinant expression of mussel foot proteins is an effective way of large-scale production of proteins. Both prokaryotic and eukaryotic hosts are used for this practice. *Escherichia coli* (bacteria), *Saccharomyces cerevisiae* (baker's yeast), *Pichia pastoris* (a methylotrophic yeast), or *Kluyveromyces lactis* (a lactic-acid–producing yeast) are the commonly used prokaryotic hosts. Similarly, plants like tobacco, potatoes, and mammals such as rabbit, mouse, and goat cells are used as eukaryotic hosts. There are several studies were conducted for the recombinant expression of mussel adhesive proteins in bacteria, yeast, mammalian cells, and plant cells (Silverman & Roberto, 2007). Filpula et al. (1990) studied molecular cloning of *Mytilus edulis* adhesive protein 1 by using the expression system *S. cerevisiae*. According to their study, foot protein 1 primary structure considered as most repetitive protein identified in the animal kingdom. Similarly, their adhesion studies revealed that the protein has a water-resistant bonding ability that depends on *in vitro* tyrosine residue modification to DOPA and the subsequent oxidation to a quinone.

In 2006a, & 2006b, Silverman and Roberto invented and patented a technique for cloning and expression of foot proteins 1 and 2 from *M. edulis* using the expression system *S. cerevisiae*. As an alternative to an expression of genes in hosts, Takeuchi et al. (1999) made an attempt to culture mussel foot cells from *M. galloprovincialis* in petri dishes. The findings indicated that the Mgfp-2 and Mgfp-3 genes were

expressed in primary and secondary cultures and that this method is appropriate for the in vitro expression of adhesive genes. This method could be a viable substitute for yeast or bacterial-based expression systems. Because of highly biased amino acid composition and repetitive sequences, foot protein 1 recombinant expression becomes laborious. Hwang et al. (2004) tried to synthesise recombinant foot protein 5 from *M. galloprovincialis* in *E. coli*. The team extracted foot protein 5 and generated recombinant Mgfp-5 coupled with a hexahistidine affinity ligand. Purified recombinant Mgfp-5 was studied for its adhesive characteristics and it was discovered that it has strong adhesive capabilities and might be used as a medicinal or underwater adhesive. In a subsequent attempt, Hwang et al. (2005) used *E. coli* to produce recombinant *M. galloprovincialis* foot protein type 3 variant A (Mgfp-3A) coupled with a hexahistidine affinity ligand. The adhesion ability of purified recombinant Mgfp-3A was compared with commercially available mussel extract adhesive Cell-Tak and recombinant Mgfp-5. The findings indicated that recombinant Mgfp-3A's adhesion strength was equivalent to Cell-Tak whereas recombinant Mgfp-5 showed greater adhesive strength than both recombinant Mgfp-3A and Cell-Tak.

The recombinant synthesis of adhesive proteins is restricted by low production yields, low purification yields, and high levels of insolubility. To resolve this issue Hwang and colleagues designed novel fusion proteins that provide greater production yields, easier purification, and improved solubility. The first hybrid mussel adhesive protein was fp-151 developed by Hwang et al. 2007c produced by the

fusion of six Mgfp-1 decapeptide repeats at both the N- and C-termini of Mgfp-5. Similarly, the same research team developed a second hybrid adhesive fp-151-RGD synthesised by the fusion of the GRGDSP residues found in fibronectin (designated RGD) to the C terminus of fp-151 (Hwang et al. 2007c). They concluded that fp-151-RGD showed superior cell adhesion and spreading abilities than fp-151, Cell-Tak, and polyL-lysine (PLL). Another recombinant fusion protein was developed by Gim et al. (2008) called fp-353 by the fusion of fusion adhesive protein fp-3A at each terminus of fp-5 in *E. coli*. Their results concluded that fp-353 can be used as a potential practical alternative bioadhesive because of its high solubility and adhesion strength and also it did not inhibit host cell growth.

Applications of mussel adhesive proteins

The mussel adhesive protein's capacity to attach to various surfaces in a wet environment distinguishes them from other adhesives and provides them with better adhesive strength than synthetic adhesives. The biocompatibility and biodegradability of MAPs make them ideal for biomedical adhesives (Ku et al., 2010). The biodegradable and non-toxic adhesives market value is increased in medical areas such as wound healing, tissue engineering, recovery from surgery, dental composites, and orthopaedic cement (Hwang et al., 2007a). Many researchers attempted to synthesise mussel-inspired synthetic polypeptides that mimic mussel adhesive protein properties. In 1998, Yu & Deming synthesised water-soluble copolypeptides by ring-opening polymerization of α-amino acid N-carboxyanhydride (NCA)

monomers, which contain l-dihydroxyphenylalanine (DOPA) and l-lysine. These copolypeptides can make moisture-resistant adhesive bonds to a variety of substrates (e.g., aluminium, steel, glass, and plastics) by mixing aqueous solutions of these copolymers with a suitable oxidizing agent (e.g., O_2, mushroom tyrosinase, Fe^{3+}, H_2O_2, or IO^{4-}).

Mussel adhesives are used as surgical adhesives because they can adhere to tissue with excellent binding strength in the presence of tissue fluids. Ninan et al. (2003) studied the binding ability of adhesive proteins extracted from *Mytilus edulis* on porcine skin. They concluded that mussel adhesive protein has biocompatibility; hence it can use in surgical applications and which shows adhesive strength similar to adhesive fibrin Tisseelt. Because of biocompatibility, mussel adhesives are utilized as a medical and dental adhesive. Lee et al. (2002) synthesised mussel-inspired adhesives called linear and branched DOPA-modified poly(ethylene glycol)s (PEG-DOPAs) containing one to four DOPA endgroups. In the presence of oxidizing agents, oxidative polymerization of DOPA endgroups occurs, resulting in polymer network formation and rapid gelation. Depending on the oxidizing agents, this gelation rapidly occurs; hence this adhesive can be used as an excellent medical adhesive. Similarly, when designing biosensors, immunosensors, or artificial tissue scaffolding and constructions, mussel adhesive proteins like the Mefp class and collagens can be immobilised on solid substrates. The findings of Yamada et al. (2000) point to the possibility of using polyphenol

oxidase, which is generated from *M. edulis* byssus structures, as a thickening agent in a various fields and applications.

Another application of mussel adhesive proteins is the development of cell adhesion materials to coat artificial surfaces and promote cell adhesion. Hwang et al. (2007b) studied the ability of modified recombinant Mgfp-5 (*Mytilus galloprovincialis* foot protein-5) as a cell adhesion agent. According to their findings, cell lines effectively adhered to recombinant Mgfp-5-coated glass surfaces, and surface-immobilized S2 cells could survive and divide for up to a week. As a result, they concluded that recombinant Mgfp-5 may be a beneficial novel cell adhesion biomaterial for anchorage-independent cells. Likewise, Mussel adhesive shows a potential application in target gene delivery into eukaryotic cells. The usage of the recombinant mussel adhesive protein fp-151 as a gene delivery medium was examined by Hwang et al. (2009). The hybrid fp-151 has an effective DNA binding capacity and shares the same proportion of basic amino acids and high theoretical pI values as histone HI proteins. They used the hybrid fp-151 as the gene delivery carrier to transfect mammalian cells (human 293T and mouse NIH/3T3) with foreign genes. The findings show that the transfection effectiveness of this hybrid protein is higher than that of the widely used Lipofectamine 2000. In order to facilitate effective gene delivery, mussel adhesive protein may potentially be exploited as a possible protein-based mediator.

INTRODUCTION

Mussel's robust adhesion to wave and wind-swept marine surfaces are achieved by high-performance tough biopolymers called byssus which consists of 40-100 byssus threads, synthesized from the foot (Aldred et al., 2007; Hagenau et al., 2009). The mussel foot extends out from the shell and finds a suitable substratum for firm adhesion. When the foot reaches the substratum, it secretes a proteinaceous plaque, and after that, it disengages from the plaque, leaving a protein thread that connects to the plaque. (Bandara et al., 2013). Adhesive proteins are secreted from different glands of the foot to the ventral groove. When the foot probes the substrate, the liquid proteins in the ventral groove exposed to saltwater, go through a curing process and create functional byssus thread and adhesive plaques. Because of complex coacervation, liquid adhesive proteins could not dissolve in seawater (Hwang et al., 2010). The adhesive strength of the byssus thread varies depending on the factors like temperature, salinity, pH, substratum choice, season, pollution and metabolic state of the mussel (Carrington, 2002).

Byssus thread comprises mainly six different types of adhesive proteins, three types of collagens and thread matrix proteins with gradient distribution. Because of this gradient distribution of proteins, different regions of the byssus thread have different mechanical properties (Hagenau et al., 2009; Torres et al., 2012). The most abundant proteins in the byssus thread are three collagens, namely, collagen-D, collagen-P, and collagen-NG which have gradient distribution. Col-P is primarily located in the proximal region of the

thread, and Col-D is located in the distal region. However, Col-NG and thread matrix proteins (TMP) are found throughout the thread. Collagens provide incredible strength and extensibility to the byssus thread (Silverman & Roberto, 2007). Mussel foot protein 1 (mfp-1), mfp-2, mfp-3, mfp- 4, mfp-5, and mfp-6 are the six different adhesive proteins. Among these proteins, mfp-3 and mfp-5 are mainly involved in the adhesion mechanism and located at the interface between the substratum and the adhesion plaque. Mfp-6 is also found in adhesive plaque and acts as a rescue protein that prevents the oxidation of DOPA. The adhesive protein 2 is located at the inner side of the plaque and is mainly involved in the stabilization of plaque by covalent disulphide links and quinine-derived cross-linking. The coupling of byssus thread and plaque is carried out by mfp-4, because it is found between preCol-D and mfp-2. The entire cuticle of the byssus thread is formed of mfp-1, which belonging the most abundant adhesive protein (Bandara et al., 2013).

DOPA (3,4 dihydroxyphenylalanine) is an unusual catabolic amino acid, act as key factor behind the adhesive ability of foot proteins. DOPA formation occurs during posttranslational modification of protein; in which tyrosine residue undergoes hydroxylation by polyphenol oxidase to form DOPA. 3,4-dihydroxyphenyl (catechol), a side chain of DOPA, can able to form strong hydrogen bonds with hydrophilic surfaces and strong complexes with metal ions, metal oxides (Fe^{3+}, Mn^{3+}), and semimetals (silicon). Mussel adhesive proteins closer to the adhesion interface have a higher proportion of DOPA residues (Papov et al., 1995). DOPA content, redox chemistry,

metal ion interactions, and open conformation of Gly are the key factors affecting the adhesion mechanism (Ohkawa, et al., 2009; Bandara et al., 2013).

Mussels are fouling organism that causes many ecological, technical, and economic problems because it accumulates on submarine boats, ships, and hulls. Biofouling creates extra drag on ship hulls causing a reduction in fuel efficiency, which leads to adding tens of billions of dollars in extra fuel costs and hundreds of millions of tons of additional CO_2 emissions in each year. Many antifouling agents were developed to overcome these issues, including metal-based compounds and synthetic organic biocides. However, these synthetic antifouling agents cause toxic effects on non-target organisms and make aquatic pollution (Wang et al., 2017). To resolve these issues, eco-friendly and natural antifouling alternatives such as chitosan, capsaicin and some enzymes were developed. In recent years, new antifouling agents are developed by mimicking natural biological materials. For example, lotus leaf self-cleaning property was attracted to the synthesis of superhydrophobic antifouling surfaces and also liquid-infused porous surfaces (SLPs) thoughts are acquired from the omniphobic capability of Nepenthes pitcher plants. Similarly, the byssus thread acts as a fouling-resistant structure, therefore mussel-inspired chemistry promotes the development of environmentally safe antifouling compounds (Wong et al., 2011; Zhang et al., 2014; Li et al., 2021).

Mussels fouling make serious ecological and economic consequences; hence deep knowledge regarding fouling is crucial for developing

antifouling strategies. Each species of mussels has its own unique adhesive mechanism. So far, the reason for such diversity in the adhesion mechanism is not understood. Mussels can expand their distribution very quickly through an invasion; hence, study of each species adhesion mechanism is very necessary (Li et al., 2018). *P. perna* is a marine brown mussel species and till date this species is not explored for studying adhesion mechanisms. This chapter mainly focused on detailed morphological and structural elucidation of *P. perna* foot and byssus thread, elemental composition analysis, chemical composition, and also thermal stability. These structural and chemical analysis results provide a significant understanding of the adhesion mechanism of *P. perna.*

MATERIALS AND METHODS

1.2.1 Test organism

The test organism selected for the present study was *Perna perna*, commonly known as brown mussel or Mexilhao mussel (Figure 1).

Taxonomic position of *P. perna* is as follows;

Kingdom : Animalia

Phylum : Mollusca

Class : Bivalvia

Subclass : Pteriomorphia

Order : Mytiloida

Family : Mytilidae

Genus : *Perna*

Species : *perna*

P. perna is native to the western Indian Ocean, specifically from the Bay of Bengal and the red sea to the tip of South Africa and the west coast of Africa. It has been introduced as an invasive species to North America and the Gulf of Mexico (Douek et al., 2021). In India, *P. perna* has restricted distribution including Pondicherry, Cuddalore, Pamban, Tuticorin, Vijapadi, Thiruchendur, Colachel, Muttom, Trivandrum, Varkala, Alleppey and Cochin (Kuriakose and Nair, 1976). On average *P. perna* is 90 mm in length but sometimes they reach up to 120 mm. Adults have thick shells, typically brown coloured and roughly oval in the ventral region but taper to a triangular shape in

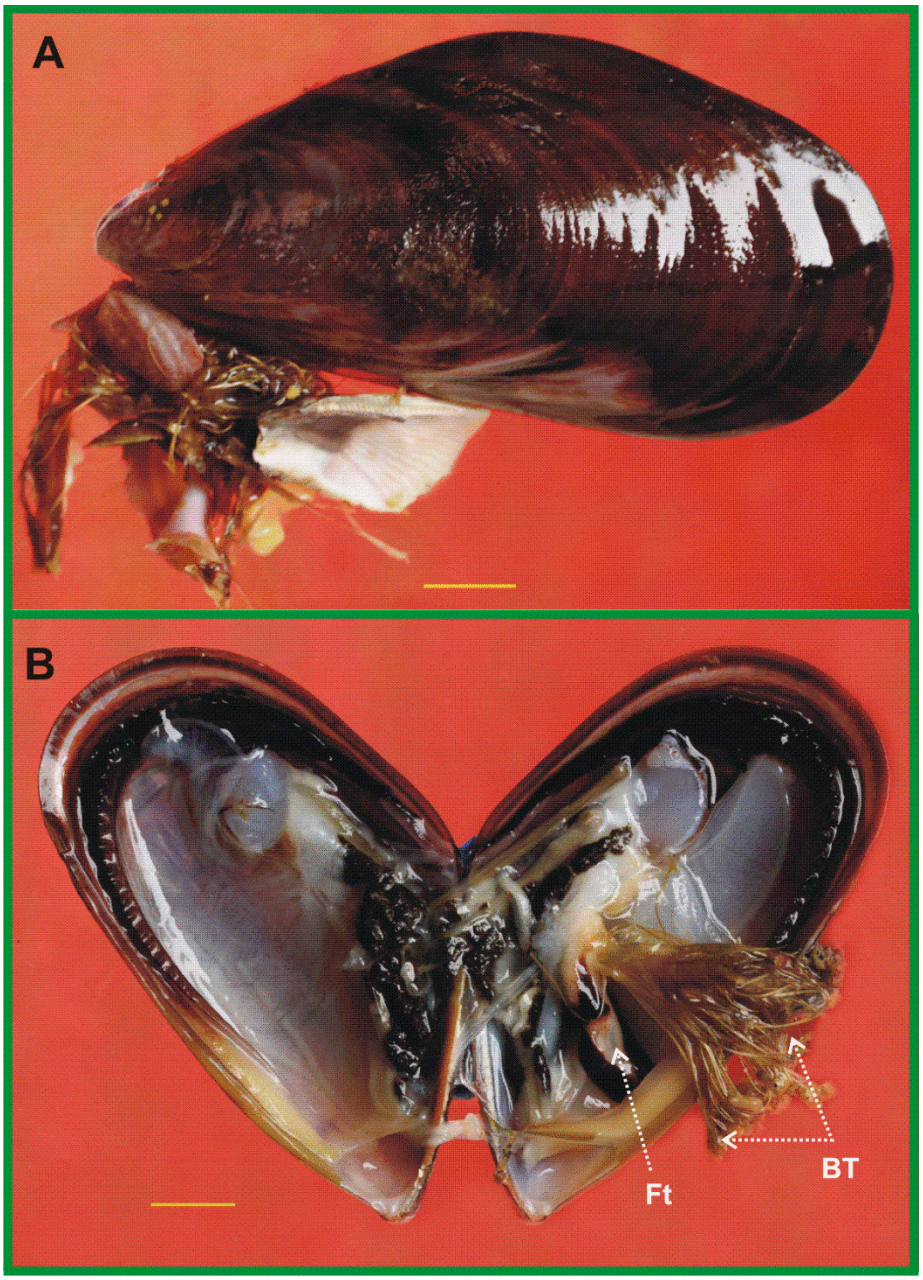

Figure 1: *Perna perna*; (**A**) entire *P. perna*, (**B**) shell opened *P. perna* showing byssus thread (BT) and Foot (Ft)

the dorsal half. Shell is broader in the anterior poster direction, the ventral margin is straight and has thin, elongated posterior retractor muscle, and both arise from a common base and run parallel. *P. perna* has two small hinge teeth on the left valve and one on the right valve. Pronounced papillae along the mantle margin are another distinguishable feature. *P. perna* exhibit sexual dimorphism, males release sperm and females release egg into the water during the spawning season. They utilize external fertilization and fertilized eggs develop into planktonic trichophore larvae, and then shelled veliger larvae. After 10-12 days of fertilization larvae undergo metamorphosis, produce byssus threads and settle on a hard substratum (Kuriakose and Nair, 1976; Hicks, 1993). *P. perna* tolerates 15-50 PSU salinities and 7.5 to 31.5°C temperatures. They are ciliary mucoid filter feeder mainly feeds phytoplanktons, zooplanktons and suspended organic materials (Hicks et al., 2000; Hicks & McMahon, 2002).

1.2.2 Sample collection

The sample *P. perna* for this study was collected from Kovalam, Thiruvananthapuram, Kerala (8.3988° N, 76.9820° E) (Figure 2). The mussels were collected from rock and transported to the laboratory in semi-sedated condition. In the laboratory, they were kept in a glass tank containing seawater with adequate aeration for further analysis.

1.2.3 Micoscopic analysis

For microscopic analysis, foot tissues and byssus threads were dissected from live mussels using a disinfected surgical blade, washed thoroughly in distilled water and preserved at -80°C for further analysis.

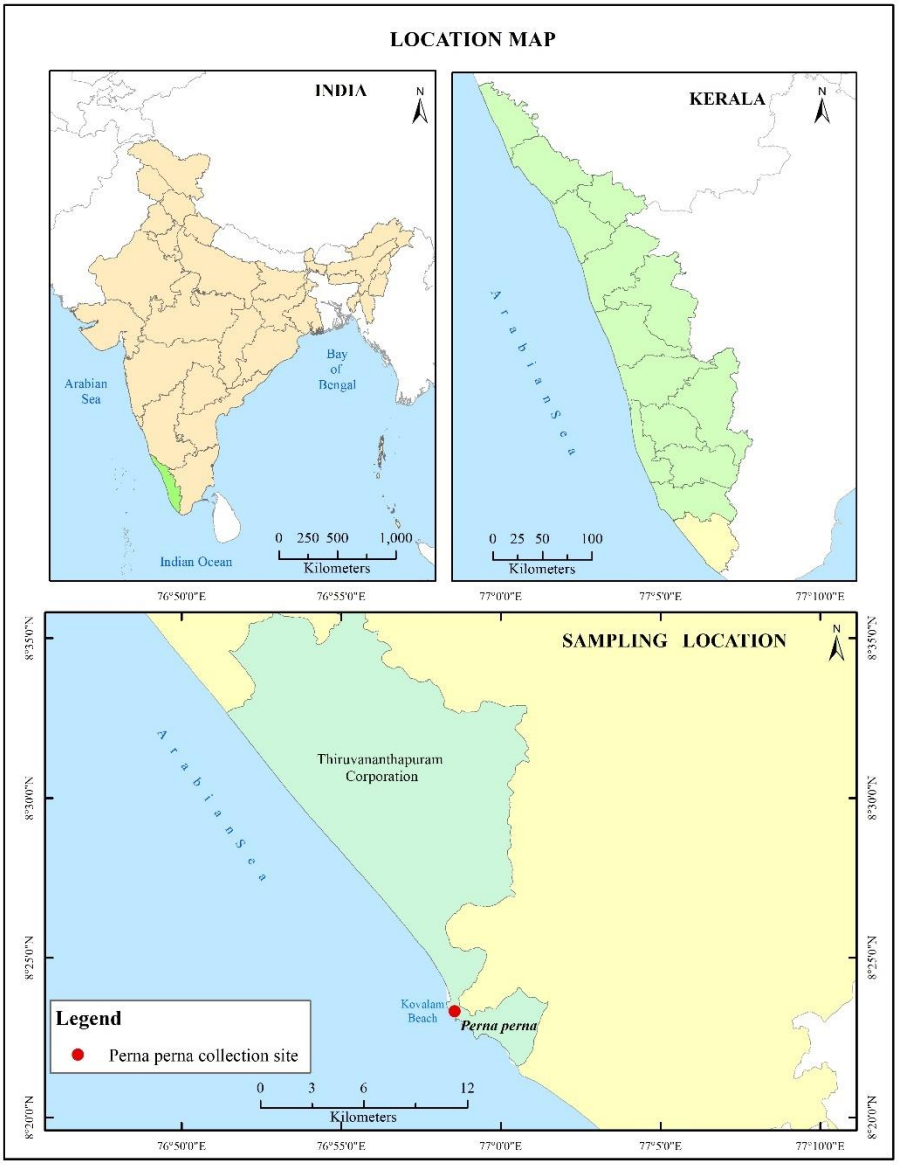

Figure 2: Collection site; *P. perna* collected from Kovalam, Thiruvananthapuram, Kerala

1.2.3a Light microscopic analysis

Light microscopic imaging of byssus thread and foot was done by using a ZEISS Stereo Zoom Microscope with Discovery V20 CCD camera 506 and cross-polarized light microscopy (Radical polarising microscope, RPL-55B). The stereo-microscopic analysis provides morphological features of the byssus thread and foot. Similarly, crossed polarized light microscopic images exhibit anatomical regions of thread by differential light scattering.

1.2.3b Scanning electron microscopic analysis

Microstructural characterization of byssus threads was done by using Field Emission Scanning Electron Microscopy (FE-SEM). Samples were prepared according to previously described method (Li et al., 2018). In brief, byssus threads were dried in an oven at 60°C for 1 hour and kept in a desiccator. Properly dried threads were mounted on conductive carbon tape and sputter-coated with gold particles for the 50s on Quorum SC 7620 sputter coater. Ultrastructure imaging was conducted using FE-SEM microscope (ZEISS GeminiSEM 300).

1.2.4 Histological analysis

The live healthy specimens were immersed in chilled seawater, and fresh foot was dissected with the serialised surgical knife. The samples were fixed in neutral buffered formalin and subsequently dehydrated in double-distilled ethanol. The dehydrated samples were cleared in methyl benzoate, passed through different gradients of xylene and paraffin wax and finally embedded in embedding wax. The blocks

were sectioned with a thickness of 5 to 6 microns by using a rotary microtome (Leica, HistoCore BIOCUT) and stained with conventional Haematoxylin and Eosin (H&E) (Feldman & Wolfe, 2014) for further examinations. Stained slides were examined in Zeiss compound microscope Scope A1, and the final full foot image was acquired using a ZEISS stereo zoom microscope, Discovery V20, CCD camera 506.

1.2.5 NBT staining

Nitroblue tetrazolium (NBT) staining is a redox cycling staining used to detect quinones and related quinonoid substances. 8 mg of NBT were dissolved in 14 ml potassium glycinate buffer at pH 10 and the bottles were kept in the dark to avoid photoreaction. The samples were stained in NBT/Glycinate buffer for 15 minutes according to the existing protocol (Qin et al., 2016). In principle, at alkaline pH quinones and related quinonoid substances catalyse the reduction of tetrazolium to formazan forming dark blue colour, in the presence of oxygen and glycine act as reductants.

1.2.6 Elemental composition analysis

1.2.6a Inductively coupled plasma mass spectrometry (ICP-MS)

The elemental composition of byssus threads and foot was measured using ICP-MS. The samples were perfectly cleaned with Milli Q water to removes contaminants and oven-dried. For ICP-MS, sample preparation was done by using acid digestion protocol (Li, et al., 2018). At first, 1 g of dried samples such as byssus threads, and foot hydrolysed in 10 ml of nitric acid (HNO_3). After the complete

dissolution of residues, added 2 drops of hydrogen peroxide (H_2O_2) to remove organic contents. When cooling the samples, the solutions makeup to 25 ml by using Milli Q water in the standard flask. The elemental compositions were determined using inductively coupled plasma mass spectrometry (Agilent 78000 ICP-MS). The determining elements include Lithium, Beryllium, Boron, Sodium, Magnesium, Aluminium, Potassium, Calcium, Vanadium, Chromium, Manganese, Iron, Cobalt, Nickel, Copper, Zinc, Gallium, Arsenic, Selenium, Rubidium, Strontium, Molybdenum, Silver, Cadmium, Tellurium, Barium, Thallium, Lead, Bismuth and Uranium. The elemental concentrations were expressed as ng/g dry weight. The percentage of each element in the corresponding categories found in byssus thread and foot were also calculated.

1.2.6b CHNS analysis

Vital elements such as carbon, hydrogen, nitrogen, and sulphur concentration in foot and thread were detected by the CHNS analyser (Thermo Scientific FLASH 2000 HT analyser). For this analysis, foot and threads were thoroughly cleaned in double distilled water and oven-dried. After proper drying the samples were finely powdered and measured the element composition. The elemental concentrations were expressed as ng/g dry weight. The percentage of each element in the corresponding categories of each sample (byssus thread and foot) was also calculated.

1.2.7 Fourier transform infrared spectroscopy (FTIR)

Fourier transform infrared spectroscopic analysis utilizes infrared light to scan the samples and provide the chemical properties of the samples.

For this analysis, byssus threads were thoroughly cleaned in double-distilled water to get rid of any impurities. After thorough drying, the materials were ground up into small pieces, powdered with potassium bromide, and pelletized. Using a FTIR spectrophotometer (Jasco-4100, Shanghai, China), the infrared examination was carried out in the spectral region of 500 to 4000 cm^{-1}. The raw FT-IR data has been processed using Origin software (Version OriginPro 9.0 64Bit). The interpretation of FTIR spectra was done based on the article "infrared spectroscopy of proteins" by Barth, (2007). The secondary structure of the proteins found in byssus threads was discovered using the amide I band in the FT-IR spectrum. The Gaussian fit was used to analyse the deconvolution of the FTIR spectrum's amide I band in order to ascertain the secondary structure, in which a specific secondary structure absorbs a specific range of amide I region (Barth, 2007).

1.2.8 Thermogravimetric analysis (TGA)

Thermogravimetric analysis is a type of analytical procedure in which the weight changes that occurs while the sample is heated at a consistent rate to determine the thermal stability of the specimen (Aldred et al., 2007). For this analysis, thoroughly washed and cleaned byssus threads were chopped into small pieces and the thermal stability was carried out in an STA 8000 simultaneous thermal analyser under the temperature range of 30-900°C with a heating rate of 10°C/min.

1.2.9 Statistical analysis

The results obtained from the experiments were statistically analysed by using the programme IBM SPSS version 20.0. All data represented as mean ± standard deviation acquired by descriptive statistics.

RESULTS

1.3.1 Byssus thread structure

Wet adhesion is the mussel's unique characteristic ability provided by adhesive holdfasts called byssus, made up of numerous threads called byssus threads. *P. perna* byssus consists of a fibrous stem rooted into the byssus retractor muscle. SEM image of the stem region (Figure 3A & 3B) showed that, byssus threads originated from the lateral region of the stem as loosely packed bundles. Morphologically, a single byssus thread of *P. perna* contains three notable portions, namely, proximal thread (Figure 3C), distal thread (Figure 3C), and adhesive plaques (Figure 3E). The proximal thread was corrugated and elastic, whereas the distal thread was smooth and stiffer. The distal thread was ended with a larger, leaf-like structure called plaque. Figure 3D showing SEM image of porous inner plaque surface of *P. perna*. The NBT-stained image (Figure 4) of the *P. perna* byssus thread showing that, the anchoring surface of the plaque was more deeply stained because these sites are DOPA-rich portions of the thread. Crossed polarized light image of the byssus thread (Figure 5) exhibiting the two distinct anatomical regions of *P. perna* byssus thread namely outer cuticle and inner core. The cuticle was dark (anisotropic), and thick coating which covers the lightly coloured isotropic soft core region.

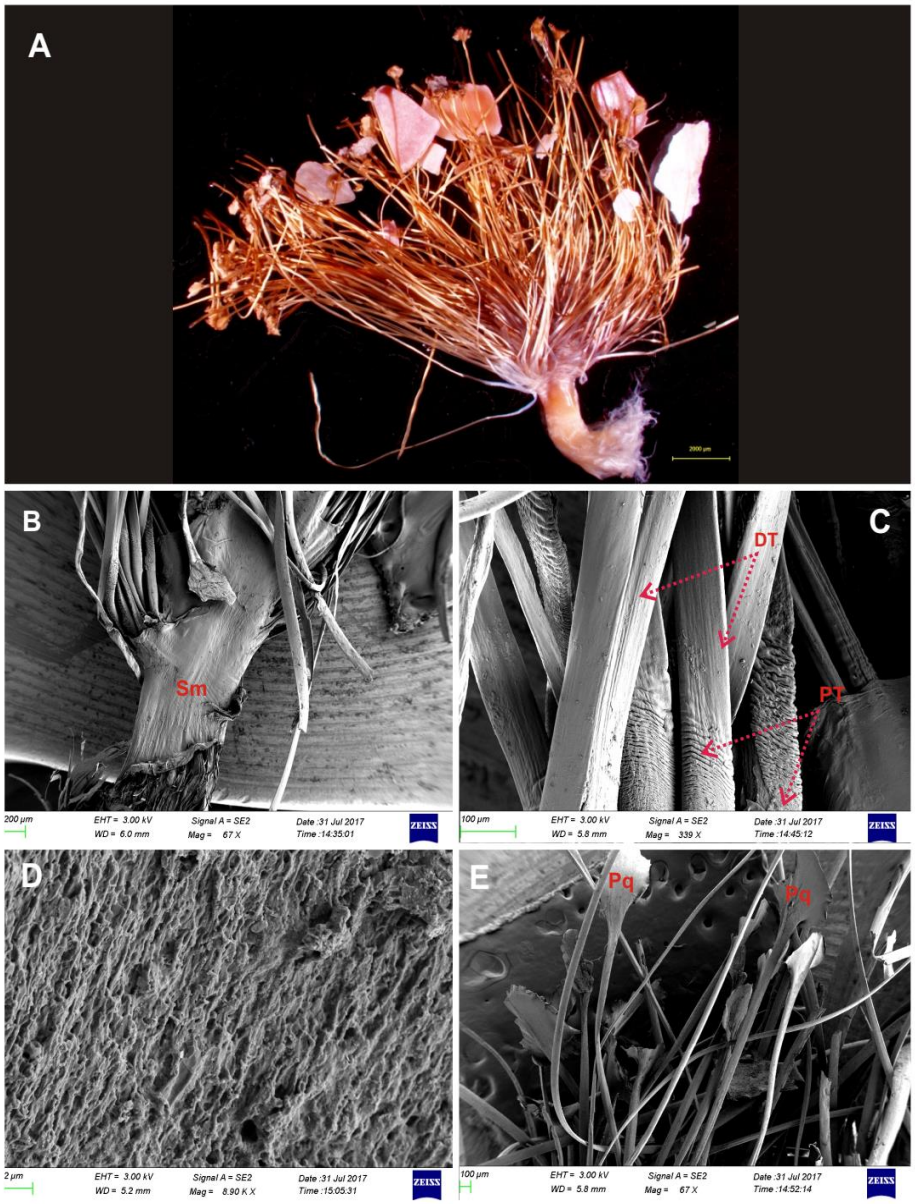

Figure 3: *P. perna* byssus structure; (**A**) entire byssus, (**B**) stem region (Sm), (**C**) proximal thread (PT) and distal thread (DT), (**D**) inner surface of plaque, (**E**) Plaque (Pq)

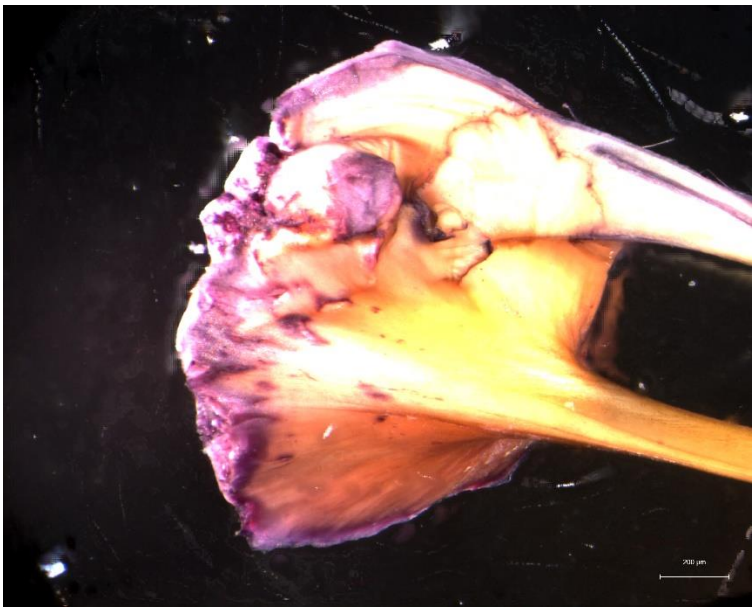

Figure 4: NBT stained *P. perna* byssus thread

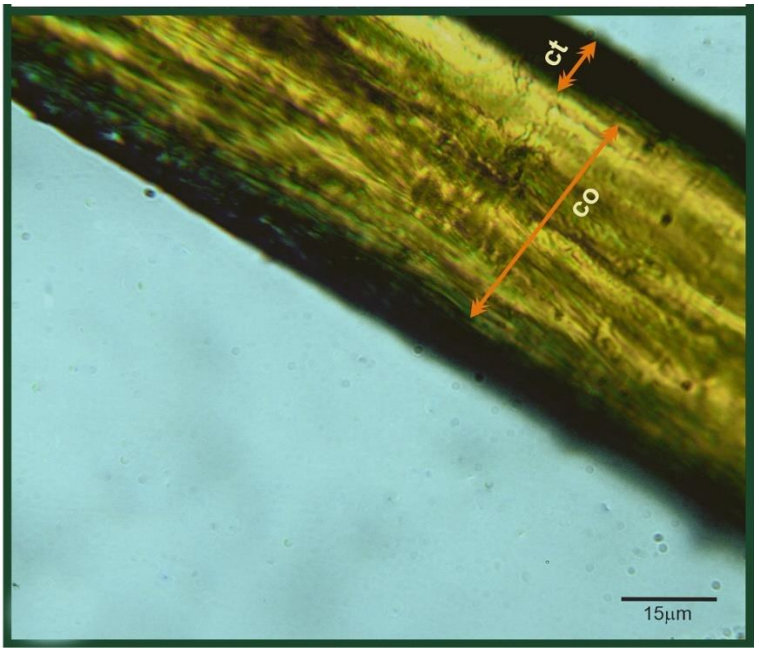

Figure 5: Crossed polarized light microscopy image of *P. perna* byssus thread

1.3.2 Foot structure

The mussel foot is a tongue-shaped muscular organ involved in locomotion, temporary attachment and more importantly, in the synthesising, storing and secretion of adhesive proteins. *Perna perna* foot had around 1-1.5 cm in length at the resting stage (Figure 6). The foot's lateral surfaces (Figure 6C) contained numerous folding, that allowed the foot to lengthen gradually. The dorsal side of the foot is flat (Figure 6A), while the ventral side has a trench-like groove from the proximal to the distal tip of the foot known as the ventral groove or pedal groove that ends in a small concavity called the distal depression (Figure 6B). The ventral groove in *P. perna* had a depth of about 915 µm. Image of the *P. perna* foot's histology (Figure 7) showed that the entire foot tissue was covered in the ciliated epithelium. Layers of mucous-secreting glands, muscle cells, and haemolymph sinuses were found beneath this ciliated epithelium. Each cilium in *P. perna* measured an average of 16.073±0.719 µm in length and 1.297±0.194 µm in width. Three major byssus glands found in *P. perna* foot (Figure 8A & 8B) are the core gland or collagen gland, accessory gland or cuticle gland and phenol gland or plaque gland. They can all be spotted surrounding the ventral groove and distal depression. A second mucus-secreting gland was located at the apex of the foot tissue (Figure 8B), and muscle fibre bundles split the ovular mucous gland into two. The figure 6A shows the bulbous stem gland located at the base of the foot and the Figure 6C exhibited the NBT stained foot of *P. perna,* which shows that ventral groove region of the foot had high concentration of DOPA.

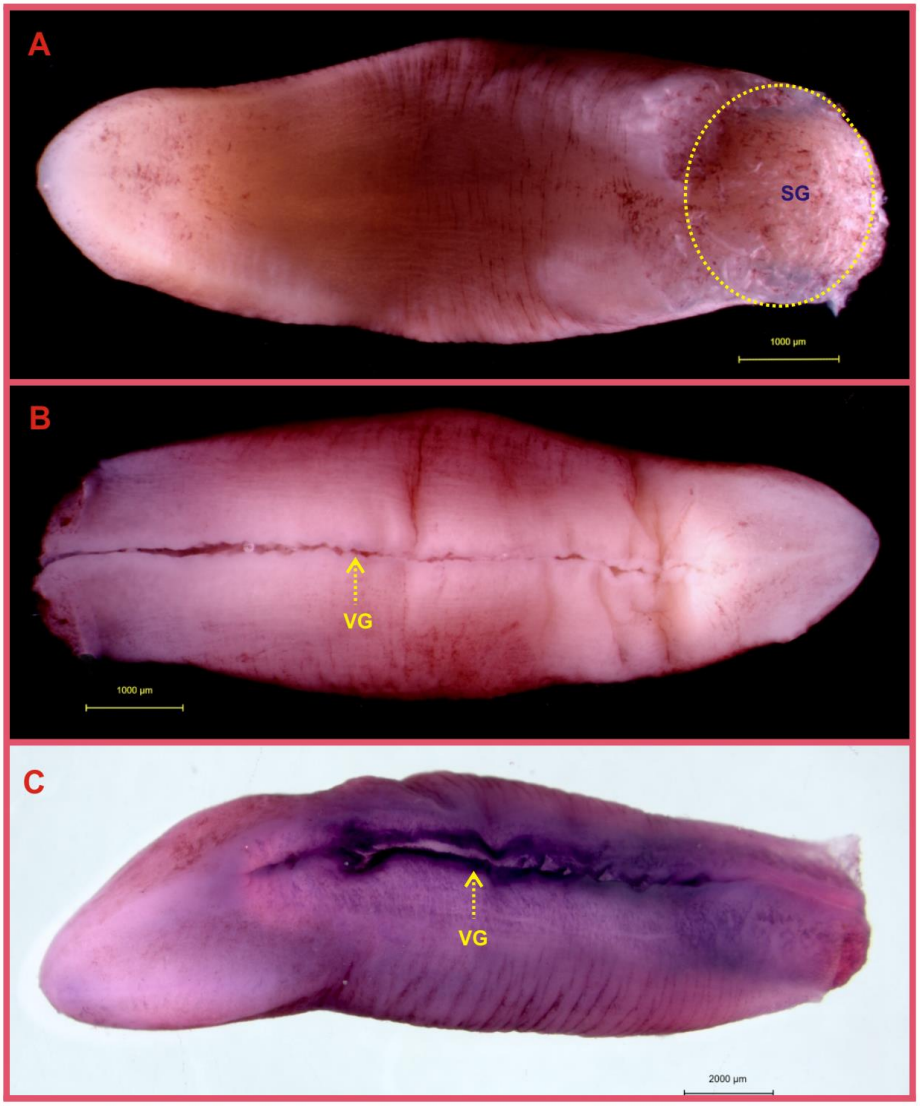

Figure 6: Foot of *P. perna*; (**A**) dorsal region of foot showing stem gland (SG), (**B**) ventral region of foot showing ventral groove (VG), (**C**) NBT stained foot showing ventral groove

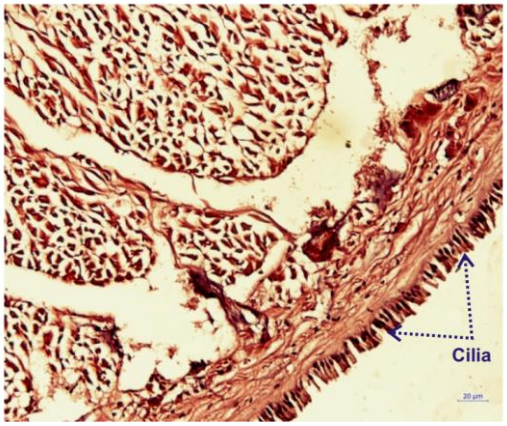

Figure 7: Foot section of *P. perna* showing outer ciliated epithelium

Figure 8: Histological sections of *P. perna* foot (**A**) Cross section of foot showing accessory gland (ag), collagen gland (cg), phenol gland (pg) and muscle tissue (mt), ventral groove (vg), epithelial cilia (ec), haemolymph sinus (hs) (**B**) Longitudinal section of foot showing phenol gland (pg) and mucous gland (mg)

1.3.3 Elemental composition analysis

The result of the elemental composition analysis gives insight into the relative amounts of various elements in the foot and thread. The elements acquired from ICP-MS and CHNS were divided into five categories: toxic, non-essential, trace, macro, and vital elements. In all test samples, vital elements concentration was exponentially high. Carbon (C), hydrogen (H), nitrogen (N) and sulphur (S) were included in the vital elements category (Table 1). Among these, carbon stands at a high concentration followed by nitrogen, hydrogen and sulphur. Macroelements were another category that included four elements, namely sodium (Na), potassium (K), magnesium (Mg), and calcium (Ca) (Table 2). Sodium was found in the highest concentration succeeded by potassium and magnesium. The foot and the thread contained two calcium isotopes such as Ca^{43} and Ca^{44}, although their concentration was extremely low. A total of eleven trace elements were recorded, including iron (Fe), copper (Cu), zinc (Zn), manganese (Mn), cobalt (Co), molybdenum (Mo), selenium (Se), vanadium (V), chromium (Cr), silver (Ag), and nickel (Ni) (Table 3). In the byssus thread, Cu>Fe>Cr were found in the highest concentration, whereas in the foot Ni>Mn>Fe>Cr>V> were dominated. Four different selenium isotopes, including Se^{76}, Se^{77}, Se^{78}, and Se^{82}, were discovered at low concentrations. Similarly, two isotopes of vanadium were also detected namely V^{51} and V^{53}. Silver and cobalt were other trace metals that had modest concentrations found in foot and thread. Non-essential elements are the fourth category of elements which include aluminium (Al), strontium (Sr), boron (B), lithium (Li) and rubidium (Rb) (Table

4). Aluminium comprised 99.5% of the byssus thread's concentration, whereas the percentage of other elements was very low. In foot tissue, aluminium stands at the highest concentration followed by boron. Toxic elements were another category including ten elements such as cadmium (Cd), lead (Pb), thallium (Tl), beryllium Be), bismuth (Bi), uranium (U), gallium (Ga), barium (Ba), arsenic (As), tellurium (Te) (Table 5). Among these, except lead and barium, all other element's concentrations were very negligible. The presence of three isotopes of lead were detected namely, Pb^{206}, Pb^{207}, and Pb^{208}.

Table 1: Vital elements composition in foot and thread

Sample	**Vital elements (ng/g dry weight)**			
	C	**H**	**N**	**S**
Foot tissue	4.438×10^8	7.119×10^7	1.212×10^8	1.244×10^7
Percentage	78%	8%	13%	1%
Thread	4.089×10^8	5.486×10^7	1.503×10^8	6.001×10^6
Percentage	65.95%	8.85%	24.24%	0.96%

Values are expressed in mean ± standard deviation.

Table 2: Macroelements composition in foot and thread

Sample	**Macro Elements (ng/g dry weight)**				
	Na	**K**	**Mg**	**Ca^{43}**	**Ca^{44}**
Foot tissue	2400.04± 422.7	544.24± 48.48	568.09± 51.75	17.35± 1.1	14.87± 4.41
Percentage	67.71%	15.35%	16.03%	0.49%	0.42%
Thread	1727.65± 77.54	458.08± 40.64	252.58± 29.03	14.58± 0.7	15.48± 1.47
Percentage	69.1%	19.45%	10.23%	0.59%	0.63%

Values are expressed in mean ± standard deviation.

Table 3: Trace elements composition in foot and thread

Sample	Trace Elements (ng/g dry weight)														
	Fe	**Cu**	**Zn**	**Mn**	**Co**	**Mo**	**Se^{76}**	**Se^{77}**	**Se^{78}**	**Se^{82}**	**V51**	**V53**	**Cr**	**Ag**	**Ni**
Foot tissue	46.15± 8.92	12.41± 1.86	4.23± 1.18	50.55± 8.51	1.59± 0.46	6.25± 1.54	3.98± 0.34	0.08± 0.05	0.33± 0.05	0.18± 0.024	0.61± 0.05	34.18± 3.77	34.77± 1.94	0.2± 0.06	56.16± 11.79
Percentage	18.34%	4.93%	1.68%	20.09%	0.63%	2.48%	1.58%	0.03%	0.13%	0.07%	0.24%	13.58%	13.81%	0.08%	22.31%
Thread	55.00± 3.1	56.98± 9.34	8.72± 0.93	21.17± 2.54	2.64± 0.62	23.54± 4.26	3.45± 0.17	0.05± 0.007	0.27± 0.03	0.14± 0.008	16.59± 1.52	25.19± 4.75	47.19± 11.67	0.29± 0.09	16.47± 4.04
Percentage	19.81%	20.52%	3.14%	7.62%	0.95%	8.46%	1.24%	0.02%	0.1%	0.05%	5.97%	9.07%	16.97%	0.10%	5.93%

Values are expressed in mean ± standard deviation.

Table 4: Non-essential elements composition in foot and thread

Sample	Non-Essential Elements (ng/g dry weight)				
	Al	**Sr**	**B**	**Li**	**Rb**
Foot tissue	470.29± 0.72	13.37± 1.67	131.03±15.23	1.82±0.51	2.04±0.66
Percentage	76.03%	2.162%	21.18%	0.29%	0.33%
Thread	23311.93± 1881.47	7.91± 1.16	106.81± 0.59	1.44± 0.17	1.08± 0.19
Percentage	99.5%	0.03%	0.23%	0.001%	0.0005%

Values are expressed in mean ± standard deviation.

Table 5: Toxic elements composition in foot and thread

Sample	**Toxic elements (ng/g dry weight)**											
	Cd	**Pb^{206}**	**Pb^{207}**	**Pb^{208}**	**Tl**	**Be**	**Bi**	**U**	**Ga**	**Ba**	**As**	**Te**
Foot tissue	1.25± 0.24	15.19± 4.66	14.24± 4.64	15.08± 5.19	0.002± 0	0.001±0	0.07± 0.03	0.02± 0.01	0.108± 0.03	19.910± 1.69	0.22± 0.19	0.006±0
Percentage	1.89%	22.99%	21.54%	22.82%	0.003%	0.002%	0.1%	0.03%	0.16%	30.12%	0.33%	0.01%
Thread	8.21± 0.66	147.99± 15.60	145.16± 15.32	146.43± 14.26	0.02± 0.004	0.001±0	0.07± 0.02	1.86± 0.07	3.531± 0.63	19.31± 2.05	0.051± 0.006	0.0003±0
Percentage	1.74%	31.31%	30.71%	30.98%	0.003%	0.0002%	0.01%	0.39%	0.75%	4.09%	0.01%	0.0006%

Values are expressed in mean ± standard deviation.

1.3.4 Fourier transform infrared spectroscopy (FTIR)

FTIR examination of the byssus thread revealed 10 absorption peaks (Figure 9 & Table 6). An amide I (1600-1800 cm^{-1}) band linked to C=O stretching vibration can be seen at a wavelength of 1652.19 cm^{-1}. Similarly, in association with N-H stretching, amide II (1470–1570 cm^{-1}) and amide III (1250–1350 cm^{-1}) bands were detected at peak locations of 1514.72 cm^{-1} and 1337.46 cm^{-1}, respectively. A broad band corresponding to N-H stretching at 3432.64 cm^{-1} was seen, yielding the amide A (3300 to 3500 cm^{-1}). C-O and CC stretching vibration of tyrosine, C-O stretching vibration of asparagine or glutamine, and also threonine were observed in IR spectrum. According to deconvoluted amide I band data from *P. perna* (Figure 10 & Table 7) byssus fibre comprises secondary structures in the proportions of 41.69% alpha helix, 35.93% beta sheet, and 20.44% beta turn.

Table 6: IR interpretation of byssus thread

Wavelength (cm^{-1})	**Group**	**Compound class**
3432.64	O-H stretching	Hydroxy group
2926.18	C-H stretching	Alkane
1652.19	C=O stretching	Amide I
1514.72	N-H stretching	Amide II
1337.46	N-H stretching	Amide III
1239.19	C-O stretching, CC stretching	Tyrosine
1160.80	C-O stretching	Asparagine or Glutamine
1077.00	C-O stretching	Threonine
855.72	C=C bending	Alkene
703.18	C-S streching	Thiol or thioether

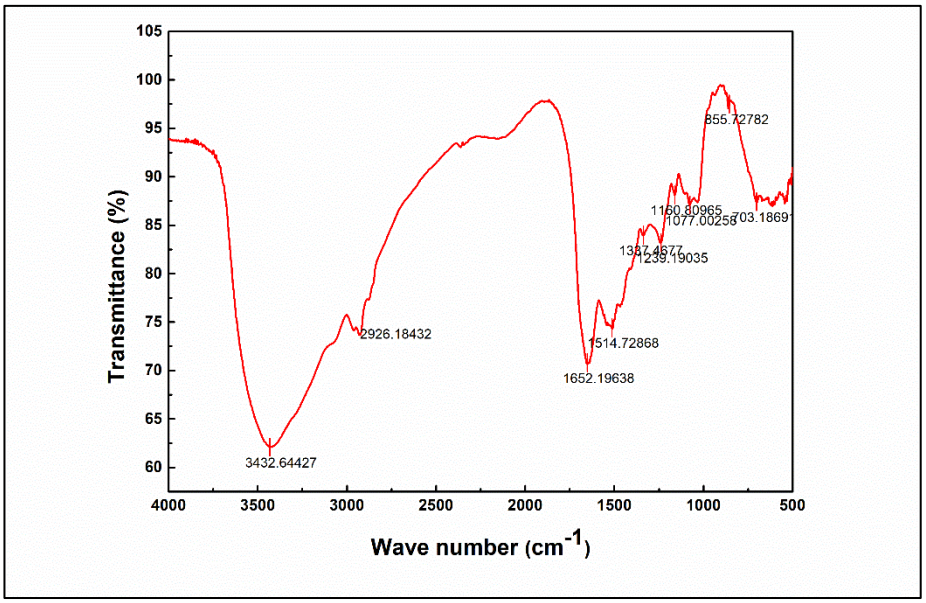

Figure 9: FTIR spectrum of *P. perna* byssus thread

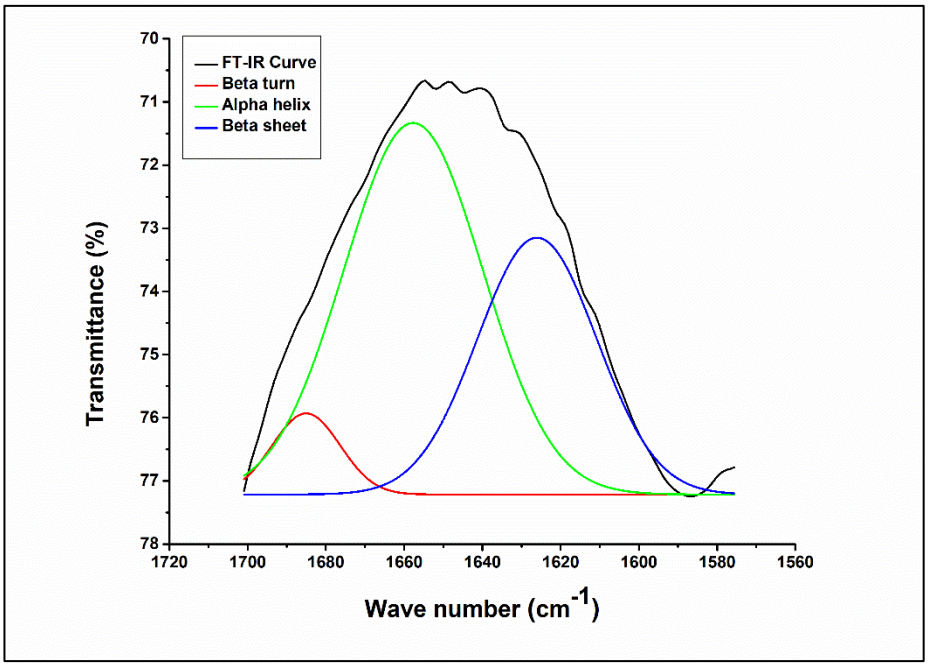

Figure 10: Amide I peak deconvolution graph

Table 7: Wavelength and percentage of secondary structures in byssus thread

Secondary structure	Wavelength (cm^{-1})	Percentage
α-Helix	1657.65127	41.69%
β-Sheet	1626.02248	35.93%
β-Turn	1685.01514	20.44%

1.3.5 Thermo gravimetric analysis (TGA)

Thermal stability of byssus threads was demonstrated in TGA curve (Figure 11). Initial weight loss of 8% in *P. perna* byssus thread indicates release of moisture content which start from 50°C, and thermal deterioration starts at 250° C.

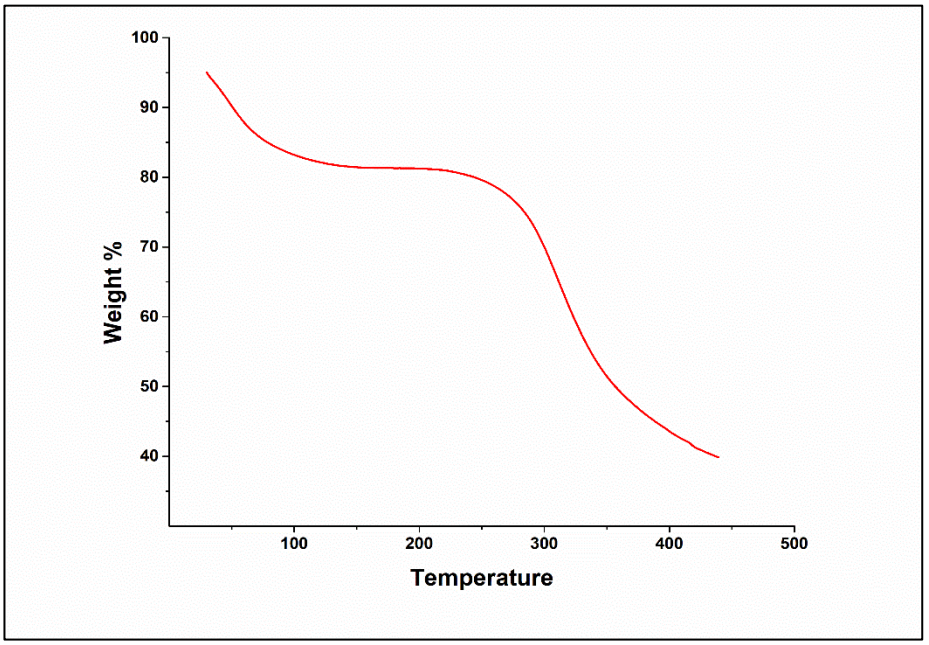

Figure 11: TGA graph of *P. perna* byssus thread

DISCUSSION

Bivalve byssus exhibit notably similar morphology, whereas byssus ultra-structural studies distinguish the differences across species. *P. perna* byssus thread had prominent proximal and distal thread regions which considered as characteristic feature of mussels belonging to the family Mytilidae. At the same time, Zebra mussel (*Dreissena polymorphano*) and *Aulacomya ater* had not noticed such ultra-structural regional differences in byssus thread (Farsad & Sone, 2012; Torres et al., 2012). In *Aulacomya ater* longitudinal and radial grooves were present throughout the byssus thread. In *P. perna,* numerous folding was found in proximal thread region whereas the distal thread region is smooth. In the proximal region, collagen containing fibrils scattered in a soft proteinaceous matrix, and folded surface provide more extensibility and flexibility, which can lengthen up to 200% from its original length. This stretchable characteristic of proximal thread gives tolerance against intertidal waves (Vaccaro and waite, 2001; Harrington and waite, 2007).

Proximal thread is followed by ten time's stiffer distal thread which contains densely packed fibrous bundles held together by intermolecular covalent and non-covalent crosslinks. The distal thread had unique stress healing and stress softening properties. Protein folding, disulphide bridges, metal ion complexes and non-covalent interactions maintain the strength of distal thread (Vaccaro and waite, 2001). Distal thread was ended with leaf like, flattened region called plaque which helps to adhere on to the substratum. In *P. perna* the

adhesive region of plaque was porous, which was an adaptation for surviving in the more turbulent intertidal environment because pores create vacuum filled conditions during adhesion leading to an increase in adhesive strength. Hence, increases the number of pores leading to increasing the adhesive strength of the plaque. Mussel species such as *Dreissena polymorpha*, *Limnoperna fortunei*, *Mytilus edulis* and *Mytilus californianus* had similar kind of porous plaques (Li, et al., 2018). In contrast, some of the mussel's species have non-porous plaques, and some others have both porous and non-porous plaques. *Geukensia demissa* is an excellent example of species that had both porous and non-porous plaques. In 2012, Farsad and Sone described that the appearance of different plaque morphology was depends on the species habitat.

NBT stained image of byssus thread revealed the presence of DOPA containing mussel foot proteins. *P. perna* plaque interface region was more DOPA rich, containing mainly mussel foot protein (mfp) 3, mfp-5 and mfp-6. Mfp-3 and mfp-5 contain high DOPA content approximately, 20-25 mol% and 27 mol% respectively, whereas mfp-6 is rich with tyrosine but contains only 4 mol% of DOPA. Mussel foot protein 2 and 4 were found in the middle region of the plaque which contains 3-5 mol% of DOPA and is located in the thread-plaque connection (Bandara et al., 2013). Crossed polarized microscopic image exhibited two anatomical regions of the *P. perna* byssus fibre namely, the outer cuticle and inner core. Many mussels including *P. perna* and *P. canaliculus* had smooth cuticular region whereas some others had biphasic granules, example *M. galloprovincialis* (Holten-

Andersen et al., 2007). The cuticle is made up of mfp-1 which has highly repetitive sequences that help to protect underlying core contents from abrasion and microbial attack. Cuticle strength varied according to the environment of mussel where they lived. The mussels in intertidal areas have more adaptive design of protective cuticle than they live in sub tidal regions (Rius & McQuaid, 2006; Holten-Andersen et al., 2007).

A well-structured byssus thread core contains three types of collagen include, proximal collagen (Col-P), distal collagen (Col-D) and pepsin-resistant non-gradient collagen (Col-NG). All collagens triple-helical domain contain $(Gly\text{-}X\text{-}Y)_n$ repetitive sequence, where Gly is glycine, X is proline and Y is hydroxylproline, which provide mechanical strength (Silverman & Roberto, 2007; Bandara et al., 2013). Proximal collagen is a unique natural copolymer located in the proximal thread region in a coiled manner, and has spectacular shock absorbing ability with 160% extensibility. Pre-collagen P has around 95 kDa molecular weight with seven domains including amino and carboxyl termini, a central large collagenous domain flanked by elastin like domain, and a small histidine-rich domain found at side of elastin like domains. At the carboxyl end of collagen, a small acidic patch is present between collagen and elastin like domains. The incredible extensibility and elastic recoil of proximal thread are provided by collagen domain and elastin like domains. Similarly, the metal binding property of collagen is carried out by histidine-rich domain which helps for crosslinking of pre-collagens (Coyne et al., 1997; Silverman & Roberto, 2007).

In the distal thread region, collagens are arranged as straight bundles and the major stiffer copolymer is distal collagen formed of seven domains. The Molecular mass of pre-collagen D is 97 kDa, and have silk fibroin domain located on either side of the central large collagen domain, which provide extraordinary stiffness and strength to the distal region. Like Col-P, distal collagen contains collagen domain, a small acidic patch, histidine-rich domain and amino and carboxyl termini (Waite et al., 1998; Silverman & Roberto, 2007). The Histidine domain is involved mainly in metal ion binding and is also which involved in self-healing (Torres et al., 2012). In addition, throughout the byssus thread contain around 76 kDa copolymer like protein called pepsin resistant non-gradient collagen, which acts as an adaptor between Col-P and Col-D. Like Col-P and Col-D, Col-NG contains a large collagen domain, acidic patch and histidine-rich termini. The collagen domain is flanked by $(X\text{-}Gly)_n$ repeats, which are found in plant cell wall proteins and histidine-rich domain contain large number of tyrosine residues compared to the other two collagens (Qin & Waite 1998; Bandara et al., 2013). Another kind of protein found in the entire byssus thread is thread matrix proteins (TMPs) which are water soluble and non-collageneous. They are involved in collagen binding, antigenicity and also in stiffening effect (Sun et al., 2002; Sagert and wait, 2009).

Rapid and robust production of the byssus apparatus was achieved by a muscular organ called the foot, which mainly participates in locomotion, temporary attachment and protein synthesis. In *P. perna,* foot was tongue-shaped organ enclosed with different types of endocrine glands involved in the production of byssus threads. The

foot contains numerous circular and longitudinal muscle bundles and also lateral surface of the foot contains numerous folding which helps to extend the foot to several lengths during the searching of suitable substratum for the attachment. The endocrine gland found in the foot secretes their protein products for the synthesis of byssus thread into the ventral groove which acts as a mould of byssus thread, producing one thread at a time (Waite, 2017). In juvenile mussels, the entire endocrine activity of the foot was done by a single bulbous stem gland. The stem gland's role is later replaced by other glands while they develop, and as a result, it becomes rudimentary (Lane, et al., 1982; Waite, 1992). The histological analysis of *P. perna* foot revealed that the foot was covered with ciliated epithelial layer underlying with mucous layer, muscular layer and hemolymph sinus. Both attaching (*Mytilus edulis*) and burrowing bivalves (*Solemya reidi*, *M. mercenaria* and *G. veneriformis*) have cilia on the foot surface. *P. perna* cilia were lengthier and wider than *Limnoperna fortunei* and *Haliotis rufescens*. In adhering mussels, the ciliated epithelial covering is involved in non-permanent adhesion through Van der Waals forces. Similarly, the ciliated epithelium helps to facilitate the movement of proteins to the ventral groove and also spread mucous secretion over the foot (Lee et al., 2012; Andrade et al., 2015).

Three major glands were found in *P. perna* foot include collagen gland or core gland, accessory gland or cuticle gland and phenol gland or plaque gland. Cuticle gland is a small gland found around the both lip of ventral groove which secrete mfp-1. The core gland is a large gland covering a major portion of the foot found just behind the cuticle gland

which secretes specialized collagens namely, Col-P, Col-D and Col-NG. Another gland called plaque gland is mainly found around distal depression and it extends some distance below the core gland. The major adhesive proteins were synthesised from the plaque gland include mfp-2, mfp-3, mfp-4, mfp-5, and mfp-6 (Priemel, et al., 2017; Silverman and Roberto, 2007). Through the injection molding process, new byssus threads are generated one by one and after all the thread-forming proteins have reached the ventral groove. Instead of these three glands, *P. perna* foot had a fourth gland called mucous secreting glands which secret sulphated mucopolysaccharides. According to the study of Hennebert et al., (2018) *M. edulis* mucous gland secrete sulphated carbohydrate containing molecules that mainly participate in locomotion and act as anti-adhesive agents for avoiding self-adhesion.

Elements play critical role in byssus threads formation and maintaining its stability. Mainly, elements reach into the byssus thread through two mechanisms including passive absorption from surrounding water and filtration by gills. In passive absorption byssus thread adsorb elements from surrounding water and in the second mechanism, metallothionines found in the gill bind with metals and which absorbed by amoebocytes, circulate in the body, and reached to foot tissue. The foot incorporates unwanted elements into newly formed thread as a part of detoxification (Swann et al., 1998; Szefer, et al., 2002; Schmitt, et al., 2015). The foot and thread were rich with vital elements including carbon, hydrogen, nitrogen and sulphur because biochemical molecules basic structure was made up of these elements. Four

macroelements, eleven trace elements and five non-essential elements were detected in both byssus thread and foot.

By binding with byssus proteins, metal ions create metal complexes that increase the protein's adhesive strength, aberration resistance, and ability to cross-link. Zhang et al. (2017) studied cadmium induced transcriptomic analysis of foot from *P. viridis*, revealed that cadmium stimulation increases transcription of foot proteins (pvfp-1 to pvfp-6) and also mussel protein tyrosinase (TYR1 to TYR5). TYR is a copper-containing enzyme with two copper binding sites (Cu (A) and Cu (B)) that functioned in conversion of tyrosine to DOPA. DOPA is considered as a key factor of mussel adhesion, hence copper plays a critical role in DOPA synthesis. Same time, metal ions can induce adhesive properties to non-adhering mussel foot proteins. For example mfp-2 is the most abundant foot protein found in the plaque but it could not involve in adhesion. However, according to the study of Hwang et al. (2010) ca^{2+} and Fe^{3+} induces adhesive property in mfp-2. Mfp-1 is also not involved in the adhesion process, whereas the byssus cuticle is referred to as ironclad. Because a single mfp-1 molecule may bind 50–75 molecules of Fe^{3+}, mfp-1 transforms into an incredibly complex macromolecular complex (Taylor et al., 1996). Byssus thread resistance and attachment strength are directly connected with metal ion concentration. The results of Holten-Anderson et al. (2009) and Seguin-Heine et al. (2014) revealed that byssus thread's mechanical properties have been significantly impacted by the decreased concentration of protein cross-linkers like Zn, Cu, Ca, and Fe, which has led to a decrease in cuticle hardness. Similarly, Al and V also act

as protein cross-linkers which complexes with DOPA residue form ionic-crosslinking lead to increase in strength and toughness of the cuticle and are also involved in self-healing (Holten-Andersen et al., 2004; Schmitt, et al., 2015)

Mussels have been used as highly efficient bio-indicators for monitoring aquatic environmental pollution (Atasaral et al., 2020). Mussel soft tissue is considered as an excellent sample for analysing short-term anthropogenic contamination processes. The elemental composition results showed that foot tissue and byssus threads contain heavy metals, lead isotopes and rare earth elements. Similarly, Benaltabet et al. (2021) reported that heavy metal, rare earth elements and lead isotope accumulation in mussel *Brachidontes pharaonis* collected from contaminated lagoon in the Gulf of Aqaba, northern Red Sea. Previous studies such as Yap et al. (2003), Szefer et al. (2002), Zhang et al. (2017), and Li et al. (2018) also revealed the accumulation of heavy metals in mussel soft tissues and byssus thread. Byssus proteins are rich with tyrosine, cysteine and histidine residues which considered as major metal binding sites. These sites can bind metal ions even after the separation from the organism. Byssus thread's ability to remove metal contaminants from water was exploited to create novel, inexpensive adsorbents that may be used in aquatic streams (Motroni et al., 2020; Anand and Vardhanan, 2021).

FTIR spectroscopy is the most powerful analytical technique for the identification of chemical composition. The first broad band found in the FT-IR spectrum of byssus thread represents the hydroxyl group.

Mainly, the byssus thread made up of protein and water. Byssus thread proteins contain tyrosine, threonine and serine residues which possess hydroxyl group. Post translational modifications were occurs in these hydroxyl groups and also it increases reactivity and solubility of amino acids. Through the formation of a hydrogen bond with water, hydroxyl groups in molecules enhance their hydrophilicity and solubility (Gargaud et al., 2015). Another important functional group found in the *P. perna* byssus thread was the thiol group which is mainly seen in cysteine residues of mfp-6, which create a redox environment and actively participate in preventing DOPA oxidation into DOPA quinone (Li et al., 2021). Amide I, Amide II and Amide III are three polypeptide backbone vibrations and three amino acids (Tyrosine, Asparagine or glutamine, and threonine) side chain vibrations were found in *P. perna* byssus thread. The amide bond is important for maintaining protein structural properties. Similar studies were conducted in *Aulacomya ater* and *M. galloprovincialis*, obtained amide bands with slight variation in peak position because backbone conformation and hydrogen-bonding pattern are varied with species (Hagenau, et al., 2009; Torres, et al., 2012).

Secondary structure analysis helps to study proteins folding and unfolding, and aggregation. Deconvolution results of *P. perna* byssus thread indicated that alpha helix is the dominating secondary structure followed by beta-helix and beta-turn. A similar study conducted by Torres et al. (2012) in *A. ater* indicated that amount of secondary structure varied with species. In *A. ater* beta sheet was predominated (~37%) followed by α-helix (~23%) and α-turn (18%). The study

conducted by Hagenau et al. (2009) revealed exciting results that the proximal and distal portions of *M. galloprovincialis* byssus thread contain different secondary structure composition. In the proximal region, the major share comprises α-helical structures (47%), subsequently by beta confirmations (15%) and triple helical structures (13%). At the same time, distal region was governed by beta structural content (70%) and collagen typical triple helices (22%).

The thermal stability of byssus threads also indicates the temperature tolerance of byssus proteins. In *P. perna*, thermal decomposition of byssus threads started at 250°C whereas in *Mytilus edulis* decomposition was occur from 217°C and in *A. ater* at 280°C (Aldred et al., 2007; Torres et al., 2013). According to these findings, the thermal stability of the byssus thread is varied by species. A major part of the byssus thread is made of three kinds of collagens. The study of Bozec & Odlyha (2011) showed that, collagens initial thermal degradation starts at 300°C and secondary degradation from 340°C. In a conclusion, this collagen characteristic demonstrated the temperature resilience of the mussel byssus thread.

CONCLUSION

The present study focused on structural elucidation and chemical formulation of foot and byssus thread from brown mussel *P. perna* using multiple approaches. The architecture of the foot provides insight into glandular organisation and ideas about the development of the byssus thread. Similarly, the byssus thread structure study opens up the area of bioadhesion mechanism. Metal ions are critical for maintaining byssus structural stability. In light of this, elemental composition analysis reveals the appropriate concentration of each metal ion, and the results also highlight the accumulation of toxic elements, which point to aquatic pollution. The detection of toxic elements in soft tissue suggests that *P. perna* can be used to analyse short-term pollution effects from a biomonitering perspective. Functional group analysis and thermal stability analysis project the strength and steadiness of the byssus thread. Biofouling is a serious threat to aquatic systems which make serious losses to maritime industries and aquaculture facilities. Structural studies provide an understanding of the mussel's adhesive mechanism, which is very crucial for developing new strategies against biofouling. Same time, biomaterials are considered as excellent models for the development of synthetic materials. Byssus thread strength is always attractive to many researchers; hence structural elucidation of byssus thread provides intuition for developing new bio-inspired materials.

INTRODUCTION

Mussels are semi-sessile organisms; they can adhere to a variety of substrates including glass, plastics, and metal oxides through a bundle of threads called byssus. The attachment of mussels in rocky, wind-swept and wave-swept seacoasts enables by glue-like proteins called mussels adhesive proteins (MAPs) or mussels foot proteins (MFPs). An unusual catabolic amino acid called 3,4-dihydroxyphenyalanine (DOPA) provides adhesive properties to mussel foot proteins (Yuvaraj et al., 2021). The oxidation of tyrosine by catechol oxidase, tyrosinase, or sodium periodate leads to the formation of DOPA residues (Bandara et al., 2013), which facilitate adhesion on both organic and inorganic substrates. DOPA oxidation forms DOPA-quinone or DOPA-semiquinone which facilitates adhesion on organic substrates through covalent bonds. Similarly, unoxidized DOPA molecules make strong adhesion with inorganic substrates (Lee et al., 2006; Guvendiren et al., 2009). Maintaining a low pH (less than 3), together with thiol chemistry, helps to address the DOPA molecule's high susceptibility to oxidation (Yuvaraj et al., 2021). Mainly six different DOPA containing proteins are present in mussels namely mussel foot protein (mfp) 1, mfp-2, mfp-3, mfp-4, mfp-5, and mfp-6. Mfp-1 is the first identified and most studied foot protein forming the byssus thread cuticle. Hydroxylation of DOPA residues by tyrosinase causes the synthesis of 3,4,5- trihydroxyphenylalanine (TOPA) in mfp-1, which has stronger adhesive properties than DOPA (Burzio & Waite, 2002).

The second abundant (25-40%) phenolic protein in the byssus thread plaque is mfp-2, acts as a major structural component. While Mfp-2 contains large amount of cysteine cross-links created by covalent disulfide bonds and it maintain the adhesive plaque matrix. (Rzepecki et al., 1992; Bandara et al., 2013). The smallest adhesive protein found in byssus thread plaque is mfp-3, which is critically involved in adhesion. The high arginine content is found in mfp-3 which undergoes post-translational modification to form 4-hydroxy-L-arginine; it can make strong hydrogen bonds. DOPA cross-links and 4-hydroxy-L-arginine hydrogen bonds are mainly involved in adhesion to the substrate surface (Even et al., 2008). Mfp-4 is a comparatively large protein found at the junction between plaque and byssus thread and is rich in glycine, arginine and histidine. Mfp-4 act as a coupling agent located between PreCOl-D and mfp-2 (Bandara et al., 2013). Mfp-5 is also a small protein actively involved in substrate adhesion. It contains seven phosphorylated serine residues and the actual function of phosphoserine is not understood. A theory suggested that phosphoserine can make calcareous bonds that help mussel adhere to another mussel shell (Waite & Qin, 2001). Mfp-6 is another small protein with low DOPA content, high tyrosine (20 mol%) and high cysteine content (11 mol%) which is mainly involved in preventing DOPA oxidation in mfp-3 and mfp-5 by thiol-mediated dopaquinone scavenging (Zhao & Waite, 2006b).

The active foot proteins involved in surface adhesion are mfp-3 and mfp-5, which are low molecular weight proteins; hence they can easily make conformational changes leading to improved adhesion (Cha et

al., 2008). Similarly, chemical bonds play a critical role in substrate adhesion. Mussel adhesive proteins contain many post-translationally modified amino acids such as DOPA, 4-Hydroxyproline, 3,4-dihydroxyproline, 4-hydroxy arginine and o-phosphoserine which can make hydrogen bonds with many surfaces. Likewise, strong non-covalent bonds can make by DOPA with mineral surfaces containing metal ions, metal oxides and silicon dioxides. The other interactions involved in the surface adhesion are (1) π-π interactions between DOPA and aromatic groups (Papov et al., 1995), (2) strong electrostatic interaction between positively charged adhesive proteins and negatively charged marine mineral surfaces (Wiegemann, 2005), (3) positively charged lysine in MAPs creates an ionic bond with negatively charged surfaces like collagen and acidic polysaccharides (Suci et al., 2000), (4) glycine open confirmation in proteins and DOPA metal ion interactions also facilitate surface adhesion (Silverman & Roberto, 2007; Wilker, 2010).

Mussel foot proteins have superior adhesive performance than man-made polymers because of their high strength and durability in a wet environment. MAP's water resistance property attracts researchers in the biomedical field and its nontoxicity, biodegradability and biocompatibility features inspire the synthesis of environment friendly adhesives. The Cell-Tak™, MAP cell and MEFP-1, MAP comp, and MAPTM are the four naturally extracted, commercially available mussel adhesive protein-based products. Cell-Tak™ is a widely used adhesive extracted from the marine mussel, *Mytilus edulis*, composed of foot protein 1 and 2 in 5% acetic acid and MAPTM is made up of

mussel foot protein 1 from *M. edulis* (Cha et al., 2008). The cost of 1 mg of Cell-Tak™ is 337 US dollars. The nature-inspired, non-toxic bioadhesives replaces synthetic adhesives because it undergoes detachment and deterioration while exposed to moisture. Marine mussel's foot proteins are considered an excellent raw material for the synthesizing new biodegradable, biocompatible, and small or non-antigenic, water-resistant bioadhesives (Castillo et al., 2017; Qvist, 2002). However, understanding of chemical, physical and functional aspects of mussel adhesive proteins is necessary for their potential. To date, mussel species *P. perna* couldn't be utilized for adhesive protein study. Therefore, the present chapter aims to develop an excellent protocol for the natural extraction of mussel foot protein from *P. perna* and also it focused on analysing characteristics of extracted protein products by using UV-Visible spectroscopy, acid-urea gel electrophoresis, atomic force microscopy and contact angle measurements.

MATERIALS AND METHODS

2.2.1 Tissue preparation for adhesive protein extraction

Foot tissue was dissected from live *P. perna* by using a disinfected surgical blade. Brown coloured mucous containing integument was scraped; tissues were thoroughly washed in deionized water and then chopped into small pieces.

2.2.2 Extraction of adhesive proteins from foot

Various protein extraction techniques from different species of mussels have been already published in many scientific articles. However, adhesive protein extraction from *P. perna* is an untouched area of research. For developing the best protein extraction method from *P. perna*, four extraction protocols were selected from previously published articles on the basis of avoiding auxiliary chemicals. Salt precipitation is one of the major steps in protein extraction. Therefore, sodium chloride (NaCl) was the salt used in all four methods taken from previous articles. Here, we used salts such as sodium sulphate (Na_2SO_4) and potassium chloride (KCl) as alternatives to NaCl. In addition, we made some modifications to previously published methods for developing a new efficient protein extraction technique from *P. perna*. Hence, a total of ten extraction methods were analysed in this chapter.

Method 1

Method 1 was taken from Xu et al. (2014). In this method, 0.5g of mussel foot was homogenized well in 1.5 ml of 5% acetic acid and continuously stirred for 30 minutes. After stirring, the samples were centrifuged in a cold centrifuge (at 4°C) at 10,000 g for 30 minutes. To the collected supernatant add 6M NaCl to salt out the proteins and kept them at room temperature for 5 hours. Again centrifuged (10,000 g, 4°C, 30 min.) sample and decanted the supernatant. Dissolve the sediment in 2% acetic acid and centrifuge (10,000 g, 4°C, 15 min.) the sample. After centrifugation, the supernatant containing adhesive proteins was stored at -20°C.

Method 1a

This was the first modified protocol of Method 1 collected from Xu et al. (2014). This method used 6M Na_2SO_4 instead of NaCl in the Salt precipitation. Similarly, the centrifugation force hiked to 12000 g from 10000g because of improper sedimentation in 10000 g and the final product is stored in 5% acetic acid.

Method 1b

Method 1b was the second modified protocol of method 1, in which KCl was used for salt precipitation instead of NaCl. In the first centrifugation step, the force was increased up to 12000 g because tissue sedimentation was not properly occurred at 10000 g and the final product is stored in 5% acetic acid.

Method 2

Method 2 also was obtained from Xu et al. (2014), in which 0.5 M NaCl solution was added to 0.5 g *P. perna* foot, homogenized well and continuously stirred for 40 minutes. The samples were centrifuged (10,000 g, 4°C, 30 min.) for collecting supernatant and fractionated by using 20% ammonium sulphate. Through centrifugation (10,000 g, 4°C, 15 min.) the precipitate formed was removed and ammonium sulphate was added to the supernatant up to a final concentration of 55%. Again centrifuged (10,000 g, 4°C, 15 min.) the sample to obtain sediments, and they dissolved in 2% acetic acid. Then, centrifuged (10,000 g, 4°C, 15 min.) the sample to acquire supernatant containing adhesive proteins and kept in -20°C for further analysis.

Method 2a

Method 2a was the modified method of method 2. In the first step of method 2, NaCl was used for protein precipitation, but in method 2a NaCl is replaced with Na_2SO_4. In the first step, proper tissue sedimentation was not found in 10000 g centrifugation; hence 10000 g was hiked to 12000 g. The final product of extraction was stored in 5% acetic acid rather than 2%.

Method 2b

In method 2b, the modification was done in the first step; KCl replaced the NaCl for salt precipitation. Similarly, centrifugal force increase from 10000 g to 12000 g was done to obtain clear supernatant and the final product was stored in 5% acetic acid.

Method 3

Method 3 was adopted from Li et al., (2011). Briefly, 0.5 g of mussel foot was mixed with 5% acetic acid and 8 M urea, then homogenized on ice, stirred for 10 minutes and centrifuged at 12000 g for 40 minutes. The supernatant was collected and added 6 M NaCl for 5 hours which precipitated proteins. The sediment was collected by centrifugation (10,000 g, 4°C, 30 min.) and dissolved in 2% acetic acid. The samples were again centrifuged (10,000 g, 4°C, 15 min.) to obtain supernatant containing adhesive proteins, which were stored at -20°C for further analysis.

Method 3a

The first modified protocol of method 3 was method 3a in which salting out of proteins was carried out with Na_2SO_4 instead of NaCl and the final product of protein was dissolved in 5% acetic acid.

Method 3b

This was the second modified method of method 3 and it was carried out with KCl for salt precipitation and the final product of protein dissolved in 5% acetic acid.

Method 4

This method was acquired from Rzepecki et al. (1992) with slight modifications. Briefly, 0.5 g of mussel feet was homogenized in 1.5 ml of 0.7% PCA, stirred for 10 minutes and the homogenate was centrifuged at 14,000 g for 30 minutes. By using acetone the

supernatant containing proteins was precipitated and centrifuged (10,000 g, 4°C, 30 min.). The sediments were dissolved in 5% acetic acid and kept at -20°C for further analysis.

2.2.3 Extraction of adhesive proteins from thread

The *P. perna* byssus threads were removed from the stem region and scraped off debris adhering to the threads and thoroughly washed in deionized water. Each thread was cut into small pieces by using a disinfected surgical blade and followed two different extraction methods for determining which method is more efficient in *P. perna*.

Method 1

In this method, the protein extraction was done based on the protocol explained by Waite et al. (1989) with slight modifications. Briefly, 15-20 threads were homogenized in 0.8 M acetic acid and 8 M urea on ice and continuously stirred for 30 minutes. Protein containing supernatant was separated by centrifugation at 12,000 g for 30 minutes. Finally, the samples were stored at -20°C for further analysis.

Modified 1a

Another extraction procedure was done with a slight modification made to method 1. In this protocol, 5% acetic acid and 6 M NaCl were used for the separation of proteins instead of urea.

Method 2

This method was taken from Gantayet et al. (2013), in which 15-20 byssus threads were homogenized in an extraction buffer containing 0.2 M sodium borate, 4 M urea, 1 mM EDTA and 10 mM ascorbic acid. After 30 minutes of continuous stirring, samples were centrifuged at 17,000 g for 8 minutes. The supernatant containing extracted proteins was stored at 20°C for further analysis.

2.2.4 Estimation of protein

Protein concentration was done by the Bradford method (1976). Measurements were taken at 595nm with a 96-well microplate spectrophotometer (BioTeK, SYNERGY HT Microplate Reader). Bovine serum albumin (BSA) was used as the standard, and the quantification of the unknown samples was determined by plotting the standard curve.

2.2.5 Acid-urea polyacrylamide gel electrophoresis

This is an analytical technique used to separate proteins on the basis of mass and charges. Acid-Urea PAGE was performed according to the method of Smith, (1984) with 15% acrylamide.

Reagents

1. Acrylamide solution (30%)

Dissolve 30 g of acrylamide and 0.8 g of bis acrylamide in distilled water and make the final volume 100 ml. This stock solution was stored in an amber bottle at 4°C.

2. Ammonium persulfate (APS)

   Dissolve 0.1 g ammonium persulfate in 1 ml distilled water

3. Reservoir buffer (0.9M acetic acid, pH 3)

   15.5 ml glacial acetic acid made up to 1000 ml with distilled water.

4. Sample buffer

   Add 1 ml HCl (1 M), 0.5 ml β-mercaptoethanol, 5.4 g urea, and 0.25 mg methyl green to 5 ml distilled water. After dissolving each component, makes up the volume into 10 ml.

5. Fixative

   Mix 45% of Methanol, 45% of distilled water and 10% glacial acetic acid.

6. Staining solutions

   i) Coomassie Brilliant Blue R-250 stain (CBBR)

      Dissolve 0.25 g Coomassie Brilliant Blue R-250 dye in 125 ml methanol. To this, add 25 ml glacial acetic acid and 100 ml distilled water.

ii) NBT stain

Dissolve 8 mg of NBT in 10 ml potassium glycinate buffer and make up to 15 ml (Paz et al., 2009).

7. Destain solution

Mix 100 ml methanol, 100 ml glacial acetic acid and 800 ml distilled water.

Gel preparation

A mini gel with 15% acrylamide was conducted and procedure described below (Table 1),

Table 1: Gel composition

Solutions	**Stacking gel**	**Separating gel**
Urea	1.2 g	3.2 g
Acrylamide	1 ml	5.33 ml
Glacial acetic acid	0.5 ml	1.33 ml
Distilled water	1.5 ml	1.33 ml
TEMED (Tetramethylethylenediamine)	30 µl	30 µl
APS (Ammonium persulfate)	150 µl	200 µl

At first, separating gels were prepared by mixing all solutions in the above table, ensuring minimum oxygen contact, pouring them into a gel cassette assembly, and allowing them to polymerase. After polymerisation of separating gel, the mixed stacking gel compositions

were poured over the separating gel and placed comb for making sample loading wells. Sample buffer mixed protein samples were placed in boiling water for 5 minutes to denature the proteins by breaking the peptide bond. These denatured samples were loaded into the wells and chambers were filled with reservoir buffer. After this, electrodes were connected and applied 15 mA electric fields to stacking gel and 25 mA to separating gel. When methyl green dye reached the bottom of the gel, disconnected the power supply and the gel was transferred to a fixative for 1 hour. After protein fixing, the gel was stained with CBBR for 45 minutes and destained with the destaining solution. In NBT staining, the gel was incubated with NBT solution at room temperature in dark for 45 minutes. Destained gels were photographed using Canon EOS 5D Mark IV.

2.2.6 UV-visible spectroscopic analysis

The detection of quinone proteins in the protein extract was also detected spectrophotometrically. The protein sample and BSA control were mixed with NBT-glycinate solution (2:1 ratio) and the reaction mixture was incubated for 30 minutes. Changes in the samples were measured through the UV-Visible spectrum at the wavelength from 300 to 800 nm.

The pH stability of adhesive protein was analysed spectrophotometrically (Priemel et al., 2020). For this study, extracted foot proteins were dissolved in NaOH (pH 8) and acetic acid (pH 3) and then kept at room temperature for 2 hours. After the incubation, the absorption spectra of samples were measured at the wavelength

from 200 to 800nm by using Cary 5000 UV-Visible spectrophotometer.

2.2.7 Atomic force microscopy

Atomic force microscopy (Park Systems, Series Xe 100) was used to analyse the surface roughness and surface topology of adhesive proteins extracted from *P. perna* (Lin et al., 2019). To perform this, foot protein extract along with BSA (2 µg/ml) as control protein were subjected to iron (10 µM) induced polymerisation of peptides on a clean dry glass coverslip and dried in a vacuum oven at 40°C for 10 minutes. The properly dried glass coverslips were loaded into the AFM device and images were taken in tapping mode.

2.2.8 Contact angle measurement

The angle formed by the intersection of the liquid-solid interface and liquid-vapor interface is termed the contact angle (Gupta & Denis, 2016). The contact angle measurements were done by the sessile drop method to understand the water affinity of adhesive protein. The protein extract, iron-treated protein sample and BSA control were individually coated on a glass coverslip and 1 µl of deionized water droplet was dropped on the protein surface. A video contact angle meter (Holmarc's Contact angle meter, O-IAD-CAM-01A) was used to capture the video of droplet spreading (Figure 1). From this video, the static image of the water droplet was cropped and the contact angle was measured using Image J software. The surface energy was calculated by using Young - Dupré equation,

$W_{SL} = Y_L (\cos\theta + 1)$

Here, W_{SL} is the interfacial tension between the liquid and solid, Y_L is the surface tension of water and θ is the contact angle.

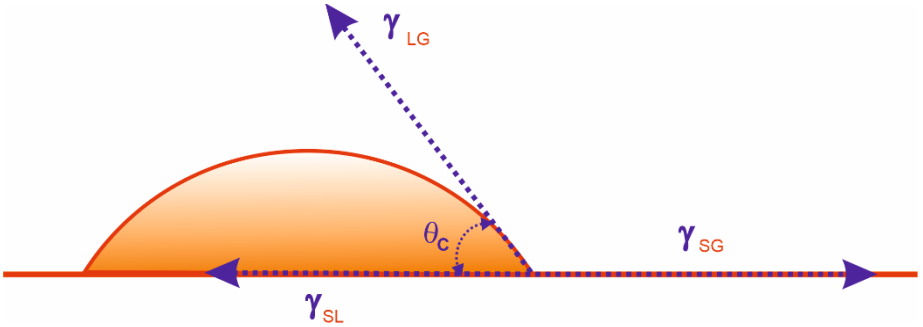

Figure 1: Contact angle and interface energies

2.2.9 Statistical analysis

The results obtained from the experiments were statistically analysed by using the programme IBM SPSS version 20.0. All data represented as mean ± standard deviation acquired by descriptive statistics and statistical significance was determined by Kruskal–Wallis one-way analysis. The results were considered statistically significant when $P<0.05$.

RESULTS

2.3.1 Protein extraction efficacy from foot

2.3.1a Estimation of protein

Table 2: Protein yield from foot tissue

Method	Total Protein yield (µg/ml)
Method 1	217.67 ± 1.99*
Method 1a	233.44 ± 5.53*
Method 1b	196 ± 3.32*
Method 2	63.1 ± 1.22
Method 2a	67.11 ± 1.03
Method 2b	61.03 ± 2.33
Method 3	131.41 ± 0.54*
Method 3a	133.395 ± 1.41*
Method 3b	122.79 ± 1.86*
Method 4	76.49 ± 1.71

Values are expressed in mean ± standard deviation. Statistical significance ($P<0.05$) represent in *

The *Perna perna* protein yield from ten protein extraction methods was represented in Table 2. The result indicated that method such as method 1, 1a, 1b, 3, 3a and 3b shows significant difference in extraction yield than others. The lowest extraction efficacy was found in method 2b (61.03 ± 2.33), followed by 2 (63.1 ± 1.22), 2a (67.11 ± 1.03), and 4 (76.49 ± 1.71). Among all extraction methods highest extraction yield was obtained in method 1a (233.44 ± 5.53) and method 1(217.67 ± 1.99). Statistically significant difference was not found between method 1 and 1b. Hence the results concluded that method 1 and 1b are the best protein yield method from *P. perna*.

2.3.1b Acid-Urea polyacrylamide gel electrophoresis

NBT staining

Out of ten extraction methods, six methods including 1, 1a, 1b, 3, 3a and 3b shows significant difference in the yield of proteins; hence they are subjected to acid urea gel electrophoresis. NBT staining was used to identifying different quinone proteins in the protein extract. The Figure 2A showing NBT stained acid urea gel of protein extracts, here single band was observed in all six samples. In contrast, the intensity of protein band (Figure 3 & 4, Table 3) was varied in different samples. The high band intensity was observed in method 1a and lowest band intensity was found in modified 3b. Method 1 also has more intensity when compared with method 3, 3b and 1b. The NBT stained gel exhibited that method 1b is more concentrated with adhesive proteins than other five protocols; hence this extract was used for all other experiments.

Table 3**:** Protein band intensity

Method	**Raw Volume**
Method 1	20806
Method 1a	21929
Method 1b	11203
Method 3	17642
Method 3a	18346
Method 3b	11034

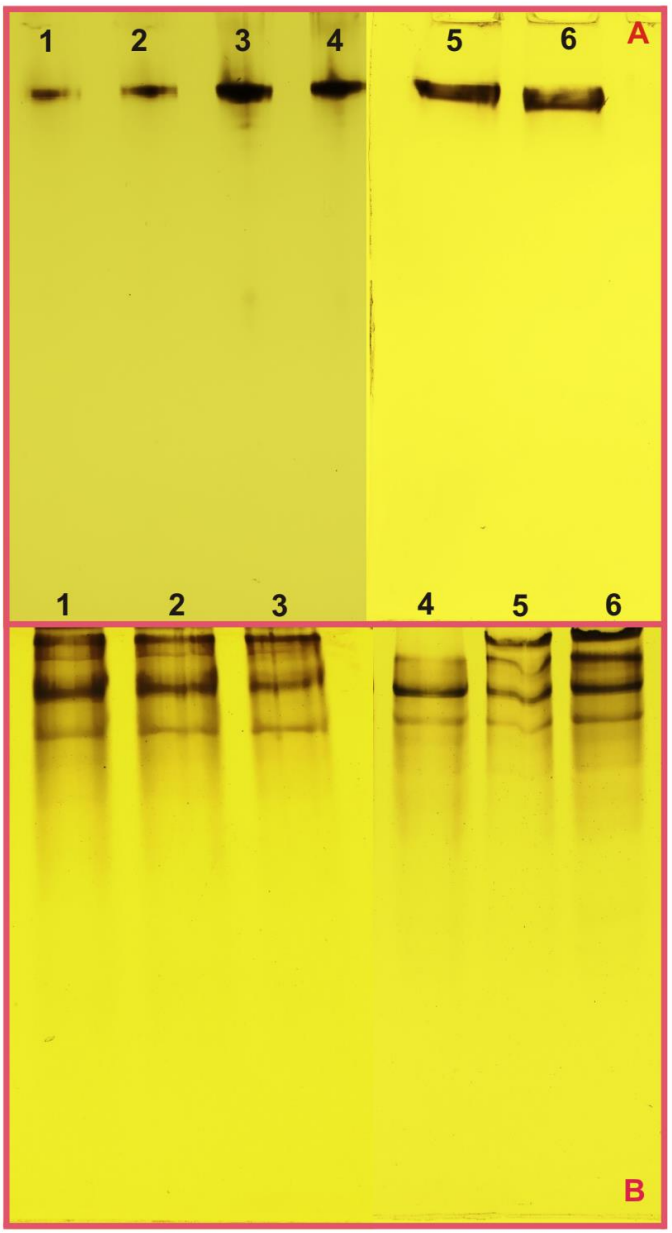

Figure 2: Acid-Urea gel electrophoresis; (**A**) NBT stained gel: Lane 1- 3b, Lane 2- 1b, Lane 3- 1a, Lane 4- 1, Lane 5- 3, Lane 6-3a (**B**) CBBR stained gel: Lane 1- 3b, Lane 2- 3a, Lane 3- 3, Lane 4- 1b, Lane 5- 1a, Lane 6- 1

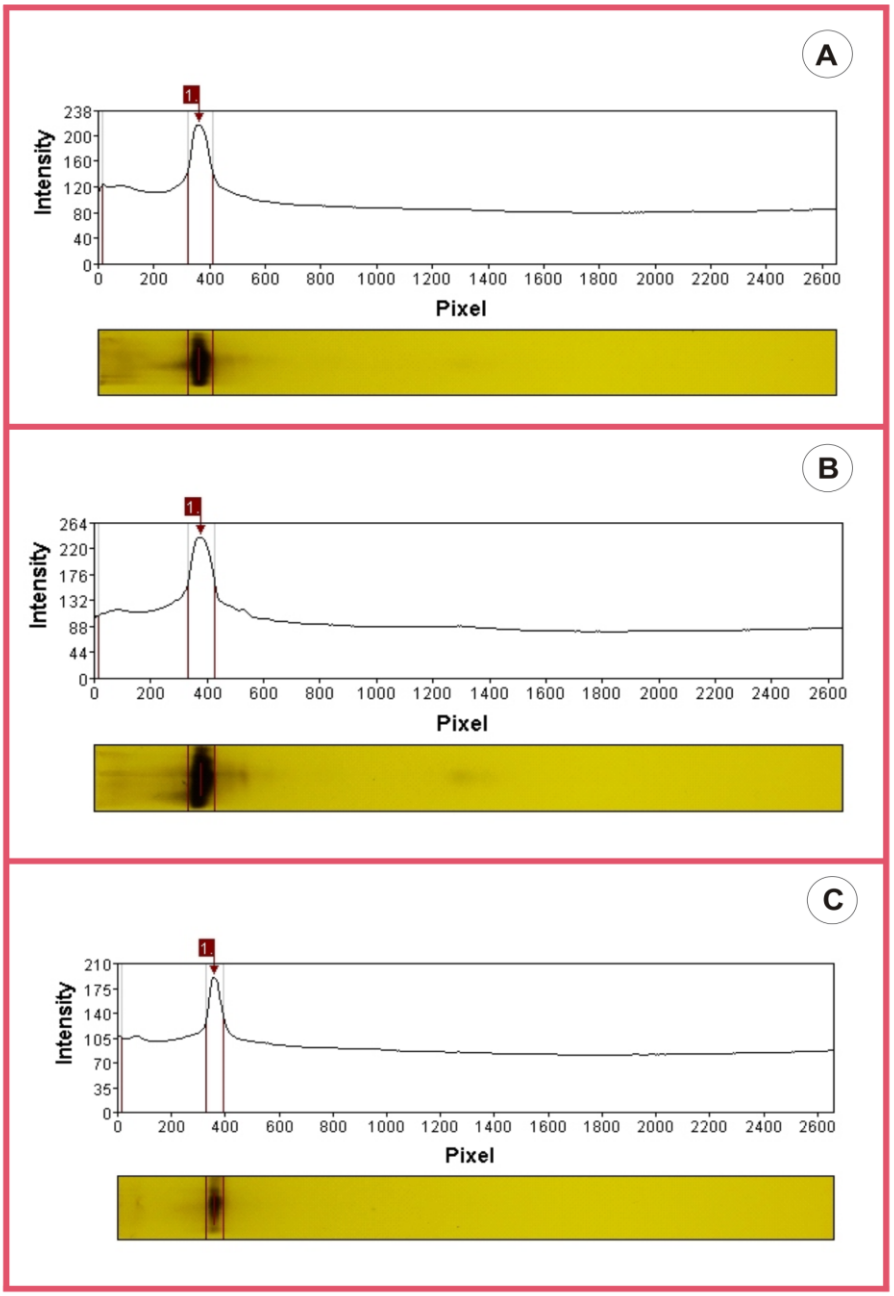

Figure 3: Band intensities of NBT stained method 1, 1a and 1b; (**A**) method 1, (**B**) method 1a, (**C**) method 1b

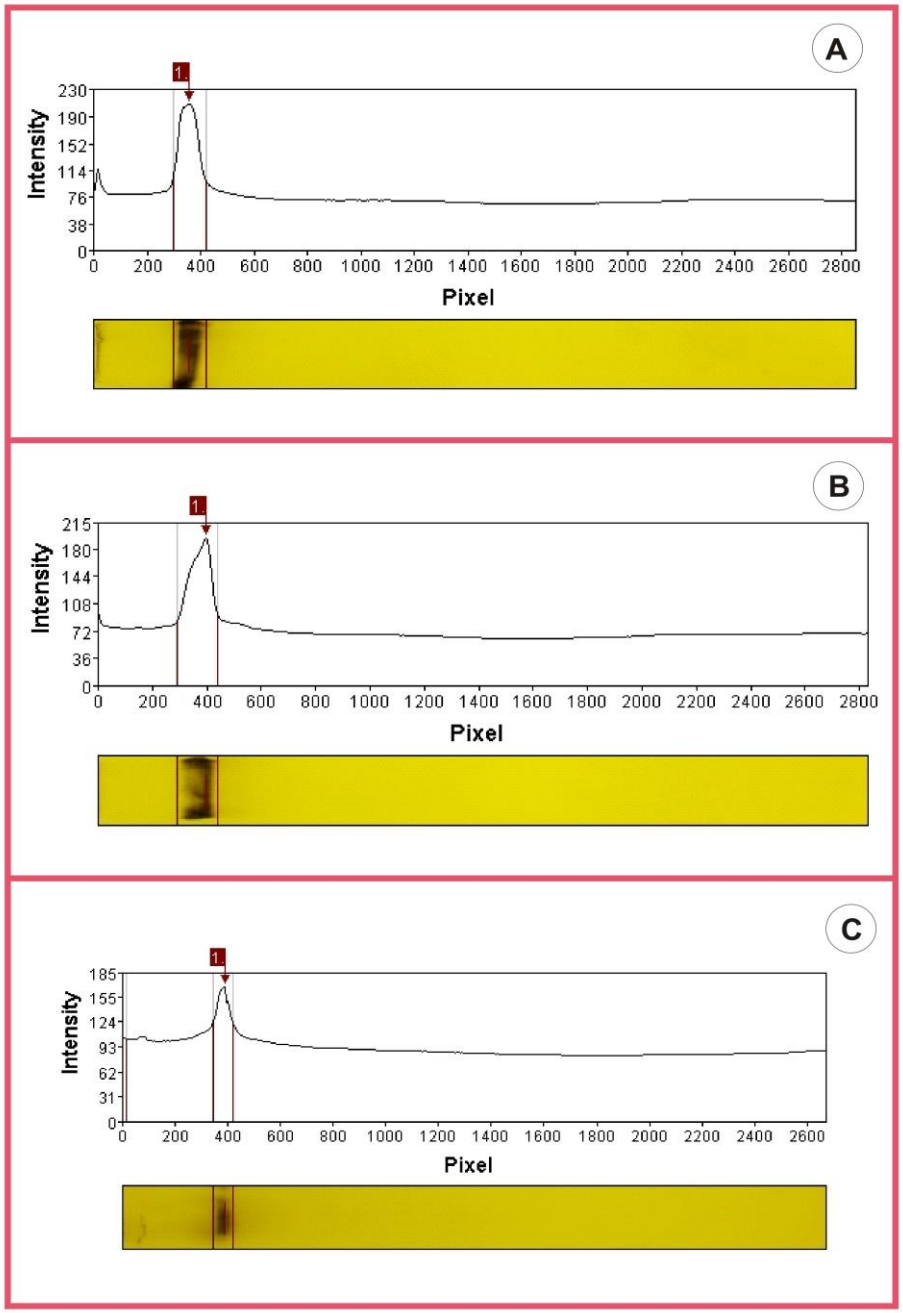

Figure 4: Band intensities of NBT stained method 3, 3a and 3b; (**A**) method 3, (**B**) method 3a, (**C**) method 3b

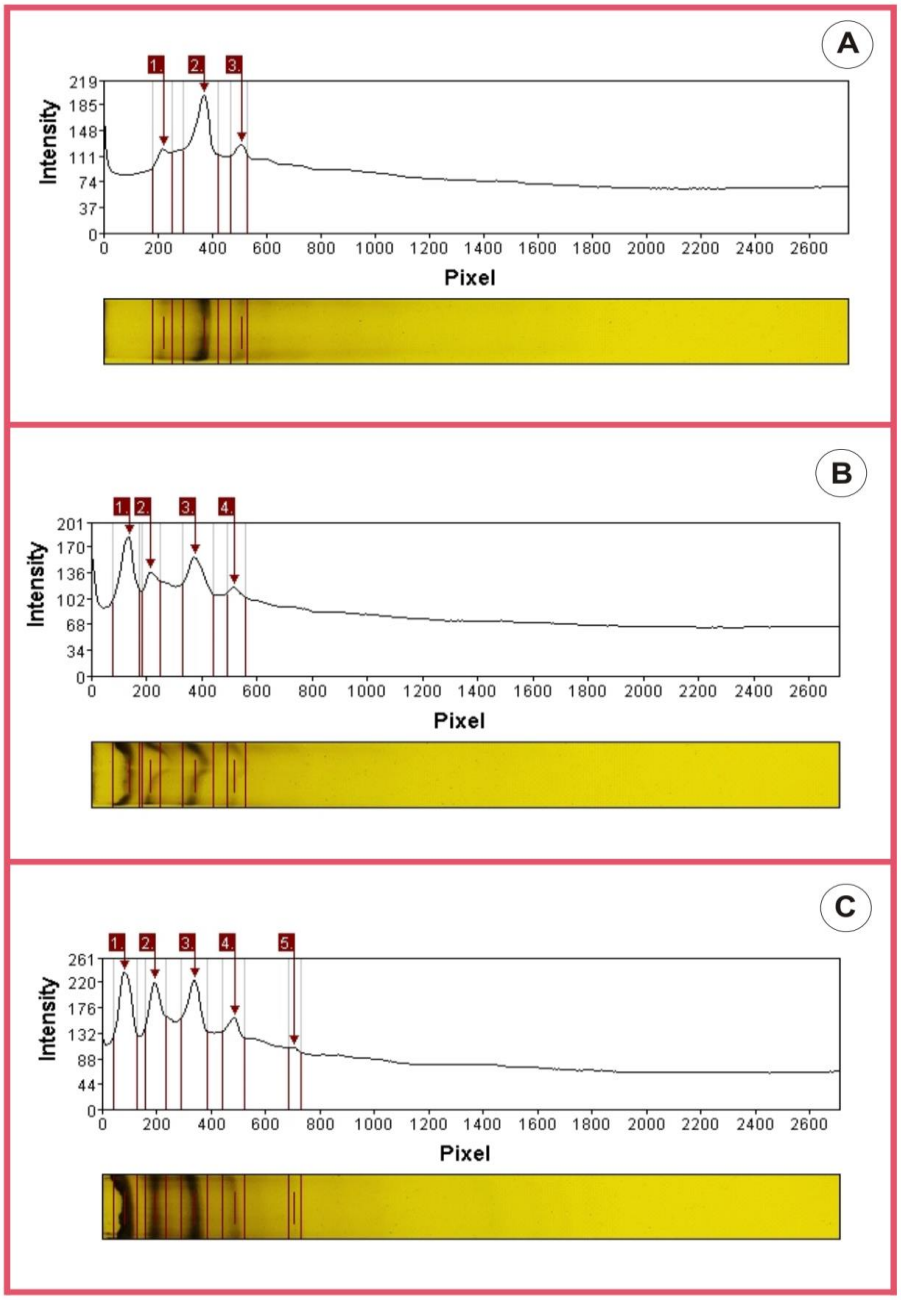

Figure 5: Band intensities of CBBR stained method 1b, 1a and 1; (**A**) method 1b, (**B**) method 1a, (**C**) method 1

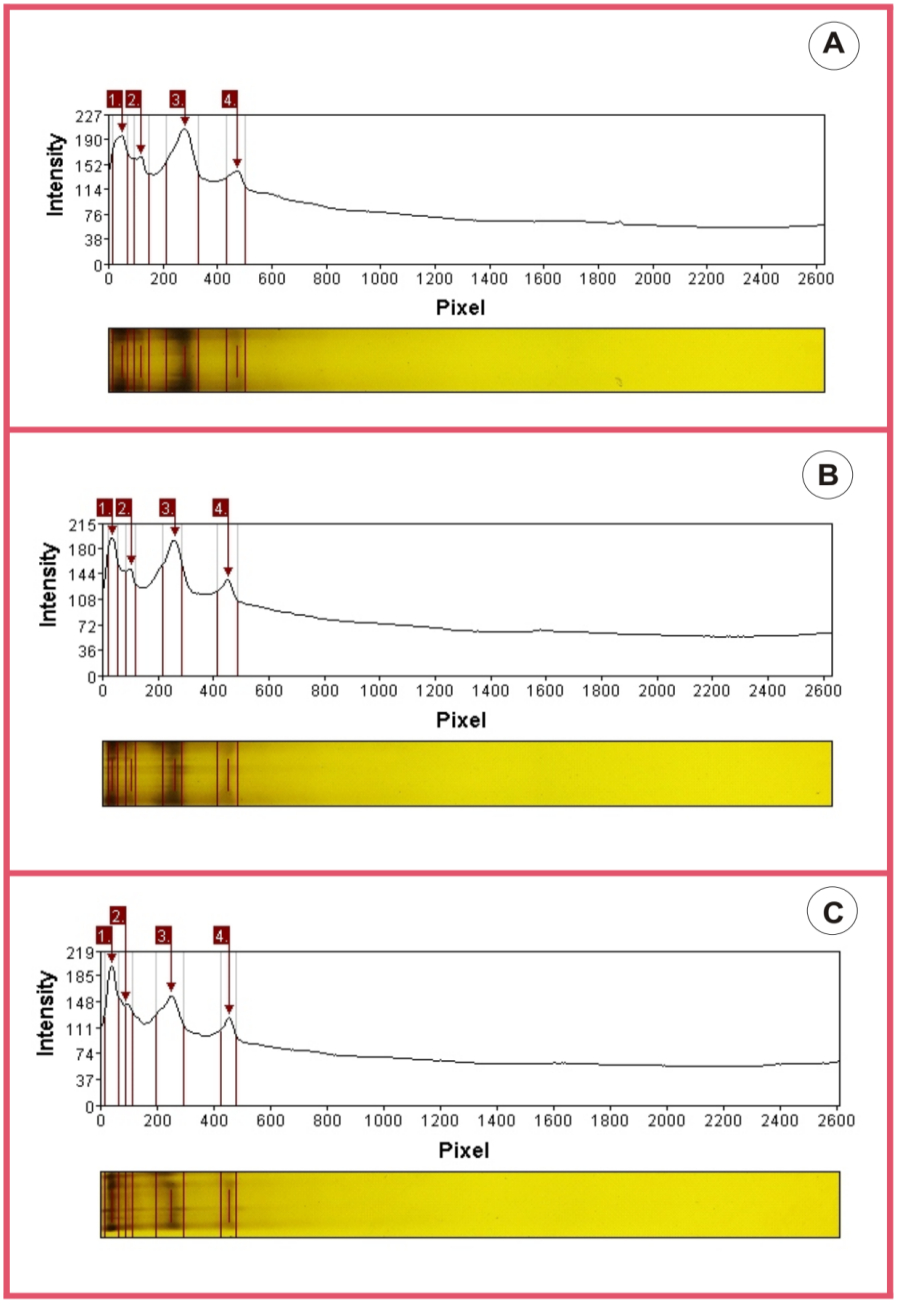

Figure 6: Band intensities of CBBR stained method 3b, 3a and 3; (**A**) method 3b, (**B**) method 3a, (**C**) method 3

Coomassie brilliant blue R-250 (CBBR) staining

CBBR staining was done to visualize the total number of proteins found in the protein extracts method 1, 1a, 1b, 3, 3a and 3b. The Figure 2B showing CBBR stained gel. In this gel, lane 1, 2, and 3 loaded with samples such as method 3b, 3a, and 3 respectively and all samples contain total of four bands. The 4^{th} lane represents 1b sample; here three protein bands were observed. The 5^{th} and 6^{th} lanes were loaded with method 1a and 1 sample respectively. The method 1a extract had total of four bands and method 1 had 5 bands. The CBBR stained gel results showed that all the extract contains maximum of five additional bands (Figure 5 & 6).

2.3.2 Protein extraction efficacy from byssus thread

Table 4: Total protein yield from byssus thread

Method	Protein yield (µg/ml)
Method 1	86.66 ± 2.39
Method 1b	85.82 ± 1.52
Method 2	55.93 ± 3.61

Values are expressed in mean ± standard deviation

A total of three extraction methods were applied to obtain best protein extraction protocol from the byssus thread of *P. perna* (Table 4). Method 1 and 1b had more protein concentration than method 2. However, a significant difference in protein extraction was not observed between the three samples.

2.3.3 Confirmation of quinone proteins

The presence of quinone proteins in the protein extract prepared by method 1b was double confirmed by UV-visible spectroscopy and the Figure 7 represent the spectrum. The NBT treated protein extract showed band at blue range (λ=469 nm) of visible spectrum, because the NBT reacted with quinone moiety to form blue colour. Whereas BSA control shows band in the green range (λ=531 nm) indicating the absence of quinone moiety. The results confirmed the presence of polyphenolic proteins in the foot extract of *P. perna*.

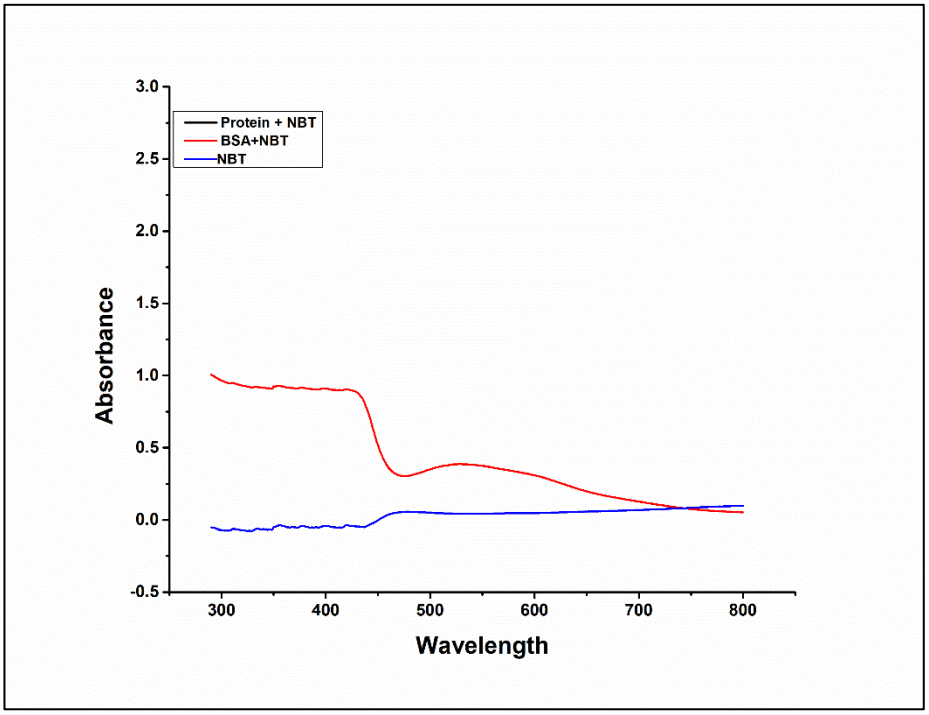

Figure 7: UV-Visible spectrum of quinone protein

2.3.4 pH stability of adhesive proteins

The pH stability of the protein extract was measured through UV-visible spectroscopy and the Figure 8 showing corresponding spectrum. The proteins kept in acidic condition show three absorption bands at 253 nm, 294 nm and 352 nm, which is the typical absorption of DOPA-catechol. However, in the alkaline condition, the spectrum appears complete shift of bands into 229 nm, 248 nm and 370nm which indicates oxidation of DOPA. This result concluded that acidic condition is more suitable for maintaining adhesive protein stability.

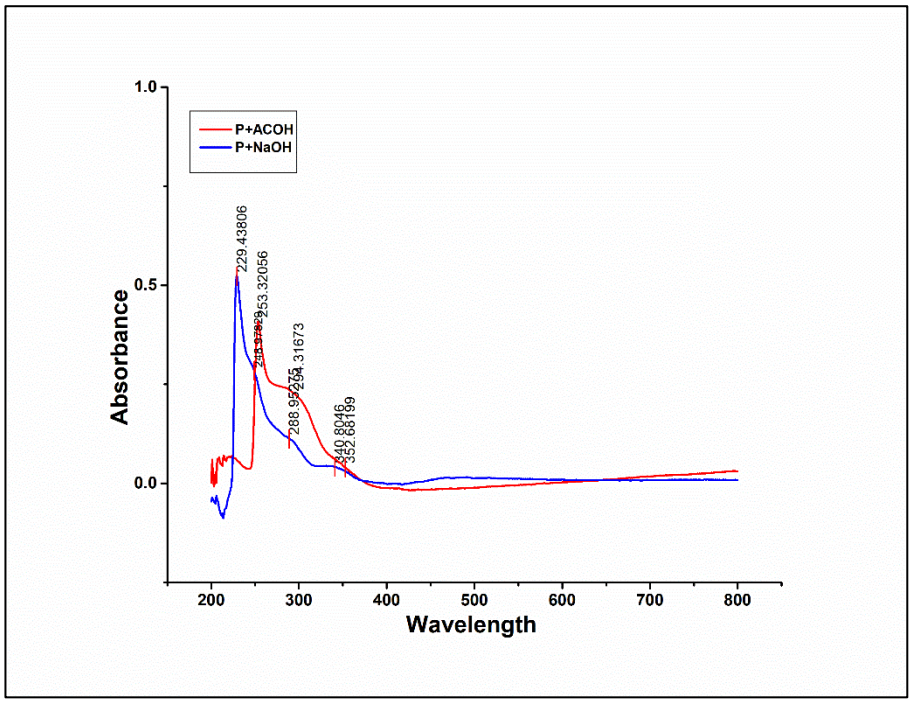

Figure 8: UV-Visible spectrum of adhesive protein showing p^H stability

2.3.5 Atomic force microscopy

Atomic force microscopy was used to understand the surface nano-texture and surface roughness of protein samples. The Figure 9 & 10 represents the two-dimensional (2D) and three-dimensional (3D) topography of samples such as protein extract, iron-treated protein extract and BSA control. Table 5 shows the surface roughness of each sample. R_a describes the average roughness of sample, which is the arithmetic average of the absolute values of the profile heights over the evaluation length. R_q is the root mean square (RMS) average of the profile heights over the evaluation length and R_z is the ten-points mean height roughness, measure of difference in height between the average off five highest peaks and five valleys in the evaluation surface (Kumar & Rao, 2012). According to Table 5, foot protein had higher roughness value than control BSA sample. When foot protein treated with iron the roughness of sample became reduced, whereas in the BSA roughness gets increases. The topology images also substantiate the roughness values because the images revealed that iron treated BSA and normal protein samples had rougher surface and normal BSA and iron treated protein samples had smoother surface Figure 9 & 10. The results concluded that iron treatment mediated impact is different in different proteins.

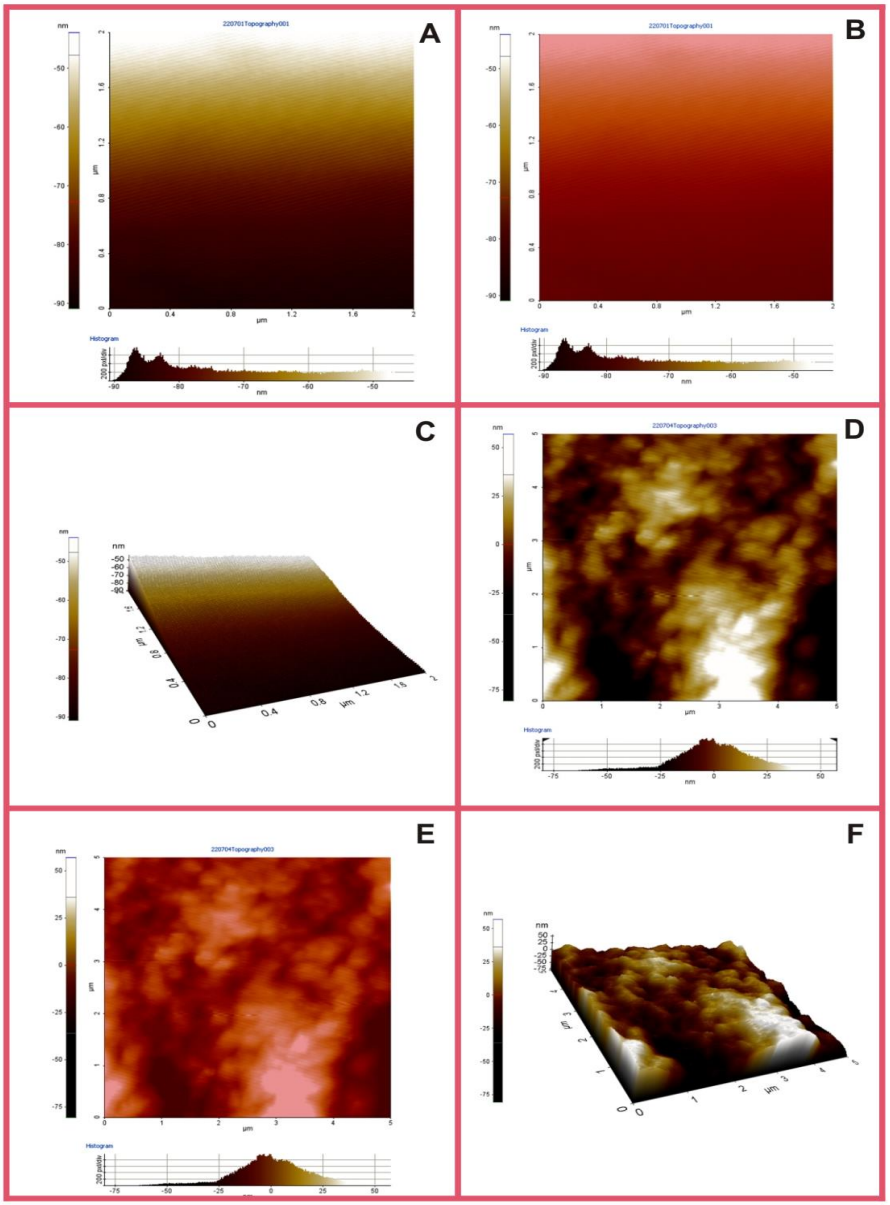

Figure 9: AFM surface analysis of BSA and iron treated BSA; (**A**) BSA surface morphology, (**B**) BSA topography, (**C**) BSA 3D image, (**D**) iron treated BSA surface morphology, (**E**) iron treated BSA topography, (**F**) iron treated BSA 3D image

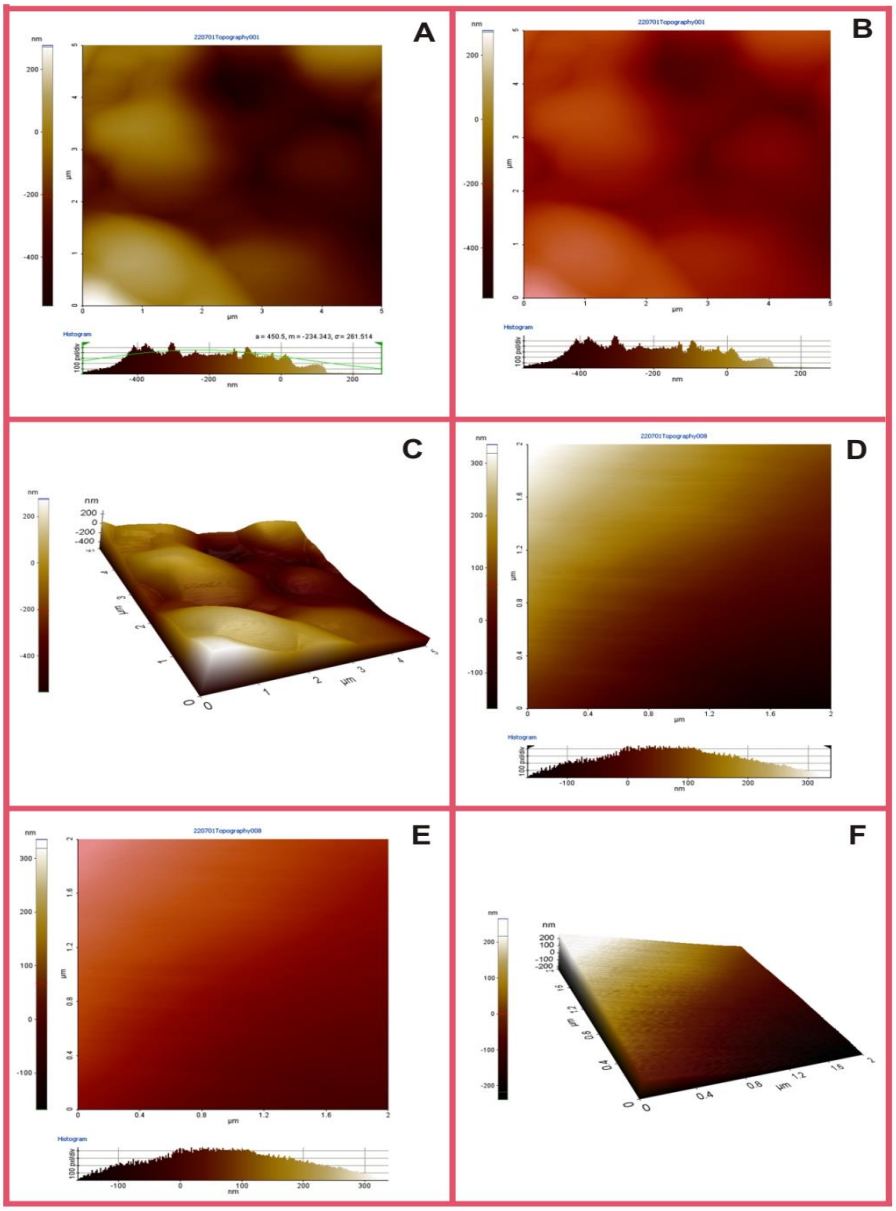

Figure 10: AFM surface analysis of adhesive protein and iron treated adhesive protein; (**A**) adhesive protein surface morphology, (**B**) adhesive protein topography, (**C**) adhesive protein 3D image, (**D**) iron treated adhesive protein surface morphology, (**E**) iron treated adhesive protein topography, (**F**) iron treated adhesive protein 3D image

Table 5: Surface roughness of samples

Sample	**Surface roughness (R_a) (nm)**	**Mean root square roughness (R_q) (nm)**	**Maximum height (R_z) (nm)**
BSA	11.466	13.115	46.409
BSA + Fe	14.064	18.385	130.805
Foot protein	141.687	166.596	826.304
Foot protein + Fe	91.703	110.774	498.529

2.3.6 Contact angle measurement

The contact angle measurements (Figure 11 & 12) and surface energy of all protein samples on glass coverslip were represented in Table 6. When contact angle of the substance increases with decreasing the wettability and adhesion strength. Water had lowest contact angle (16.72°) and highest surface energy. Foot protein had higher contact angle and lower surface energy than control sample BSA. Iron treated protein sample had improved contact angle (43.09°) than untreated protein sample (39.68°). The results concluded that iron treatment increases the hydrophobic nature and low wettability in foot proteins which causes decrease in surface energy.

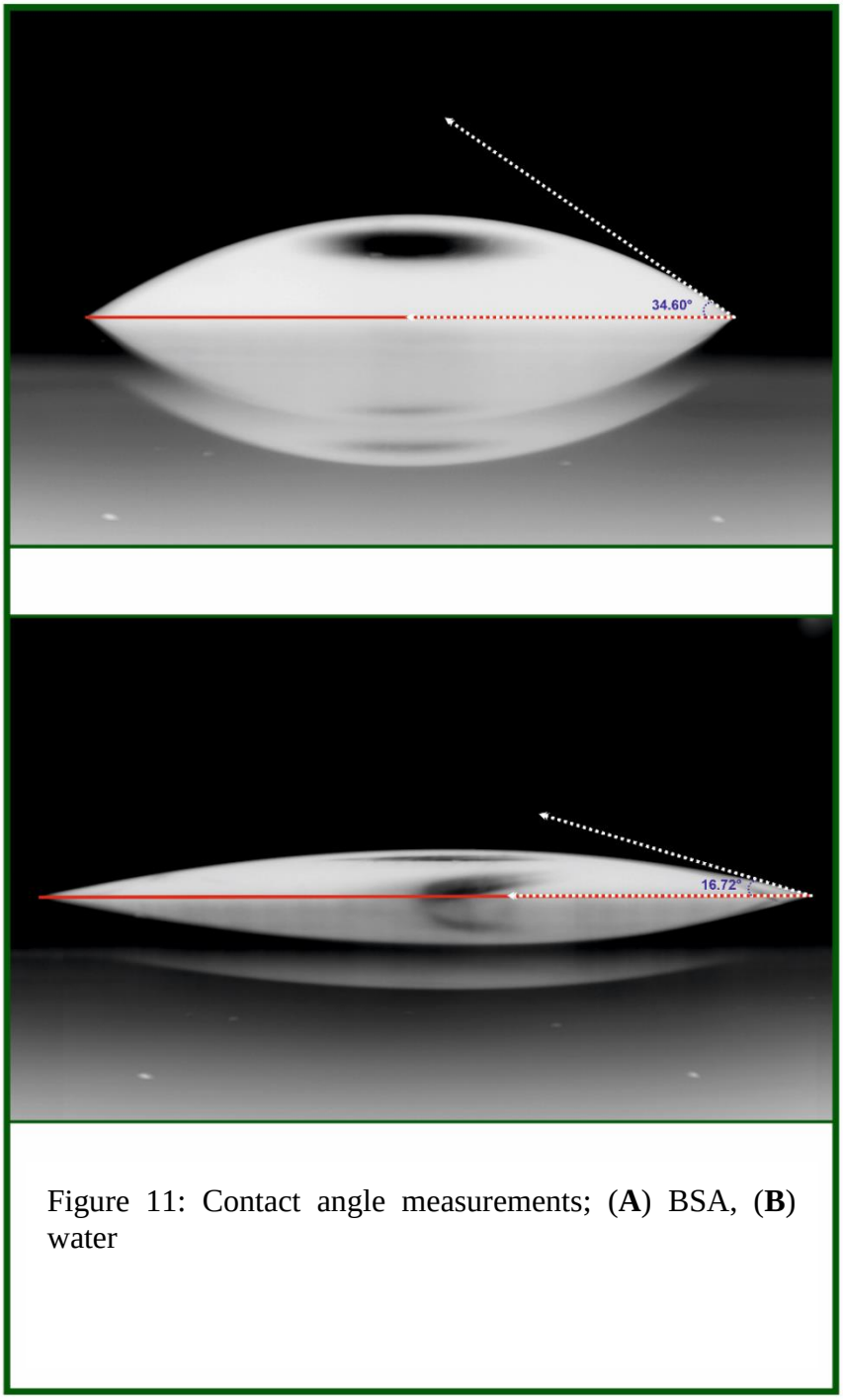

Figure 11: Contact angle measurements; (**A**) BSA, (**B**) water

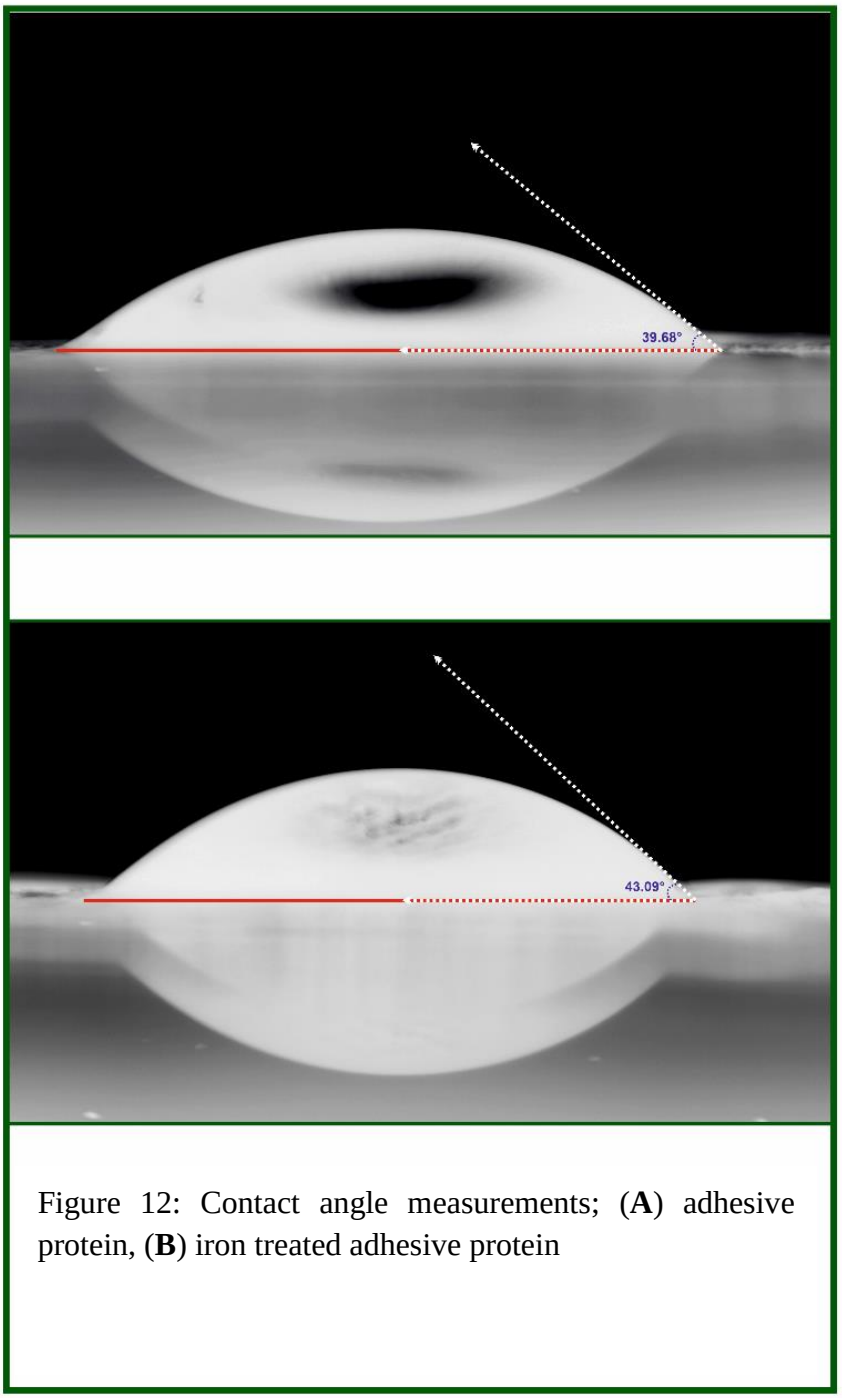

Figure 12: Contact angle measurements; (**A**) adhesive protein, (**B**) iron treated adhesive protein

Table 6: Contact angle measurements of samples

Sample	**Contact angle**	**Surface energy (J/m^2)**
Water	16.72°	0.1909
BSA	34.60°	0.1326
Foot protein	39.68°	0.1275
Foot protein + Fe	43.09°	0.1149

DISCUSSION

High commercial values of native mussel adhesives open to vast research scope to develop new strategies for adhesive protein extraction. To date, efficient protein extraction methods have not been developed from *P. perna*. According to results of foot protein extraction from *P. perna*, significant protein yield was obtained in methods 1, 1a, 1b, 3, 3a and 3b. All the above-mentioned extractions were started by using acetic acid and salt. Foot proteins are only stable at acidic pH because DOPA is spontaneously oxidised to dopaquinone at neutral or alkaline pH, which abolished the adhesive ability of foot proteins. High oxidation susceptibility of DOPA makes critical challenges to foot protein adhesion (Martinez Rodriguez et al., 2015; Yuvaraj et al., 2021). Hence acid-based extractions are more suitable for maintaining the adhesive ability and more appropriate for the production of native adhesive proteins. According to our results, NaCl, Na_2SO_4, and KCl are good agents for the salt-induced precipitation of adhesive proteins. Among these salts, NaCl and Na_2SO_4 are more cost-effective have high salt stability and have salt reactivity. In our results, Na_2SO_4 mediated salting out provides a comparatively high yield.

The NBT-stained acid urea gel images of six protein extracts revealed that all the samples contain a single adhesive protein band with different band intensities. The intensity of the band is directly proportional to the DOPA content. The highest intensity was observed in method 1a>1>3a>3 and the lowest intensity was observed in modified 1b and 3b. The highest molecular mass foot protein is mfp-1

with molecular mass ~108 kDa and which is the most abundant foot protein. Anderson and waite (2001) extracted foot protein-1 from *Dreissena bugensis*, Ohkawa et al. (2004) purified foot protein 1 from *Perna viridis*, Zhoa & waite (2005) extracted fp-1 from *P. canaliculus*, and Holten-Andersen et al. (2009b) purified fp-1 from *Mytilus californianus*. In all the above mentioned foot protein 1 studies, the fp-1 band in the NBT stained gel was similar to the present NBT gel band; Hence when comparing with these studies confirmed that our protein extract contains a single polyphenolic adhesive protein which was foot protein 1. Mfp-1 was the first identified polyphenolic protein in mussels, mainly concentrated in the byssus thread cuticle (Bandara et al., 2013).

The NBT stained gel image revealed that method 1b and method 3b was not efficient for foot protein extraction because of low band intensity. Similarly, Urea is used in methods 3, and 3a, which is a protein denaturing agent. Urea actively participates in the unfolding of proteins by competing with native interactions, which first destabilizes the β sheet and causing the loss of three-dimensional structure and natural function of the protein (Das and Mukhopadhyay, 2009; Camilloni et al., 2008). Therefore, Urea mediated extraction leads to loss of functional status of protein; hence these two (methods 3 and 3a) methods are not suitable for functional foot protein extraction. The remaining two extractions, NaCl mediated salting out was done in method 1 and Na_2SO_4 was used in method 1b. Among these salts, Na_2SO_4 is more cost-effective, has high salt stability and low salt reactivity and also which is very effective at stabilizing proteins (Hani

et al., 2019). Similarly, Na_2SO_4 is a divalent ion containing salt which also can enhance the adhesive strength of the protein sample (Frank and Belfort, 2002). In our results, Na_2SO_4 mediated salting out provides a comparatively high yield of protein. Hyde et al., 2017 studied salting out strategies using Hofmeister series and revealed that Na_2SO_4 is an excellent agent for salt fractionation because of its low cost, efficiency and chemical inertness conditions. The overall results from adhesive protein extraction from the foot indicated that the modified 1a method is more efficient for the synthesising of natural foot proteins.

The results of protein extraction from the thread indicated that, the yield of protein is comparatively low, while a better extraction yield was acquired from methods 1 and 1b. Byssus thread is considered as mari-culture waste and it can easily be available without cost. According to previous studies, approximately 10,000 mussels are required to extract 1g of naturally derived mussel foot protein (Cha et al., 2008; Castillo et al., 2017). Large scale commercial synthesis of adhesive proteins was achieved by recombinant DNA technology. At the same time, highly biased amino acid composition, different codon usage preference between mussels and expression system and small expression quantity make hindrances to the successful production (Cha et al., 2008). Hence the development of an efficient protein extraction methodology from byssus threads becomes a milestone invention.

The confirmation of quinone proteins in the extract was double confirmed by UV-visible spectroscopy. At alkaline pH and the

presence of reductant glycine, quinone proteins and related quinonoid substances catalyse redox cycling; occurs reduction of tetrazolium into blue-black compound formazan by free oxygen radicle (Paz et al., 1991). Because of this redox reaction in foot protein extract, NBT treated samples got peaks in the blue range band and due to the lack of quinone moiety in BSA which comes in the green range. The colour change in NBT-treated foot proteins was also reported by Zhong et al. (2014) and Priemel et al. (2020).

The pH stability of protein extract was also determined by UV-Visible spectroscopy. DOPA oxidation in alkaline pH was analysed by using UV-Visible spectroscopy, which was reported in the studies of Mirshafian et al. (2016) and Priemel et al. (2020). According to their results DOPA oxidation leads to alteration in some peak band positions, some of them get increased and some get decreased. The present study observed that in acidic pH peak positions were marked at 253nm, 294nm and 352nm. However, in alkaline pH the peaks such as 253nm and 293nm get decreased to 229nm and 248nm respectively and the 352nm peak value was increased to 370nm. According to Mirshafian et al. (2016) and Priemel et al. (2020), 350nm absorbance is indicating intact DOPA and increases the value with increases in the DOPA oxidation to DOPA quinone.

The study of Martinez Rodriguez et al. (2015) revealed the pH sensitivity of mussel adhesive proteins. According to their results, during byssus thread formation marine mussels create acidic pH under the foot. Acidic pH accomplished several functions, which limited

mfp-DOPA oxidation and maintained cateholic functionalities of adhesive proteins. Similarly, at low pH cateholic moiety of DOPA adsorb to surface, oxides by H-bonding and metal ion coordination. Low pH conditions also help to maintain protein insolubility when they are exposed to seawater (pH 8.2) and are also involved in quinone cross-linking by metal chelation (Lee et al., 2011). Similarly, the study of Wei et al. (2013) in mfp-3 exhibited the solemnity of pH in foot protein adhesion. According to their results, DOPA adhesiveness terminates when pH increased from acidic to neutral and basic. The results of Lu et al. (2012) also revealed that cohesive strength between *Mytilus californianus* foot protein-1 (mcfp-1) and mica was increased in acidic solution.

Hydrophobic interactions, electrostatic interactions and inter-residue H-bonding are the major factors for increased cohesion within adhesive proteins. AFM results revealed the surface roughness and topography of polyphenolic protein extract and BSA. The study of Sherman et al. (2009) revealed the relationship between stickiness and surface roughness. According to their conclusions, sticker substances had more surface roughness than non- or less sticky substances. Here, foot proteins are sticky which is mainly involved in the adhesion mechanism hence they got an extremely high roughness value than BSA; BSA is a non-sticky protein. Surface roughness determines the adhesion ability of substances. According to Lin et al. (2019), the surface roughness of the substance increases with decreasing adhesion strength. The raw foot protein extract had higher surface roughness, whereas when the extract was treated with iron, it became reduced.

These results were also reflected in surface topology images. Iron-treated samples had smooth surfaces whereas raw extract had peaks and valleys. This effect is due to metal chelation in polyphenolic protein, here DOPA bind with Fe^{3+} to form highly stable catecholato-Fe^{3+} complexes which mediate protein crosslinking, and causes increased adhesive strength (Harrington et al., 2010). Naturally, the concentration of metals like iron, zinc, copper and manganese is 100,000 fold higher in byssus thread than in surrounding water because of metal ion involvement during adhesion (Monahan & Wilker, 2004). A single Fe^{3+} molecule can bind with three MAPs strands to form $Fe(DOPA)_3$ tricomplexes. These complexes further react with oxygen and form radical species which actively involved in protein coupling or help to bind with the substrate (Sever et al., 2004). According to Monahan & Wilker, (2003) Fe^{3+} and Mn^{3+} concentrations were higher in adhesive plaques than Fe^{2+}, Al^{3+}, and Cr^{3+} because Fe^{3+} and Mn^{3+} are involved in oxidation of DOPA to DOPA quinone and actively involved in protein curing.

In 2003, Monahan and Wilker studied adhesive protein crosslinking by using chloride and nitrate metal ions. Their results highlighted that Fe^{3+} ability for adhesive protein crosslinking, catechol oxidation and curing of glue. Similarly, Zeng et al. (2009) studied strong reversible Fe^{3+} mediated bridging between DOPA-containing protein films in water. Their results emphasized that DOPA-Fe^{3+} complexes can make strong bridging between two mfp 1 coated surfaces and this property has considerable scope in wet industrial and biomedical applications. In 2002, Frank and Belfort studied ionic effects on adhesion of *Mytilus*

edulis foot protein 1 on silica. Their results revealed that divalent ions containing salts such as $MgCl_2$, $CaCl_2$ and Na_2SO_4 induce more adhesion strength than monovalent ions containing salts such as NaCl and KCl. The highest adhesion was found in the trivalent ion containing salt called $FeCl_3$. In the present study, extraction was done by using Na_2SO_4 and also sample was treated with $FeCl_3$, which led to increased adhesion ability. These results confirmed that the ionic composition of the sample determines the adhesive ability of the protein.

The water affinity of protein extract was analysed by contact angle measurement. Here, the water molecule spread over the bare glass because glass is a hydrophilic substance; hence contact angle of the water molecule was deceased (Gupta & Denis, 2016). Amino acid composition, size and shape of the protein molecule, and intermolecular and intramolecular cross-links are the factors depending on the surface hydrophobicity of proteins (Vnučec et al., 2017). BSA protein can adsorb on both hydrophobic and hydrophilic surfaces whereas interaction strength was higher on the hydrophilic surface than on the hydrophobic surface (Jeyachandran et al., 2009). Here, glass is a hydrophilic surface, so the BSA molecule shows high adsorption strength and low contact angle. In mussel foot protein 1, hydrophobic amino acid content was higher than hydrophilic amino acid (Anderson & waite, 2002; Zhao and waite, 2005; Holten-Andersen et al., 2009a). Whereas hydrophilic amino acids such as threonine, serine, tyrosine, asparagine, glutamine etc. are found on the surface of the protein and because of the large dipole moments they attract water molecules. Hence foot protein extract shows hydrophilic nature on glass. In the

iron-treated sample, the contact angle was much higher because iron facilitates protein cross-linking. Hydrophobic interactions occur during protein cross-linking which increasing the hydrophobicity of protein (Fan et al., 2018). Hence contact angle of iron treated sample on glass was increased and wettability and adhesion strength were decreased.

Understanding the adhesive mechanism of mussel foot proteins to a variety of surfaces opens up new insight into developing biomimetic coatings and adhesives. Yu et al. (2013) analysed the hydrophobic and hydrophilic interactions of mussel foot proteins with organic thin films such as hydrophobic methyl (CH_3) and hydrophilic alcohol (OH) terminated SAM (self-assembled monolayer) surfaces between pH 3 and pH 7.5. Their results highlighted that mussel foot proteins strongly adhere to CH_3 terminated surfaces in acidic pH via hydrophobic interactions and also weakly to hydrophilic OH terminated SAM surfaces. Similarly, Lu et al. (2013) also measured the adhesive strength of *Mytilus californianus* foot proteins such as mfp-1, mfp-3 and mfp-5 to four different substrates (mica, silicon dioxide, polymethylmethacrylate and polystyrene). Their results also revealed that hydrophilic substrate (mica) shows less adhesion force and increasing adhesion force with increasing hydrophobicity. These results supported the present work because *P. perna* foot protein extract also shows weak binding force in the hydrophilic glass substrate. Also, when comparing with results of Lu et al. (2013) and Yu et al. (2013) *P. perna* extract had more adhesive strength. *P. perna* adhesive protein extraction and their characterisation were new to the scientific community and these results provide new scope for the generation of coating and adhesives.

CONCLUSION

The present study focused on developing a new and efficient methodology for the native extraction of adhesive proteins from *P. perna* foot and also analyse its properties. Native and recombinant mussel adhesives have high commercial value and hence many extraction protocols have existed. Whereas adhesive protein extraction from *P. perna* was not established and the present work mainly focused on the extraction of functionally active adhesive proteins. The results highlighted that Na_2SO_4 mediated salting out was excellent and efficient for native adhesive protein extraction. Because, Na_2SO_4 is chemically inert, have efficiency and low cost, and also which enhances adhesion ability more than the other two salts such as NaCl and KCl. From all extraction methods, a single polyphenolic protein band was obtained, which was a high molecular protein. Among six adhesive polyphenolic proteins only foot protein 1 is the high molecular weight protein and also which is the most abundant protein. Compared with other similar studies the single band of the extracted protein can be confirmed as foot protein 1. The presence of polyphenolic proteins and pH stability were determined by using UV-visible spectroscopy. The results showed that, acidic pH was suitable for maintaining a functionally active state of adhesive proteins and neutral or basic pH causes DOPA oxidation, which reduces the adhesive performance of proteins.

Atomic force microscopy was performed to understanding the surface topography and roughness, which exhibit the adhesive strength of the

protein sample. The results showed that iron treatment enhances adhesive strength because it reduces the roughness of protein samples. Basically when decreasing the roughness of samples lead to increasing the adhesive performance. Similarly, contact angle measurement was performed for understanding the water affinity of the protein sample. The result implies that protein samples have hydrophilic nature whereas iron treatment reduces its hydrophilicity because protein cross-linking occurs during the treatment. Similarly, the adhesive force of the sample in the hydrophilic glass substrate was analysed. The results indicated that the extracted proteins adhesion strength was low in the hydrophilic substrate. In contrast, the *P. perna* protein extract had more strength than other species of mussel adhesive proteins. Native mussel adhesives have high commercial value and applications. Many native adhesives are currently commercially available. The foot protein extraction from *P. perna* mussel species was not studied well and data was not available. Hence the present work became a milestone in the field of *P. perna* adhesive protein research.

INTRODUCTION

Mussels' fascinating wet adhesion mechanism always attracts researchers to develop environment-friendly adhesives and several biomimetic materials. Mussel secret protein glue act as water resistant adhesive material that can adhere to all type of surfaces like plastic, glass, teflon, metal etc. Water adhesion is the major attraction of mussel foot proteins because synthetic adhesives are easily removed by water (Stewart et al., 2011). Six mussel foot proteins (mfp-1 to mfp-6) are involved in the water-resistant adhesion mechanism. Permanent strong adhesion of foot proteins is achieved mainly by DOPA, which is the post-translationally modified tyrosine residue. The DOPA content in adhesive proteins is actively involved in adhesion to the surface and cohesion between proteins (Cha et al., 2008; Kaushik et al., 2015). DOPA content, redox chemistry, metal interactions etc. are the major factors dependent on the adhesion mechanism (Bandara et al., 2013).

Adhesives are part of daily life and most of them are chemically processed. Synthetic adhesives like formaldehyde-urea and formaldehyde-phenol glues create several adverse effects. Same time, mussel adhesion is considered stronger than epoxy and phenolic resins. Adhesives derived from proteins are biodegradable, biocompatible, non-toxic, cheap and renewable (Yuvaraj et al., 2021). Mussel adhesive proteins do not elicit immunogenicity; hence they can use as a medical adhesive to the human body (Sáez et al., 1991). The mussel adhesive proteins have a wide range of applications, including wound healing, preventing blood loss without causing inflammation, replacing metal amalgam in the dental procedure, used in tissue engineering,

used as drug delivery systems, used for the development of biosensors, used as adhesive biofilm for immobilizing cells and enzymes, act as complicated bone fracture healers and also works as anticorrosive agent (Silverman & Roberto, 2007; Bandara et al., 2013).

Mussel adhesive protein sequence characterisation helps to design biomimetic analogue of MAPs (Waite, 2002). The substances that mimic the biologically originated compounds are called biomimetic materials and mussel adhesive proteins are highly attracted to this field because it shows similar activity on both biological and non-biological surfaces. Many researchers actively studied the production of underwater adhesives with properties of mussel foot proteins (Silverman & Roberto, 2007). DOPA and hydroxyproline-containing decapeptide synthesis was the first step of biomimetics. MAP analogues are synthesised mainly by random polymerisation of DOPA with lysine, glutamic acid etc., which make a strong bond with metal and glass surfaces (Bandara et al., 2013). Among the foot proteins, mfp-1, mfp-3 and mfp-5 are rich in DOPA content; hence they are more attracted to the synthesis of natural adhesives (Kaushik et al., 2015). The significance of mussel adhesive proteins is incomparable, whereas due to the extremely limited production, the practical applications of such proteins become quite restricted. Naturally extracted mussel adhesive proteins are commercially available, but around 10,000 mussels are required for the synthesis of 1g of mfp-1 (Cha et al., 2008).

Low extraction yield and the high production cost was the limitation of natural extraction which is overcome by recombinant DNA technology. Several studies were conducted for the genetic production of fp-1, fp-5 and fp-3 in different expression systems like *E. coli*, Yeast and plant cells. Mfp-5 is considered a potent bioadhesive and recombinant mfp-5 shows high adhesion ability than natural mussel adhesive Cell-Tak™ (Hwang et al., 2004). Highly biased amino acid composition, different codon usage preferences between mussel and other expression systems and small expression quantity are the factors that influence the massive synthesis of adhesive proteins through different expression systems (Kitamura et al., 1999). Hybrid mussel adhesive proteins were developed to overcome the low production yield from expression. For example, a new novel hybrid mussel adhesive protein called fp-151 was synthesised by fusing six mgfp-1 decapeptide repeats at N and C termini of mfp-5. These hybrid bioadhesives provide significantly higher yield, adhesion strength and biocompatibility with various cell types (Hwang et al., 2007b). Because of its high commercial value, mussel adhesion-related studies are actively continued for the last two decades. At the same time, adhesive studies from mussel species *P. perna* were limited. Hence, *P. perna* adhesive protein studies provide new insight into the development of adhesive materials with more applications. The present chapter discussed gene sequencing of adhesive protein from *P. perna* and its insilico characterisation.

MATERIALS AND METHODS

3.2.1 Tissue collection

Foot tissue was used to extract RNA of foot protein genes. Hence, it dissected from freeze sedated *P. perna* specimen by using a sterilized surgical blade. The tissue was then lightly washed in RNases-free DEPC (diethyl pyrocarbonate) treated water and chopped into small pieces.

3.2.2 RNA extraction

RNA is highly prone to degradation by RNase enzymes; hence all the glassware, vials and micro tips used for extraction were sterilized with DEPC-treated water. For the extraction (Rio et al., 2010), 1 ml TRIzol reagent was added to 100 mg foot tissue and homogenized well. The homogenized sample was incubated at room temperature for 5 minutes for the complete dissociation of nucleoprotein complexes. After incubation, the samples were centrifuged to remove the sediments and transfer the supernatant into a new vial. To the supernatant, added 0.2 ml of chloroform and vortex vigorously for 15 seconds. Then incubate the sample for 5 minutes and centrifuge at 12,000 g for 15 minutes at 4° C. Following the centrifugation, three phases are formed in the sample including the upper colourless aqueous RNA-containing phase, middle interphase and lower red phenol-chloroform phase. The upper RNA phase carefully transfers to a new vial without disturbing other phases. Added 0.5 ml of isopropyl alcohol to the RNA sample and incubated for 10 minutes at room temperature. The sample was

centrifuged at 12000 g for 10 minutes at 4° C. During the centrifugation, RNA precipitated as a gel-like pellet on the side or bottom of the vial. After centrifugation, completely removed the supernatant and RNA pellets washed by adding 1 ml 75% ethanol to the sample, mixed by vortexing and centrifuged at 7,500 g for 5 minutes at 4° C. Repeat this step again and remove all ethanol content by air drying for 5-10 minutes. Finally, RNA dissolved in DEPC-treated water. The integrity of RNA was confirmed by 1% agarose gel electrophoresis with ethidium bromide staining (Rio et al., 2010) and images were taken using gel doc (G-box F3, UK). Quantification of RNA and purity of samples were measured with a Nanodrop spectrophotometer (Eppendorf Biospectrometer).

3.2.3 cDNA synthesis

The extracted RNA was converted to cDNA using the Thermo Fisher Verso cDNA synthesis kit according to the manufacturer's instructions. The presence of RNA was confirmed by 1% agarose gel electrophoresis with ethidium bromide staining (Rio et al., 2010) and quantification of RNA and purity of samples were conducted with a Nanodrop spectrophotometer (Eppendorf Biospectrometer).

3.2.4 RNA stability determination

RNA is highly unstable and quickly degraded; hence RNA integrity in different storage conditions is mostly recommended in gene expression studies. For RNA stability determination, the samples were stored in three distinct conditions: tissue immersed in TRIzol reagent and kept at

-80° C, tissue directly kept at -80° C, and at -20° C for three months and the RNA extraction efficacy was determined. The extracted RNA was converted into cDNA and analysed its purity and integrity. The RNA and cDNA integrity was determined by agarose gel electrophoresis, stained with ethidium bromide (Rio et al., 2010) and the images were taken using gel doc (Syngene, G-box F3, UK). The concentration and purity of RNA and cDNA were determined by a Nanodrop spectrophotometer (Eppendorf Biospectrometer). The freshly extracted RNA was used as a control for comparing the changes. The extracted RNA storage efficiency was determined by keeping the RNA samples at different temperatures (-80° C & -20° C) for three months, and later cDNA conversion was carried out.

3.2.5 Gene sequencing

Primers

There is no data is available regarding the *P. perna* foot proteins gene sequences. Hence, for this study primer data was collected from a research article published by Zhang et al. (2019). In this article, they carried out foot protein gene sequencing of *P. viridis*. Both *P. perna* and *P. viridis* come under the same genus; hence for the present study, *P. viridis* foot protein 6 (Pvfp 6) primers were used.

Primer sequence used:

Pvfp6 forward: ATGATAAGTGCAGTTTGTATATATTTC

Pvfp6 reverse: TTTGTATCCATAACCACATGC

PCR amplification

Two variants of the *P. perna* foot protein 6 gene were amplified separately using two different PCR conditions with the same primers. The PCR reaction mixture is described in Table 1 and reactions were conducted in the gradient thermal cycler (Sure Cycler 8800, Agilent Technologies, USA). The PCR conditions were shown in Table 2.

Table 1: PCR reaction mixture for cDNA amplification

Reaction mixture	**Volume (µl)**
Master mix	10
Forward primer	1
Reverse primer	1
cDNA	Variable
Nuclease free water	Variable

Table 2: PCR conditions for foot protein 6

PCR condition	**Ppfp-6(1)**	**Ppfp-6(2)**
Hot start	98°C 1 min	94°C 5 min
Denaturation	98°C 5 Sec	94°C 30 sec
Annealing	54°C 10 sec	52°C 10 sec
Elongation	72°C 15 sec	72°C 1 min
No. of cycles	40	40

After the amplification PCR product was subjected to 1% agarose gel electrophoresis, stained with ethidium bromide (Rio et al., 2010) and

documented using gel doc (Syngene, G-box F3, UK). For measuring the size of the PCR product 1Kb DNA Ladder (Thermo Scientific GeneRuler, #SM 0242) was loaded in the gel.

DNA sequencing

Before sequencing, the obtained PCR products were cleaned using ExoSAP-IT. For this, 5 µl of PCR product was mixed with 2 µl of ExoSAP-IT and incubated at 37^{o} C for 15 minutes followed by enzyme inactivation at 80^{o} C for 15 minutes. The cleaned PCR products were sequenced by Sanger's dideoxy chain termination method (Sanger and Coulson, 1975) at Rajiv Gandhi Centre for Biotechnology (RGCB), Thiruvananthapuram, Kerala, India.

3.2.6 DNA sequence alignment and analysis

The chromatogram containing forward and reverse DNA sequences were analysed using the software BioEdit. The noise sequences were cleaned and multiple aligned using the Clustral W programme (Thompson et al., 1994). Conserved regions found in two variants and conserved region of foot protein 6 between two species (*P. perna* and *P. viridis*) were determined using BioEdit. The amino acid composition of the final DNA sequence was determined by using the online programme Expasy. The final FASTA format of nucleotide and protein sequences was deposited in NCBI GenBank (National Centre for Biotechnology Information) and obtained the accession number assigned for all the sequences submitted.

3.2.7 Phylogenetic analysis

The available foot protein 6 variants sequences from species such as *M. californianus*, *M. coruscus*, *P. viridis* and *P. perna* were collected from the NCBI database. The phylogenetic analysis was performed with Maximum-Likelihood algorithms using molecular evolutionary genetic analysis version 6 (MEGA 6) (Tamura et al., 2013). This method enables statistically-based hypothesis testing and the description of major features of sequence evolution, including rate heterogeneity, transition/transversion (ti/tv) rate ratios, and compositional bias (Goldman, 1990).

3.2.8 *Insilico* analysis of foot protein 6

3.2.8a Physio-chemical characterization

Physico-chemical characterisations of two variants of *P. perna* foot protein 6 were achieved using three online websites including the ProtParam tool – Expasy, CELLO v.2.5: subCELlular LOcalization predictor and Interpro. ProtParam tool – Expasy is a computational tool used to determine physical and chemical parameters of protein including molecular weight, theoretical pI, amino acid composition, atomic composition, extinction coefficient, estimated half-life, instability index, aliphatic index and grand average of hydropathicity (GRAVY) (Gasteiger et al., 2005). In addition, computational analysis of subcellular localisation of two variants of foot protein 6 was discovered by CELLO v.2.5: subCELlular Localization predictor (Yu et al., 2006) and molecular function were identified by Interpro.

3.2.8b Signal peptide prediction

The translocation of proteins is achieved by a short amino terminal part called signal peptides found in the protein. The signal peptide in the two variants of foot protein 6 was predicted by using SignalP - 6.0 web servers (Teufel et al., 2022).

3.2.8c Secondary structure prediction

The prediction of the secondary structure of two variants of foot protein 6 was done using a self-optimized prediction method (SOPMA). Prediction of secondary structure in SOPMA is done based on the homologue method. Homologous amino acid sequences have similar secondary structures. During the search for protein structure, this method finds out homologous amino acid sequences similar to query protein from the collection of protein database (Geourjon and Deleage, 1994).

3.2.8d Tertiary structure prediction

Protein tertiary structure prediction tools create the three-dimensional shape of protein molecules by arranging secondary structures as well as their side chains into three-dimension space. The software builds the structure based on the target protein sequence similarities with relative sequences; hence this method is called comparative modelling or homology modelling. The tertiary structure of two variants of *Perna perna* foot protein 6 was obtained using SWISS-MODEL, which is an automated protein structure homology modelling server (Waterhouse et al., 2018). The constructed protein models were visualized by using

the PyMol tool. After the homology modelling, the structure validation was done to discover the perfect model of the protein. In the present study, validation was done based on the QMEAN value (Benkert et al., 2018) and using the online server SAVES. For this study, two programmes of SAVES were used including PROCHCEK (Laskowski et al., 1993) and ERRAT (Colovos & Yeates, 1993). In PROCHECK validation was conducted based on the Ramachandran plot, and in ERRAT which is based on non-bonded atomic interactions.

3.2.8e Prediction of motif, domain and superfamily

Motif-Scan and Interpro are the two online servers used for predicting functional motif, domain and superfamily of two variants of the *Perna perna* foot protein 6. Motif-scan provides details about motifs found in the protein sequence and Interpro is a database that predicts functional details of proteins like family, domain and important sites. In addition, interpro estimates functional analysis of proteins by scanning the sequence against predictive models called signatures collected from several databases (Blum et al., 2021).

3.2.8f Posttranslational modification predictions

Posttranslational modifications (PTMs) are covalent processing events that make proteins functionally active. Different types of posttranslational modifications were occurred in proteins. In this study, two major PTM predictions were conducted including phosphorylation and glycosylation. Netphos 3.1 was the online server used to predict serine, threonine or tyrosine phosphorylation sites in two variants of

foot protein 6 (Blom et al., 1999). Similarly, GlycoPred (Hamby & Hirst, 2008) online server was used to predict glycosylation sites.

3.2.8g Antioxidant and metal ion binding properties prediction

The peculiar antioxidant and chelating properties of two variants of mussel foot protein 6 peptides were predicted using the online server AnOxPePred (Olsen et al., 2020). Metal Ion-Binding site prediction was conducted using the online prediction server MIB2: Metal Ion-binding site prediction and modelling server (Lu et al., 2022).

RESULTS

3.3.1 RNA purity and yield

The purity of RNA, extracted from *P. perna* foot tissue stored in different conditions was determined spectroscopically using 260/280 ratio and 260/230 ratio and purity analysis results were tabulated in table 3. 260/280 ratio of pure RNA is ~ 2.0 and the lower value indicates the presence of protein, phenol or other contaminants. Similarly, the 260/230 ratio of pure nucleic acid is 1.8 to 2.2 and the lower value indicates contamination (Desjardins & Conklin, 2010). In the present study, all samples had a good quality RNA except the -20° C stored sample (Table 3). 260/230 ratio of -20° C was 1.66 ± 0.08, which was lower than the optimum value. The RNA quantification results were represented in Figure 1. A significantly higher quantity of RNA was extracted from fresh and -80° C stored foot tissue ($P<0.05$). A low quantity of RNA was extracted from tissue stored at -20° C. The sample stored in trizol reagent shows a moderate quantity of RNA.

Table 3: RNA purity from different storage conditions

Storage condition	**260/280**	**260/230**
Fresh	1.95 ± 0.03	2.06 ± 0.23
Trizol	1.91 ± 0.04	1.98 ± 0.08
-80° C	1.95 ± 0.08	2.09 ± 0.15
-20° C	1.92 ± 0.01	1.66 ± 0.08

Values are expressed in mean ± Standard deviation

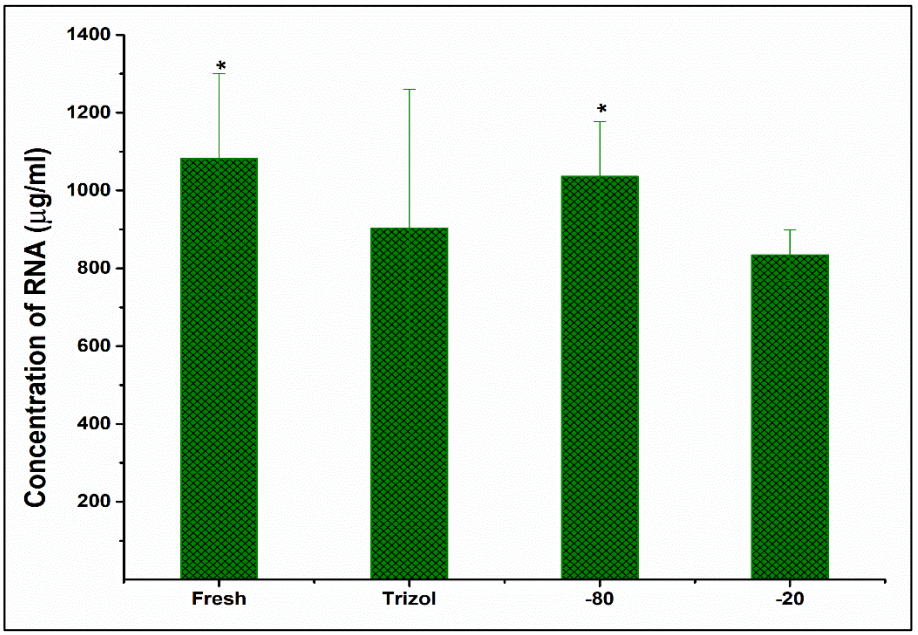

The symbol * indicating significance P<0.05

Figure 1: RNA yield from different storage conditions

3.3.2 cDNA purity and yield

cDNA purity was determined using a nanodrop spectrophotometer by calculating the 260/280 ratio and 260/230 ratio. In pure DNA, the 260/280 ratio was ~ 1.8 and the lower value indicates the presence of protein, phenol or other contaminants. Similarly, the 260/230 ratio of pure nucleic acid was 1.8 to 2.2 and the lower value indicates contamination (Desjardins & Conklin, 2010). In the present study, cDNA purity from different storage conditions was tabulated in Table 4. Here, all the samples show optimal purity; hence they can use for further analysis. The cDNA quantification results were represented in Figure 2. All the samples had a somewhat similar quantity of cDNA; hence a significant difference was not observed between the samples.

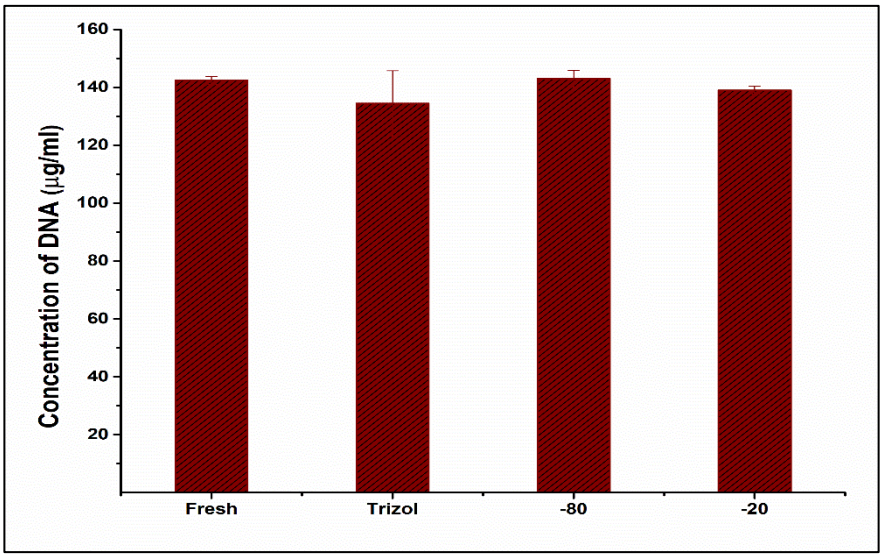

Figure 2: cDNA yield from different storage conditions

Table 4: cDNA purity from different storage conditions

Storage condition	260/280	260/230
Fresh	1.765 ± 0.04	2.075 ± 0.12
Trizol	1.755 ± 0.04	1.97 ± 0.03
-80° C	1.775 ± 0.04	2.06 ± 0.08
-20° C	1.765 ± 0.01	1.98 ± 0.01

Values are expressed in mean ± Standard deviation

3.3.3 RNA and cDNA integrity

The integrity of RNA and cDNA determine their efficiency to use for the next level of application. Figure 3 represents the agarose gel electrophoresis run with RNA (Figure 3A) and corresponding cDNA (Figure 3B) extracted from three month stored tissue in different storage conditions. Good RNA integrity was obtained from all four samples (Fresh, trizol, -80° C, -20° C). Similarly, cDNA synthesised from RNA extracted from different storage conditions also had high

Hence all these samples can use for further analysis. The integrity of three-month stored RNA and its cDNA conversion efficiency was demonstrated in Figure 4. The results highlighted that the RNA sample (Figure 4A: Lane 3) stored at -20° C shows degradation, whereas the sample kept at -80° C had acceptable integrity. Similarly, the cDNA of the sample stored at -80° C (Figure 4B: Lane 1, 3, 4) shows adequate cDNA integrity, whereas cDNA (Figure 4B: Lane 2) synthesised from -20° C stored RNA shows poor quality. Hence results confirmed that -80° C is an excellent storage condition for RNA.

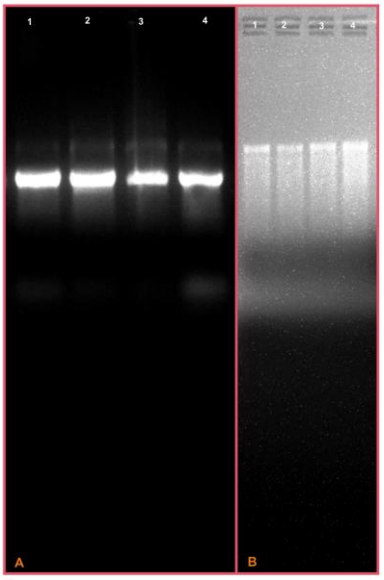

Figure 3: RNA and cDNA integrity in samples extracted from three month stored tissue; (**A**) RNA gel: Lane 1- RNA extracted from Fresh foot tissue, Lane 2- RNA extracted from -80° C stored tissue, Lane 3- RNA extracted from tissue stored in trizol and Lane 4- RNA extracted from -20° C stored tissue, (**B**) cDNA gel: Lane 1- cDNA from -20° C stored tissue RNA, Lane 2- cDNA from trizol stored tissue RNA, Lane 3- cDNA from -80° C stored tissue RNA and Lane 4- cDNA from fresh tissue RNA

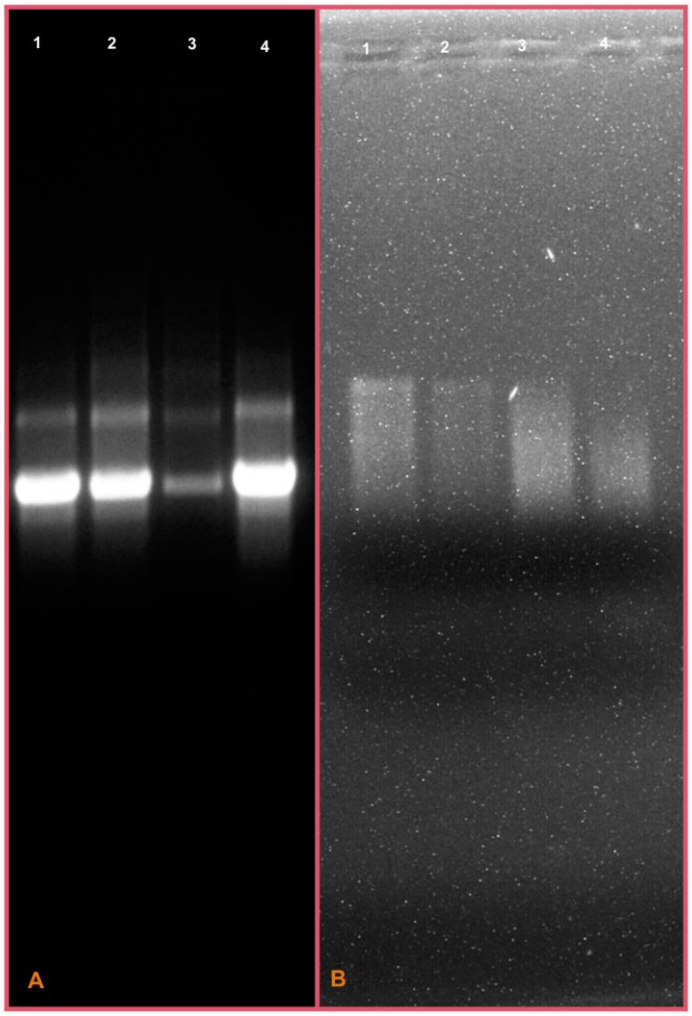

Figure 4: RNA and cDNA integrity in three month stored RNA sample; (**A**) RNA gel: Lane 1, 2, 4 - RNA stored in -80° C and Lane 3- RNA stored in -20° C, (**B**) cDNA gel: : Lane 1, 3, 4- cDNA from -80° C stored RNA and Lane 2- cDNA from -20° C stored RNA.

3.3.4 DNA sequencing

Two variants of *P. perna* foot protein 6 were obtained through DNA sequencing and designated as Ppfp-6(1) and Ppfp-6(2) respectively (Figure 5). In the designation first two letters indicate the genus and

species name (*Perna perna*), the second two letters denote the "foot protein", the first number indicates protein number (6) and the number put in the bracket denotes the variant number.

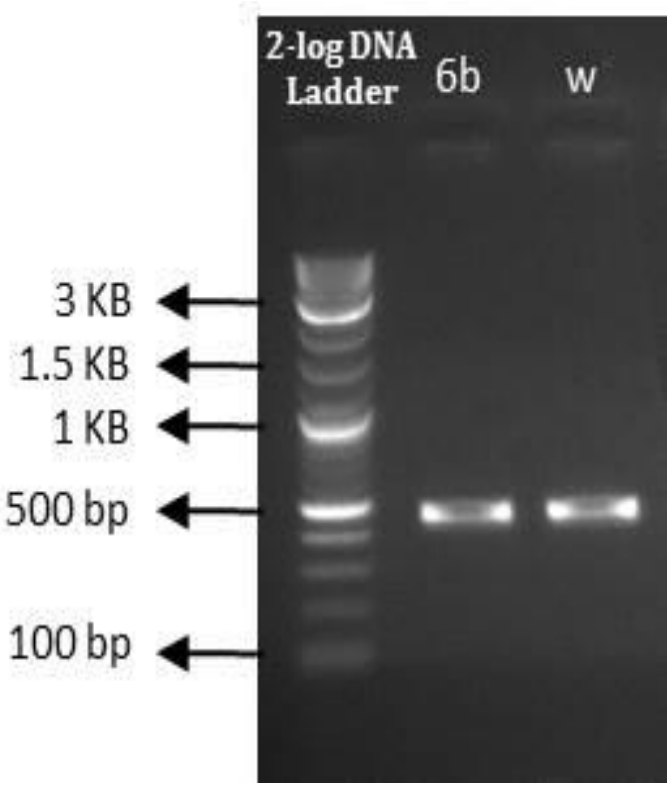

Figure 5: PCR gel showing two variants of *P. perna* foot protein 6, Lane 1- DNA ladder, Lane 2- Ppfp-6(1), Lane 3- Ppfp-6(2)

Ppfp-6(1)

The NCBI accession number of *P. perna* foot protein 6 variants 1 is OL623835, a 376 base pair length sequence with molecular mass 11.62 kDa. The molecular barcode of Ppfp-6(1) is represented in Figure 6. The cDNA sequence is as follows,

```
TTTTTATGATAAGTGCAGTTTGTATATATTTCTTTCTAGTCGGCCAG
ATACAGGCTGGTGTATACATACCATTTGAAAAACCCGGACAGTGTCC
AGTCACTCGCGGTATTACACCATGCGTTTGCATACCAGAAAACTCTG
AATGCAGGTTTGATTCTAACTGTCCTGGAGCCATGAAGTGTTGTGAT
TTTGGATGTGGCTGCAACAAGAGATGTGTTCCACCAGTGCCATCGCC
TTTACAATGTTATTACAATGGACAGTACTATCCTATCGGAGYTCATT
TCCCCGTCTGTTGATGGATGTAATACATRTTATTGCAACGATGATGG
GACCGTTATGTGTACTCTTAAAGCATGTGGTTATGGATACAAAAAAA
```

The Ppfp-6(1) open reading frame (ORF) contain 96 amino acids and the sequence is as follows,

```
MISAVCIYFFLVGQIQAGVYIPFEKPGQCPVTRGITPCVCIPENSEC
RFDSNCPGAMKCCDFGCGCNKRCVPPVPSPLQCYYNGQYYPIGVHFP
VC
```

Figure 6: Molecular barcode of Ppfp-6(1)

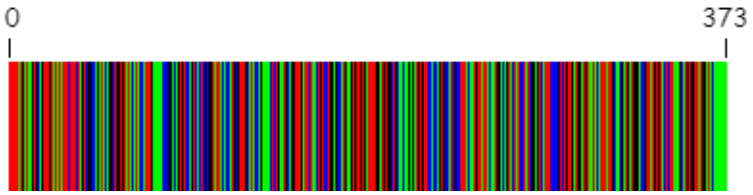

Ppfp-6(2)

The NCBI accession number of *P. perna* foot protein 6 variants 2 is OL623836, a 370 base pair length sequence with 11.45 kDa. The molecular barcode of Ppfp-6(1) is represented in Figure 7. The cDNA sequence is as follows,

```
TTATGATAAGTGCAGTTTGTATATATTTCTTTCTAGTCGGCCAGATA
CAGGCTGGTGTATACATACCATTTGAAAAACCCGGACAGTGTCCAGT
CACTCGCGGTATTACACCATGCGTTTGCATACCAGAAAACTCTGAAT
GCAGGTTTGATTCTAACTGTCCTGGAGCCATGAAGTGTTGTGATTTT
GGATGTGGCTGCAACAAGAGATGTGTTCCACCAGTGCCATCGCCTTT
ACAATGTTATTACAATGGACAGTACTATCCTATCGGAGYTCATTTCC
CGTYTGTTGATGGATGTAATACATGTTATTGCAACGATGATGGGACC
GTTATGTGTACTCTTAAAGCATGTGGTTATGGATACAAAAA
```

The Ppfp-6(2) open reading frame (ORF) contain 122 amino acids and the sequence is as follows,

```
MISAVCIYFFLVGQIQAGVYIPFEKPGQCPVTRGITPCVCIPENSEC
RFDSNCPGAMKCCDFGCGCNKRCVPPVPSPLQCYYNGQYYPIGVHFP
FVDGCNTCYCNDDGTVMCTLKACGYGYK
```

Figure 7: Molecular barcode of Ppfp-6(2)

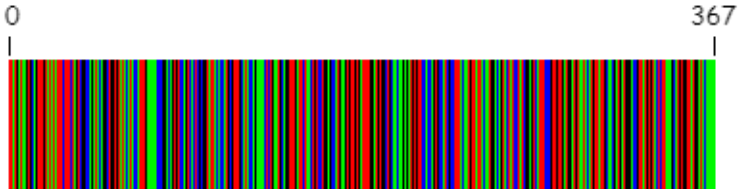

3.3.5 Conserved sequences

The sequence differences between the two variants of *P. perna* foot protein 6 and *P. viridis* foot protein 6 were represented in Figure 8. The variants of *P. perna* foot protein 6 had three conserved sequences located in the positions 4 to 286, 291 to 310, and 312 to 374, indicating that these sequence regions are common to both variants. Interspecies comparison of foot protein 6 indicated that *P. perna* and *P. viridis* foot protein 6 sequences had four conserved sequences located at positions, 68 to 89, 91 to 338, 353 to 372 and 374 to 434.

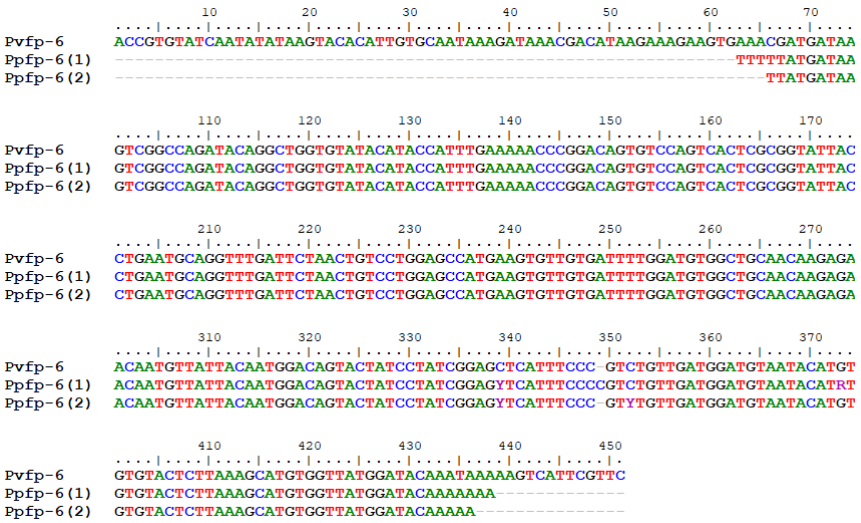

Figure 8: Multiple sequence alignment of foot protein 6 sequences from *P. perna* and *P. viridis*

3.3.6 Phylogenetic analysis

The phylogenetic tree represents the evolutionary relationship between foot protein 6 of different species of mussel (Figure 9). The tree reflected that the first divergence in foot protein 6 occured at the genus level. Two genera of mussels, *Perna* and *Mytilus* originate from a common ancestor. In the *Perna* genus, *P. viridis* foot protein 6 and *P. perna* foot protein 6 variant 2 (Ppfp-6(2) was sister groups and *P. perna* foot protein 6 variant 1 (Ppfp-6(1) have a different lineage. The *M. coruscus* foot protein 6 and its variant 9 was sister groups and they could not show common ancestry with other variants. *M. californianus* foot protein 6 variant 2 and 3 share common ancestries, but variant 1 has a different lineage.

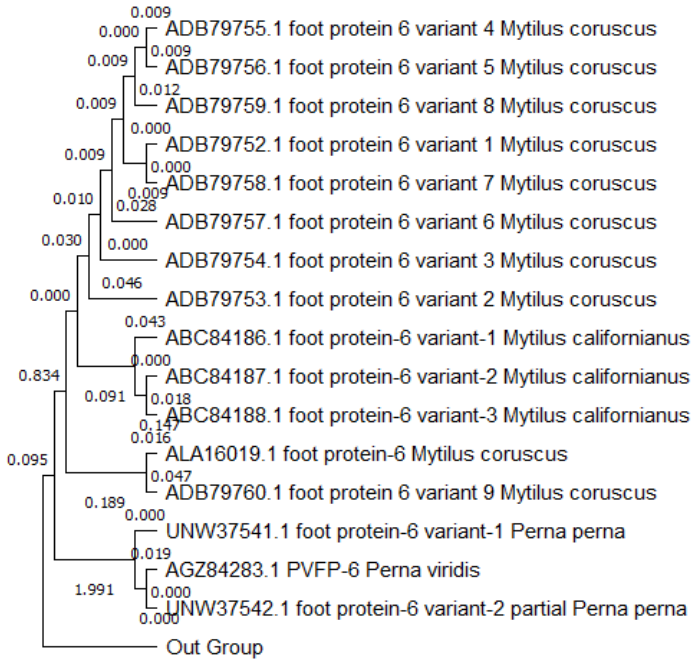

Figure 9: Phylogenetic tree of mussel foot protein 6

3.3.7 *Insilico* analysis of foot protein 6

3.3.7a Physio-chemical characterization

Table 5 shows the physio-chemical characterisation results of *P. perna* foot protein 6 variants 1 and 2. The Ppfp-6(1) contains 96 amino acids and among these, cysteine (13) and proline (12) were the highest in number followed by valine (9) and glycine (9) (Table 6). Similarly, Ppfp-6(2) contains 122 amino acids and cysteine (17), glycine (13), proline (12), valine (10) and tyrosine (9) are the abundant amino acids (Table 6). The theoretical isoelectric point of Ppfp-6(1) was 7.39 indicating the protein is basic and Ppfp-6(2) was 6.48 indicating the acidic nature of the protein. The instability index of both variants of foot protein 6 had a value above 40 suggesting that both variants are unstable. Similarly, the aliphatic index of both variants had a value above 50 indicating high thermal stability of proteins. The gravy value indicates the hydropathicity of proteins and in two variants of *P. perna* foot protein 6, the gravy value is positive indicating that all two proteins are hydrophobic.

Table 5: Physio-chemical characterisation of two variants of foot protein 6

Conditions	**Ppfp-6(1)**	**Ppfp-6(2)**
Total number of amino acids	96	122
Molecular weight	10.541 kDa	13.366 kDa
Theoretical pI	7.39	6.48
Atomic composition	$C_{467}H_{703}N_{119}O_{128}S_{15}$	$C_{580}H_{873}N_{149}O_{169}S_{20}$
Half-life in hours (in vivo)	Yeast – 20 hrs E. coli – 10 hrs	Yeast – 20 hrs E. coli – 10 hrs
Instability index	48.31	41.01
Aliphatic index	66.88	59.02
Gravy (Grand average of hydropathicity)	0.237	0.118
Subcellular localisation	Extracellular	Extracellular
Molecular Function	Peptidase inhibitor activity	Peptidase inhibitor activity

Table 6: Amino acid composition in two variants of foot protein 6

Amino acids	**Ppfp-6(1)**		**Ppfp-6(2)**	
	Number	**Percentage**	**Number**	**Percentage**
Alanine (A)	3	3.1	4	3.3
Arginine (R)	3	3.1	3	2.5
Asparagine (N)	4	4.2	6	4.9
Aspartic acid (D)	2	2.1	5	4.1
Cysteine (C)	13	13.5	17	13.9
Glutamine (Q)	5	5.2	5	4.1
Glutamic acid (E)	3	3.1	3	2.5
Glycine (G)	9	9.4	13	10.7
Histidine (H)	1	1.0	1	0.8
Isoleucine (I)	7	7.3	7	5.7
Leucine (L)	2	2.1	3	2.5
Lysine (K)	3	3.1	5	4.1
Methionine (M)	2	2.1	3	2.5
Phenylalanine (F)	6	6.2	7	5.7
Proline (P)	12	12.5	12	9.8
Serine (S)	4	4.2	4	3.3
Threonine (T)	2	2.1	5	4.1
Tryptophan (W)	0	0	0	0
Tyrosine (Y)	6	6.2	9	7.4
Valine (V)	9	9.4	10	8.2
Pyrrolysine (O)	0	0	0	0
Selenocysteine (U)	0	0	0	0

3.3.7b Signal peptide prediction

The two variants of *P. perna* foot protein 6 contain standard secretory signal peptides (Figure 10) transported by the Sec translocon and cleaved by Signal Peptidase I (Sec/SPI) and it was a 17 amino acid sequence possesses three regions, namely N-terminal N-region, middle

H-region and C-terminal C-region. In both variants, the first two amino acid residues come in N-region, the middle hydrophobic H-region contains 10 residues and the C-region holds 5 residues. The end of the C-region (Position 17) was considered a cleavage site (CS) and later sequences were called mature proteins.

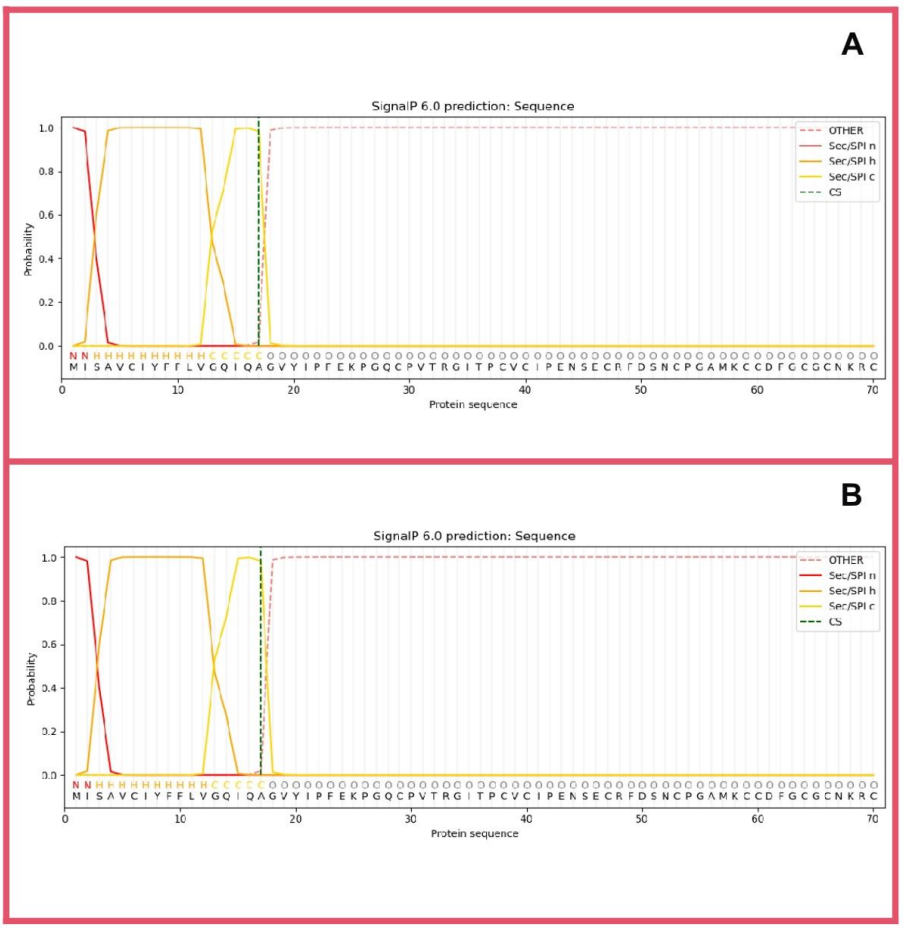

Figure 10: Signal peptide predictions of two variants of *Perna perna* foot protein 6; (**A**) signal peptide of Ppfp-6(1) (**B**) signal peptide of Ppfp-6(2)

3.3.7c Secondary structure prediction

The secondary structure prediction results of two variants of *P. perna* foot protein 6 (Table 7, Figure 11) showed that random coils were the more predominant structure found in both variants followed by extended strand and the alpha helix was the least abundant structure. Variant 2 had more secondary structures than variant 1.

Table 7: Secondary structure prediction of two variants of foot protein 6

Structure	Ppfp-6(1)		Ppfp-6(2)	
	Number	Percentage	Number	Percentage
Alpha helix (Hh)	4	4.17	7	5.74
Extended strand (Ee)	18	18.75	34	27.87
Beta turn (Tt)	6	6.25	12	9.84
Random coil (Cc)	68	70.83	69	56.56

Figure 11: Secondary structure in two variants of *P. perna* foot protein 6; (**A**) secondary structure of Ppfp-6(1) (**B**) secondary structure of Ppfp-6(2)

3.3.7d Tertiary structure prediction

Figure 12 represents the tertiary structure of two variants of *P. perna* foot protein 6. The validation of the tertiary structure was done based on the Ramachandran plot, ERRAT value and QMEAN value. Figure 13 and 14 were Ramachandran plot of variant 1 and 2 respectively. Similarly, Table 8 and 9 shows the validation results of variant 1 and 2. In a good protein model, the QMEAN value must be greater than -4.0, the ERRAT value should be above 80 and 90% of residues in the Ramachandran plot occupied at the core and additional allowed region. QMEAN value of both protein variant models was -1.02 and -0.58 respectively and ERRAT value of variant 1 was 81.8182 and variant 2 was 90.90. The Ramachandran plot (Figure 13 & 14) of the two variants shows that 100% of the residues appear in the core and additional allowed regions; hence the models of both variants are extremely stable.

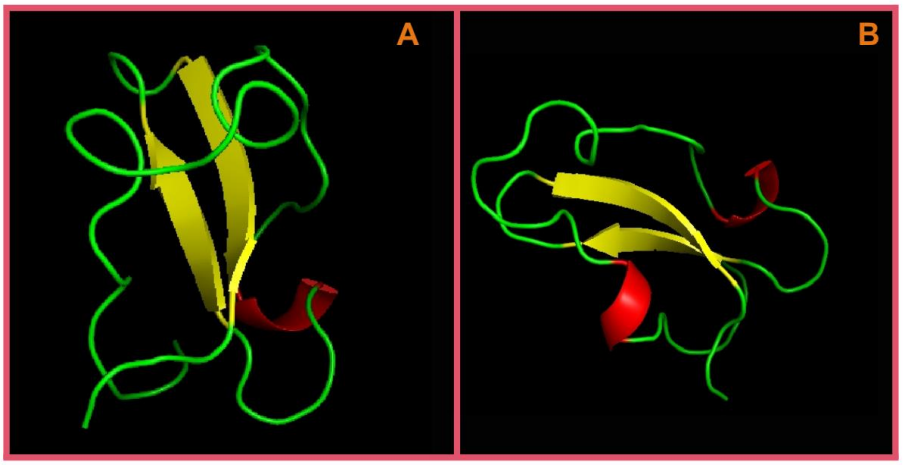

Figure 12: Tertiary structure of two variants of foot protein 6; (**A**) tertiary structure of Ppfp-6(1) (**B**) tertiary structure of Ppfp-6(2)

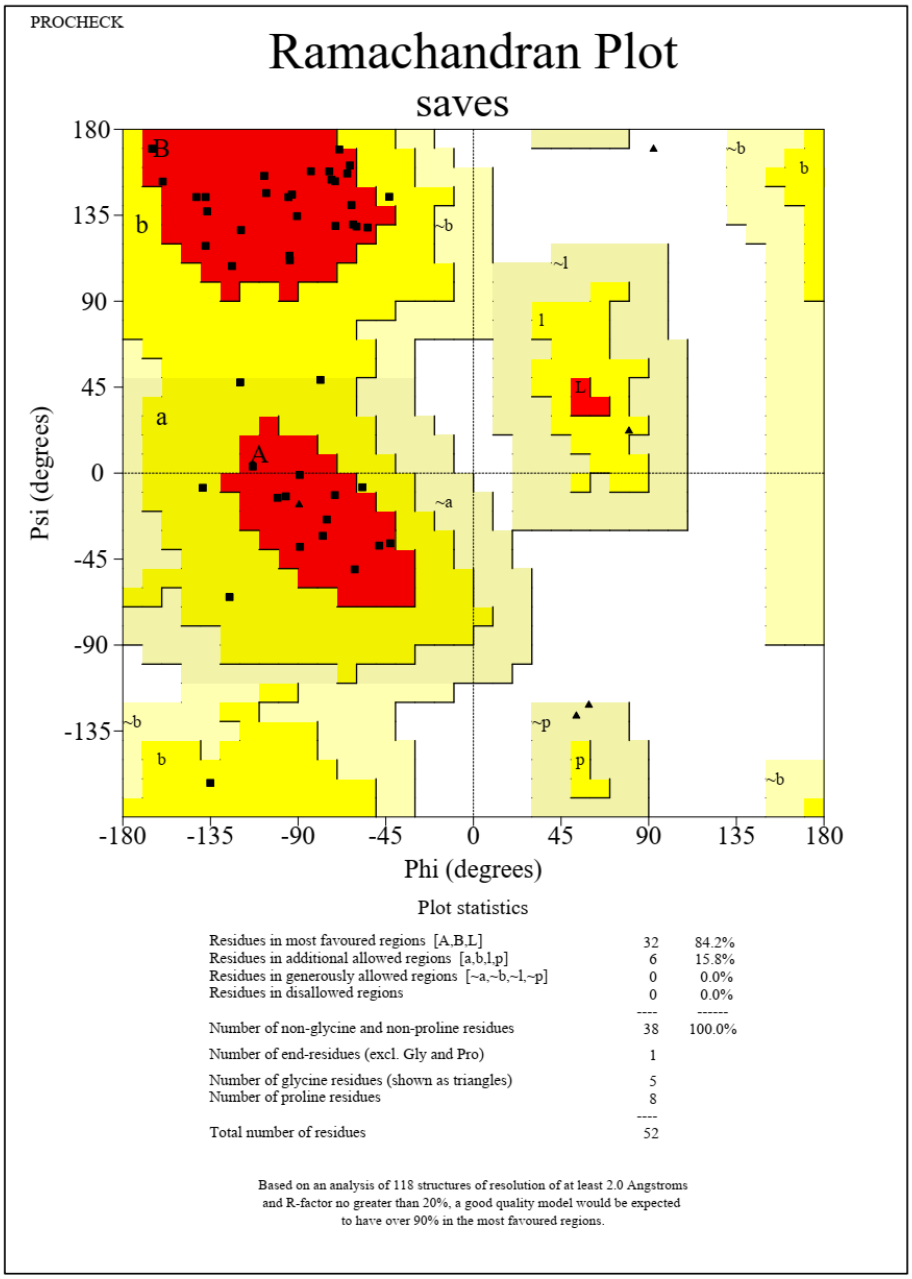

Plot statistics

Residues in most favoured regions [A,B,L]	32	84.2%
Residues in additional allowed regions [a,b,l,p]	6	15.8%
Residues in generously allowed regions [~a,~b,~l,~p]	0	0.0%
Residues in disallowed regions	0	0.0%
Number of non-glycine and non-proline residues	38	100.0%
Number of end-residues (excl. Gly and Pro)	1	
Number of glycine residues (shown as triangles)	5	
Number of proline residues	8	
Total number of residues	52	

Based on an analysis of 118 structures of resolution of at least 2.0 Angstroms and R-factor no greater than 20%, a good quality model would be expected to have over 90% in the most favoured regions.

saves_01.ps

Figure 13: Ramachandran plot of foot protein 6 variant 1

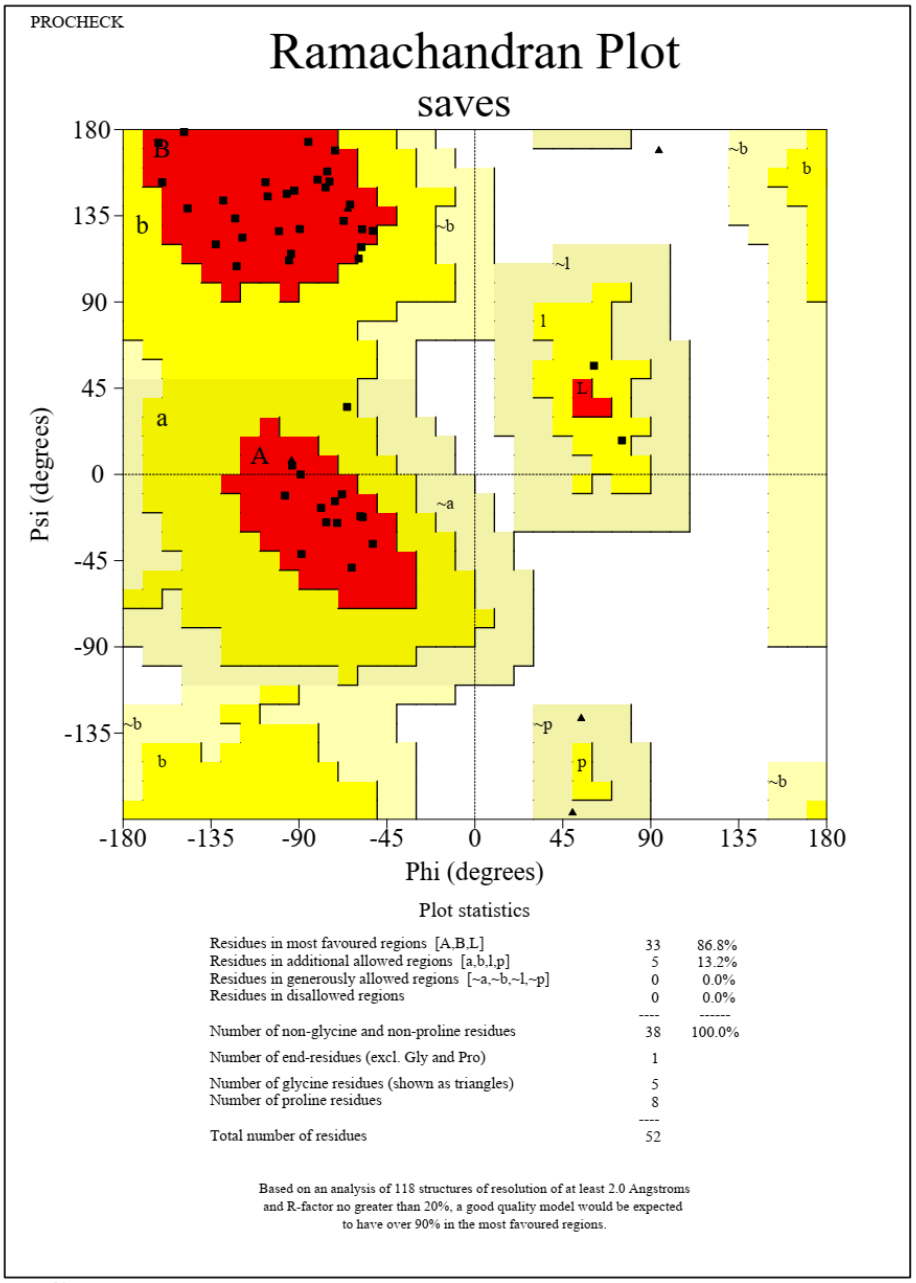

Figure 14: Ramachandran plot of foot protein 6 variant 2

Table 8: Teritiary structure validation results of Ppfp-6(1)

Parameter	Value
Residues in most favoured regions of Ramachandran plot	84.2%
Residues in additional allowed regions of Ramachandran plot	15.8%
Residue in generously allowed regions of Ramachandran plot	0%
Residues in disallowed regions of Ramachandran plot	0%
ERRAT value	81.8182
QMEAN value	-1.02

Table 9: Teritiary structure validation results of Ppfp-6(2)

Parameter	Value
Residues in most favoured regions of Ramachandran plot	86.8%
Residues in additional allowed regions of Ramachandran plot	13.2%
Residue in generously allowed regions of Ramachandran plot	0%
Residues in disallowed regions of Ramachandran plot	0%
ERRAT value	90.90
QMEAN value	-0.58

3.3.7e Prediction of motif, domain and superfamily

The motif, domain and family prediction results of the foot protein 6 two variants were tabulated in Tables 10 and 11. Here, variant 2 had an extra motif and domain called Pacifastin inhibitor (LCMII) than variant 1. However, the two variants belong to the superfamily called Elafin-like superfamily.

Table 10: Functional Motif, Domain and Family Prediction- Ppfp-6(1)

Structure	**Name**	**No. of sites**	**Amino acid residues**	**E value**
Motif	*Cysteine-rich region profile*	1	38-117	0.0044
	WAP-type 'four-disulfide core' domain profile	1	22-74	$2.8e^{-08}$
Domain	WAP-type 'four-disulfide core' domain	4	22-74, 22-31, 46-53, 65-73	1.68e-07
Superfamily	Elafin-like superfamily			

Table 11: Functional Motif, Domain and Family Prediction- Ppfp-6(2)

Structure	**Name**	**No. of sites**	**Amino acid residues**	**E value**
Motif	*Cysteine-rich region profile*	1	38-70	0.0078
	WAP-type 'four-disulfide core' domain profile	1	22-74	$2.8e^{-08}$
	Pacifastin inhibitor (LCMII)	1	95-118	2.9e-08
Domain	WAP-type 'four-disulfide core' domain	4	22-74, 22-31, 46-53, 65-73	4.70e-07
	Pacifastin inhibitor (LCMII)	1	95-122	5.19e-04
Superfamily	Elafin-like superfamily			

3.3.7f Posttranslational modifications predictions

Prediction of phosphorylation sites

The phosphorylation site prediction results of two variants of foot protein 6 were tabulated in Tables 12 and 13. Here, Ppfp-6(1) had two serine and single threonine and tyrosine phosphorylation sites. Similarly the Ppfp-6(2) had a total of 7 phosphorylation sites including three threonine, two serine and two tyrosine residues.

Table 12: Phosphorylation site of Serine, Threonine and Tyrosine residue in Ppfp-6(1)

Residue	Amino acid Location	Score	Kinase
Threonine (T)	36	0.896	Unspecified
Serine (S)	51	0.506	cGMP-dependent protein kinase or protein kinase G (PKG)
Serine (S)	76	0.646	Cyclin dependent kinase 5 (cdk5)
Tyrosine (Y)	86	0.657	Unspecified

Table 13: Phosphorylation site of Serine, Threonine and Tyrosine residue in Ppfp-6(2)

Residue	Amino acid Location	Score	Kinase
Threonine (T)	36	0.896	Unspecified
Serine (S)	51	0.506	cGMP-dependent protein kinase or protein kinase G (PKG)
Serine (S)	76	0.646	Cyclin dependent kinase 5 (cdk5)
Tyrosine (Y)	86	0.657	Unspecified
Tyrosine (Y)	103	0.862	Unspecified
Threonine (T)	109	0.540	Protein kinase C (PKC)
Threonine (T)	113	0.838	Protein kinase C (PKC)

Prediction of glycosylation sites

The glycosylation site prediction results (Table 14) exhibited that Ppfp-6(1) had 4 glycosylation sites which include two serine residues and two asparagine residues. Similarly, Ppfp-6(2) had three glycosylation sites including two serine and one asparagine residue.

Table 14: Prediction of glycosylation sites in Ppfp6-(1) and Ppfp6-(2)

Ppfp6-(1)		**Ppfp6-(1)**	
Residue	**Amino acid Location**	**Residue**	**Amino acid Location**
Serine (S)	3	Serine (S)	3
Serine (S)	45	Serine (S)	45
Asparagine (N)	52	Asparagine (N)	52
Asparagine (N)	83		

3.3.7g Prediction of antioxidant and metal chelating peptides

The antioxidant and metal-chelating peptide prediction results (Tables 15, 16, 17, 18) of two variants of foot protein 6 indicated that both variants had excellent antioxidant peptides but the metal-chelating activity of peptides was reduced. The free radical scavenging activity (FRS) and metal chelating activity score always from 0 to 1. The value above 0.5 indicates that the peptide had good antioxidant activity. The variant Ppfp-6(1) had a total of 15 antioxidant peptides and among them, 13 had an FRS value above 0.5. Similarly, 15 metal chelating peptides are present in Ppfp-6(1), but all had CHEL score below 0.5. In the case of Ppfp-6(2), 21 antioxidant and 21 metal-chelating peptides were recognized. Here 19 had superior antioxidant activity, whereas all peptides had poor metal chelating activity.

Table 15: Free radical scavenging peptides of Ppfp-6(1)

# FRS score		
0.71636528	PPVPSPLQCYYNGQYYPIGV	Sequence
0.70660526	VPPVPSPLQCYYNGQYYPIG	Sequence
0.70333326	PVPSPLQCYYNGQYYPIGV	Sequence
# ----------		
0.57952726	IYFFLVGQIQAGVYIPFEKP	Sequence
0.56950098	VGQIQAGVYIPFEKPGQCPV	Sequence
0.5631187	CIYFFLVGQIQAGVYIPFEK	Sequence
# ----------		
0.53067589	MISAVCIYFFLVGQIQAGV	Sequence
0.52738929	MISAVCIYFFLVGQIQAG	Sequence
0.52385694	ISAVCIYFFLVGQIQAG	Sequence
# ----------		
0.52990437	RCVPPVPSPLQCYY	Sequence
0.52502048	KRCVPPVPSPLQCYYNG	Sequence
0.51929617	CNKRCVPPVPSPLQCYYNGQ	Sequence
# ----------		
0.50431842	PVTRGITPCVCIPENSECRF	Sequence
0.48796406	VTRGITPCVCIPENSECRF	Sequence
0.48003149	ENSECRFDSNCPGAMKCCDF	Sequence
#		

Table 16: Metal chelating peptides of Ppfp-6(1)

# CHEL score		
0.27846742	CVPPVPSPLQ	Sequence
0.27707002	RCVPPVPSPLQ	Sequence
0.27696991	NKRCVPPVPSPLQ	Sequence
# ----------	----------	
0.25820005	IYFFLVGQIQ	Sequence
0.25358707	CIYFFLVGQIQA	Sequence
0.25046948	IYFFLVGQIQA	Sequence
# ----------	----------	
0.25762209	ECRFDSNCPGAM	Sequence
0.25354016	SECRFDSNCPGAMK	Sequence
0.25030711	TPCVCIPENSECRFD	Sequence
# ----------	----------	
0.25474861	IPFEKPGQCP	Sequence
0.2466418	IPFEKPGQCPV	Sequence
0.24201325	YFFLVGQIQA	Sequence
# ----------	----------	
0.23344752	PVPSPLQCYYNGQ	Sequence
0.231114	PPVPSPLQCYYNGQY	Sequence
0.22837465	RCVPPVPSPLQCYYNGQYY	Sequence

Table 17: Free radical scavenging peptides of Ppfp-6(2)

# FRS score		
0.71636528	PPVPSPLQCYYNGQYYPIGV	Sequence
0.7066052	VPPVPSPLQCYYNGQYYPIG	Sequence
0.70333326	PVPSPLQCYYNGQYYPIGV	Sequence
# ----------	----------	
0.57952726	IYFFLVGQIQAGVYIPFEKP	Sequence
0.56950098	VGQIQAGVYIPFEKPGQCPV	Sequence
0.5631187	CIYFFLVGQIQAGVYIPFEK	Sequence
# ----------	----------	
0.53909814	FPFVDGCNTCYCNDDGTVM	Sequence
0.53729314	FPFVDGCNTCYCNDDGTV	Sequence
0.53711426	PFVDGCNTCYCNDDGTV	Sequence
# ----------	----------	
0.53387737	YPIGVHFPFVDGC	Sequence
0.52752697	NGQYYPIGVHFPFVDGCNT	Sequence
0.52024275	GQYYPIGVHFPFVDGCNTC	Sequence
# ----------	----------	
0.53067589	MISAVCIYFFLVGQIQAGV	Sequence
0.52738929	MISAVCIYFFLVGQIQAG	Sequence
0.52385694	ISAVCIYFFLVGQIQAG	Sequence
# ----------	----------	
0.52990437	RCVPPVPSPLQCYY	Sequence
0.52502048	KRCVPPVPSPLQCYYNG	Sequence
0.51929617	CNKRCVPPVPSPLQCYYNGQ	Sequence
# ----------	----------	
0.50431842	PVTRGITPCVCIPENSECRF	Sequence
0.48796406	VTRGITPCVCIPENSECRF	Sequence
0.48003149	ENSECRFDSNCPGAMKCCDF	Sequence
# ----------	----------	

Table 18: Metal chelating peptides of Ppfp-6(2)

# CHEL score		
0.27846742	CVPPVPSPLQ	Sequence
0.27707002	RCVPPVPSPLQ	Sequence
0.27696991	NKRCVPPVPSPLQ	Sequence
# ----------	----------	----------
0.25820005	IYFFLVGQIQ	Sequence
0.25358707	CIYFFLVGQIQA	Sequence
0.25046948	IYFFLVGQIQA	Sequence
# ----------	----------	----------
0.25762209	ECRFDSNCPGAM	Sequence
0.25354016	SECRFDSNCPGAMK	Sequence
0.25030711	TPCVCIPENSECRFD	Sequence
# ----------	----------	----------
0.25474861	IPFEKPGQCP	Sequence
0.2466418	IPFEKPGQCPV	Sequence
0.24201325	YFFLVGQIQA	Sequence
# ----------	----------	----------
0.25143933	PIGVHFPFVD	Sequence
0.24653617	PIGVHFPFVDG	Sequence
0.23941955	YPIGVHFPFVDG	Sequence
# ----------	----------	----------
0.22833292	CNDDGTVMCTLK	Sequence
0.22735119	NDDGTVMCTL	Sequence
0.22545798	NDDGTVMCTLK	Sequence
# ----------	----------	----------
0.22666101	YPIGVHFPFVDGC	Sequence
0.22547705	PIGVHFPFVDGC	Sequence
0.21921478	IGVHFPFVDGC	Sequence

3.3.7h Metal ion binding properties prediction

The binding sites of different metal ions on Ppfp-6(1) were tabulated in Table 19. Fe^{2+}, Fe^{3+}, Mg^{2+}, Cd^{2+}, Ni^{2+}, Cu^{+}, Co^{2+}, Ca^{2+}, Mn^{2+} was the major metal ions bind with Ppfp-6(1). Cu^{+} had more binding pockets and Mg^{2+} had the least binding pockets but more binding scores were found in Mg^{2+}. The Ppfp-6(2) metal binding pockets were predicted in Table 20. Here, Fe^{3+}, Fe^{2+}, Mg^{2+}, Cd^{2+}, Ni^{2+}, Cu^{+}, Cu^{2+}, Ca^{2+} are the major metals bind with Ppfp-6(2). Cu^{+} had more binding pockets but binding strength was high in Cd^{2+} and the least binding pockets were recorded in Ni^{2+}.

Table 19: Metal binding sites of Ppfp-6(1)

Residue number	Amino acid	Score
Fe^{3+}		
29	CYS	2.542
47	CYS	2.613
53	CYS	2.613
60	CYS	2.542
64	CYS	2.648
66	CYS	2.648
70	CYS	2.104
Mg^{2+}		
32	THR	3.681
68	LYS	3.681
Cd^{2+}		
47	CYS	2.790
50	ASP	1.601
53	CYS	2.790
59	CYS	2.790
64	CYS	2.009
66	CYS	2.009
70	CYS	2.790
Fe^{2+}		
47	CYS	2.175
53	CYS	2.175
58	LYS	2.175
59	CYS	2.175
Ni^{2+}		
64	CYS	2.205
65	GLY	2.205
66	CYS	2.205
Cu^{+}		
29	CYS	1.320
32	THR	0.882
46	GLU	0.952
47	CYS	1.908
49	PHE	0.764
53	CYS	1.908

54	PRO	0.968
59	CYS	0.764
60	CYS	1.320
64	CYS	2.218
65	GLY	2.218
66	CYS	2.218
69	ARG	1.908
70	CYS	1.908
71	VAL	1.289
Co^{2+}		
43	GLU	4.252
64	CYS	3.585
66	CYS	4.252
Cu^{2+}		
52	ASN	1.937
53	CYS	1.937
59	CYS	1.937
70	CYS	1.937
Ca^{2+}		
28	GLN	1.863
29	CYS	1.863
52	ASN	2.403
53	CYS	2.403
59	CYS	2.403
70	CYS	2.403
Mn^{2+}		
61	ASP	2.479
62	PHE	2.479
67	ASN	2.479

Table 20: Metal binding sites of Ppfp-6(2)

Residue number	Amino acid	Score
Fe^{3+}		
29	CYS	2.740
45	SER	2.426
47	CYS	2.706
53	CYS	2.706
59	CYS	1.908
60	CYS	2.740
70	CYS	2.426
Mg^{2+}		
24	GLU	2.813
25	LYS	2.238
33	ARG	2.466
50	ASP	2.813
53	CYS	2.238
59	CYS	2.466
61	ASP	2.653
Cd^{2+}		
47	CYS	4.041
53	CYS	4.041
60	CYS	4.041
Fe^{2+}		
47	CYS	2.175
53	CYS	2.175
58	LYS	2.175
59	CYS	2.175
Ni^{2+}		
29	CYS	2.240
60	CYS	2.240
Cu^{+}		
29	CYS	1.499
35	ILE	1.027
38	CYS	1.027
46	GLU	1.687
47	CYS	1.816

51	SER	1.816
53	CYS	1.976
54	PRO	1.451
59	CYS	2.399
60	CYS	2.399
70	CYS	2.399
71	VAL	1.873
Cu^{2+}		
28	GLN	1.863
29	CYS	1.863
52	ASN	2.403
53	CYS	2.403
59	CYS	2.403
70	CYS	2.403
Ca^{2+}		
28	GLN	1.863
29	CYS	1.863
52	ASN	2.403
53	CYS	2.403
59	CYS	2.403
70	CYS	2.403

DISCUSSION

RNA content in an organism may vary with environmental, physiological and genetic factors. The concept of a biobank aims to store tissue for research or diagnostic purposes with intact morphology, protein, DNA and RNA content. RNA is a very delicate molecular component; hence it has greater susceptibility to degradation. Therefore, the purity and integrity of RNA are very crucial for further analysis such as real-time quantitative PCR, cDNA library construction, expression microarray, RNA mapping etc. (Botling & Micke, 2010). Recombinant production of mussel foot proteins resolves the low productivity issue. RNA extraction is the pioneering step of recombinant DNA technology. Huang et al. (2017) studied the effect of storage temperature and duration of blood samples on DNA and RNA qualities. Their results concluded that storing blood samples at low temperatures dramatically damages RNA and extracted RNA storage at low temperatures does not prevent degradation. The present study results of RNA extraction from different storage conditions and cDNA synthesis indicated that superior quality RNA and cDNA were extracted from all the samples and also RNA and cDNA integrity were adequate. The high quantity of RNA was extracted from fresh and -80° C stored tissue. Similar results were obtained in Auer et al. (2014) study on human tissue specimens. They reported that long-term human tissue storage at -80° C provides good quality RNA than it stored in vapour phase liquid nitrogen. The matching results were also published in Andreasson et al. (2013) study on the long-term -80° C storage effect of RNA from endocrine tissue. Similarly, the optimum storage

time and temperature for maintaining RNA integrity in the fish liver was studied by Vehniainen et al. (2019) revealed that storage at -20° C for 6 months preserves RNA integrity.

The present results show that samples except RNA stored at -20° C for three months had good integrity; the RNA integrity is essential for further studies and should be maintained. The tissue contains a large amount of hydrolytic RNase enzymes which cleave RNA. Some are active at low-temperature conditions; hence base or enzyme-catalysed hydrolysis of RNA occurs continuously (Fleige & Pfaffl, 2006; Fabre et al., 2014). This may be the reason for the degradation of RNA stored at -20°C samples. Mutter et al. (2004) studied RNA integrity after storing at -20° C for 2 months. Their results imply that some ribonuclease can cleave frozen RNA at -20° C. High-quality RNA is free from proteins, RNases, and DNA (Fleige & Pfaffl, 2006). The quality of RNA depends on several factors such as the source of RNA, RNA isolation procedure, sampling techniques etc. In addition, RNA quality may be compromised in stored for an extended period or under less-than-ideal conditions. The current RNA integration study revealed that storage of foot tissue in trizol does not significantly changes extraction yield and purity and also which is expensive. Hence storage of tissue and RNA at -80°C is a more efficient and cost-effective strategy.

P. perna is an unexplored adhesive protein resource and this present study was a pioneer attempt at *P. perna* foot protein gene sequencing and its further investigations. Mussel shows natural and induced

polyploidy. Polyploidy causes an increasing number of chromosomes in an organism and leads to variation in gene sequences in each chromosome (Piferrer et al., 2009). In the present study, two variants of foot protein 6 were obtained and sequenced. Previously, three variants of *M. californianus*, 10 variants of *M. coruscus* and single mussel foot protein 6 from *P. viridis* were reported (Anand & Vardhanan, 2020). The conserved domain analysis and phylogenetic analysis results exhibited that *P. perna* foot protein sequences are highly similar to *P. viridis*. Clear genus-level DNA sequence changes were observed in phylogenetic analysis. From a common ancestor, two genera such as *Perna* and *Mytilus* were separated and each genus had its own unique foot protein gene sequences. Mussels foot protein phylogenetic analysis was studied by Anand and Vardhanan (2020) and their results emphasized that *P. viridis* hold in a single clade without sister taxa and *M. coruscus* foot protein 6 and it's variant 9 share the last common ancestry.

Zhao and Waite (2006b) studied *M. californianus* foot protein 6 and their results highlighted that foot protein 6 is an 11.6 kDa molecular weight protein with basic PI. Similarly, Nicklish et al. (2013) synthesised recombinant foot protein 6 variant 1 from *M. californianus*. According to their results, the molecular mass of Mcfp-6 variant 1 gets increased to 13.6 kDa with basic PI. The computational analysis results of three variants of *M. californianus* had molecular weights of 13.92 kDa, 13.91 kDa and 13.82 kDa respectively with basic PI in each. Similarly, all variants of foot protein 6 from *M. coruscus* had basic PI but variants 1 to 6 had a molecular

weight of around 14 kDa and variants 7 to 9 had a molecular weight of around 11 kDa. Whereas, *P. viridis* foot protein 6 had an acidic PI (6.48) with a molecular mass of 13.26 kDa (Anand and Vardhanan, 2020). In the present results, variant 2 of foot protein 6 shows high similarity with molecular mass and PI of *P. viridis*. These results revealed that foot protein genes show gene sequence specificity.

The Ppfp-6(1) was 96 amino acid length protein and the Ppfp-6(2) had 122 amino acids. Among these, cysteine, proline, glycine and valine are the predominant amino acids. The study of Zhao and Waite (2006b) reported that *M. californianus* foot protein 6 is 121 amino acid sequence length protein dominated by tyrosine, glycine and aspartate. The computational analysis of *P. viridis* foot protein 6 revealed that they were abundant with cysteine, glycine and proline. Cysteine is the more predominant amino acid in *P. perna* and *P. viridis* foot protein 6. The cysteine undergoes ionization in a basic solution to form thiolate anions (Burns et al., 2016). Hence, because of the high cysteine content in foot protein 6, it was considered a thiol-rich protein. Cysteine-thiol moiety found in foot protein 6 is involved in antioxidant activity. According to Yu et al. (2011), the thiol group found in the mfp-6 act as a reducing agent for dopaquinone formed in mfp-3 and enables further adsorption of mfp-3. The cysteine residue is also involved in the stabilization of the tertiary and quaternary structure of proteins through disulphide bonds (Burns et al., 2016). The amino acid tyrosine plays a critical role in foot proteins because post-translational modification of tyrosine forms DOPA. The study by Zhao and Waite (2006b) reported that foot protein 6 had high tyrosine content but

DOPA content was less. The phenol groups of intact tyrosine residues in the mfp-6 act as proton and electron reservoirs for the antioxidant activity of the protein. Similarly, tyrosine found in mfp-6 is involved in some hydrophobic interactions with hydrophobic surfaces (Nicklisch et al., 2013).

Signal peptides are 15 to 30 amino acid long short peptides located at the N-terminal extension of newly formed protein and involved in protein translocation. After the protein translocation, the enzyme signal peptidase cleaves the signal peptide at the universally conserved cleavage site and released mature protein (Creuzenet et al., 1993; Kapp et al., 2009). In the present study, two variants of *P. perna* foot protein 6 had 17 amino acid length secretory signal peptides. Anand and Vardhanan (2020) reported that *P. viridis* foot protein 6 had 19 amino acid length signal peptides. *P. perna* foot protein 6 two variants had Sec-dependent signal peptides. The difference between Sec and Tat type signal peptides includes, (1) the N-terminal region of Tat had more amino acids than Sec (2) the Sec had weaker hydrophobicity at the hydrophobic region than Tat (3) the N-terminus of Tat had double arginine ('RR') residue, which was absent in Sec (Liu et al., 2021). The signal peptides are actively involved in the transmembrane transport of proteins; hence changes or mutation in single amino acid negatively affects protein translocation. The major target of the protein expression system was the secretion of recombinant protein into the growth medium, which was undertaken by signal peptides. Signal peptide-mediated secretory production of target protein help to

decrease production cost because cell disruption was not required (Freudl, 2018).

The pattern of hydrogen bonding formed between atoms of the polypeptide backbone is determining the secondary structure of the protein (Sneha & Doss, 2016). Among secondary structures, α-helix and β-strands are most commonly found in nature (Lyu et al., 2021). In *P. perna* two variants of foot protein 6, strands are more abundant than the helix. The most abundant secondary structure in the two variants of foot protein 6 is random coils, which act as a connecting link between strands and helix. Secondary structure plays a critical role in determining protein tertiary structure and protein folding, which is considered as intermediate between primary and tertiary structure. Furthermore, using a minimum energy conformation based on entropy, protein folding is a thermodynamic process that produces a three-dimensional structure. The 3D structure of the protein is built using homology modelling, also known as comparative modelling, which compares the input protein sequence to the template protein sequence (Kumar et al., 2019). In protein structure prediction studies, the Ramachandran plot is used to determine the stereochemical quality of the structure. The plot analysed the Phi (φ) and Psi (ψ) torsion angles for each residue in the protein. In the Ramachandran plot, the residues in favoured and additional allowed regions have no or negligible steric clashes, whereas generously allowed and disallowed regions have steric hindrances. Hence, for better stereochemical quality of protein structure, 90% of the residues must include in allowed regions (Agnihotry et al., 2022). In *P. perna* mussel foot protein 6 two

variants, 100% of residues included in the allowed region. In the plot, red regions are the core or most favoured regions here steric hindrances are absent. The yellow areas marked "additionally allowed" correspond to conformations that might be feasible. The beige colour boxes represent generously allowed regions and the white colour indicated sterically disallowed regions for all amino acids except glycine because it lacks a side chain (Hollingsworth & Karplus, 2010; Elsliger & Wilson, 2012).

Identification of motifs, domains and superfamily of proteins is a critical part of sequence characterisation. The motif is a small region of protein sequence with a distinct function. Different proteins share the same motif with similar functions. Similarly, an independently functioning specific structural unit of protein is called domain (Xiong, 2006). In *P. perna*, both variants of foot protein 6 contain common motifs called cysteine-rich region profile and WAP-type four disulphide core domain profile and variant 2 contains a unique motif called pacifastin inhibitor (LCMII). Cysteine-rich motifs help to maintain structural integrity through Disulphide Bridge. Similar cysteine-rich motifs are found in *M. edulis* foot protein 2. Like foot protein 6, foot protein 2 also contains low DOPA content and it stabilizes plaque matrix by re-arrangement of disulphide bond to form inter-molecular cross-links (Rzepecki et al., 1992). The two variants of foot protein 6 from *P. perna* had four WAP-type four disulphide core domains. WAP (whey acidic protein) four-disulfide core domain contains proteins found in vertebrates and invertebrates, plus some cereal plants and bacteria. WAP domains are widely distributed and

their tightly coiled confirmations provide stability and strength to proteins. The WAP domain showed a wide range of functions include, act as an antisepsis and proteinase inhibitor, calcium transport or deposition etc. The presence of the WAP domain is also reported in proteins found in mollusc shells such as green lip abalone *Haliotis laevigata*, and Mediterranean mussel *M. galloprovincialis* (Smith, 2011). The study of Algrain et al., 2022 reported that sea star footprint protein 8 (sfp8), sfp3 and sfp15 contain several WAP domains which provide stability through multiple intramolecular disulphide bridges in harsh physical conditions and also play a critical role in antibacterial activity. Genomic and transcriptomics study in green mussel *P. viridis* by Inoue et al., 2021 observed that increased number of WAP-type disulfide core domains found in the *P. viridis* genome. According to their conclusions WAP domain had proteinase inhibitor activity which helps to protect byssus protein from proteinases until the crosslinking and polymerisation are complete. Like the WAP-type disulfide core domain, the pacifastin inhibitor (LCMII) domain found in variant 2 is cysteine-rich and had serine proteinase inhibitor activity which helps to avoid unwanted proteolysis. The above-described findings suggested that the WAP domain and pacifastin inhibitor domain found in foot protein 6 of *P. perna* play a critical role in the protection of other byssus plaque proteins and maintaining structural stability. Based on the motifs and domains comprises of two variants of foot protein 6, these proteins are included in the elafin-like superfamily that shows protease inhibitor proteins.

Posttranslational modifications (PTMs) are the reversible or irreversible chemical modifications that occur in protein after translation which induces conformational changes, by proteolytic cleavage and adding a modifying group, such as acetyl, phosphoryl, glycosyl and methyl, to one or more amino acids (Wang et al., 2014; Ramazi & Zahiri, 2021). PTMs affect many protein characteristics including functional activation, lifespan, protein-protein interactions, protein folding and solubility and protein localisation (Ryšlavá et al., 2013). Among PTMs, phosphorylation is the covalent addition of phosphate group to amino acids which is the most common and essential modification that occurs through enzymes and protein kinases. This is a reversible mechanism involving the addition of the phosphate group (PO_4) to the polar R group of different amino acids (Ardito et al., 2017). The most studied phosphorylation is serine, threonine and tyrosine phosphorylation to form acid-stable phosphomonoesters which mediate several signal transduction pathways (Cieśla et al., 2011). *P. perna* variant 2 of foot protein 6 had more serine, threonine and tyrosine phosphorylation sites than variant 1. Protein kinases are responsible for the mechanism of phosphorylation. There are seven subfamilies of protein kinases. In both variants of foot protein 6 from *P. perna*, serine residue at position 51 was phosphorylated by cGMP-dependent protein kinase or protein kinase G (PKG), which is included in the protein kinase subfamily AGC. These kinases are a group of Ser/Thr protein kinases that are regulated by second messenger cGMP. Similarly, in variant 2 of foot protein 6, threonine residue at positions 109 and 113 were

phosphorylated by protein kinase C, which is also included in the AGC subfamily, mainly involved in signal transduction (Pearce et al., 2010; Cieśla et al., 2011). Serine residues located at position 76 in both variants of foot protein 6 were phosphorylated by proline-directed serine/threonine kinase called Cyclin-dependent kinase 5 (cdk5), which included in protein kinase subfamily CMGC (Cieśla et al., 2011).

Similarly, glycosylation is one of the reversible and most complex PTM in which covalent linking of oligosaccharides to the specific amino acid residue was occurred by the enzyme glycosyltransferase. The major target amino acids of glycosylation are serine, threonine, asparagine and tryptophan (Ohtsubo & Marth, 2006; Ramazi & Zahiri, 2021). In *P. perna* variants 1 and 2 of foot protein 6 had common glycosylation sites at position 3 (serine), 45 (serine) and 52 (Asparagine). Whereas in variant 1, an additional glycosylation site at position 83 (Asparagine) was also recorded. There are different kinds of glycosylation were reported based on the linkage between amino acids and sugar. Commonly, N-glycosylation was found in asparagine in which sugar is attached to an amino group. Likewise, serine and threonine had O-glycosylation; here sugar interacted with the hydroxyl group of an amino acid (Jentoft, 1990; Imperiali & Hendrickson, 1995).

Antioxidants are molecules that fight against free radicals thereby reducing oxidative stress. Free radical scavengers (FRS) are a group of molecules; that can inhibit or quench free radicals even in low concentration (Olsen et al., 2020). Antioxidant FRS peptides are

derived from natural proteins and are safe, cost-effective and efficient with additional bioactive properties like hypocholesterolemic, antimicrobial etc. Similarly, chelator peptides prevent the formation of free radicals by forming complexes with metal ions (Sarmadi & Ismail, 2010; Nwachukwu & Aluko, 2019). Both variants of *P. perna* foot protein 6 had excellent antioxidant peptides but the chelator activity of peptides was low. Nicklisch et al. (2013) studied the antioxidant efficacy of recombinant mussel foot protein 6 variant 1 (rmfp-6.1) from *M. californianus.* According to their results, rmfp-6.1 had excellent DPPH scavenging activity than vitamin C and they rescue oxidation depended on adhesion loss by reduction of dopaquinone back to DOPA. The study of Yu et al. (2011) demonstrates the thiol-rich mfp-6 ability to restore DOPA from oxidation. The unique chemistry of the thiol or thiolate group of cysteine provides antioxidant properties to mfp-6. Many studies reported the antioxidant ability of cysteine-containing peptides. Cysteine provides sulphur hydrogen for trapping radicals. The use of natural bioactive peptides as antioxidants has high commercial value because synthetic antioxidants make severe adverse effects. Many studies were conducted for the synthesis of natural antioxidant peptides from different proteins of various organisms. Yesiltas et al. (2022) synthesised antioxidant peptides from potato, seaweed, microbial and spinach proteins. Similarly, Wu et al. (2020) predicted antioxidant peptides in potato protein hydrolysate. Likewise, 11 bioactive antioxidants were synthesised from different fish proteins (Thaha et al., 2021). These research results highlighted

the scope of mussel foot protein 6 two variants as antioxidant peptides.

Metal ions play a critical role in maintaining protein structure, function and stability and some amino acids have additional metal ion binding capacity (Shimazaki et al., 2009). In *P. perna* two variants of mussel foot protein 6, cysteine show high metal binding capacity. The results enlighten that cysteine can bind with a variety of metals. In mussel foot proteins metal ions are involved in protein crosslinking and adhesion. The thiol group of cysteine is actively involved in the metal binding which permits metal control of redox activity and also cysteine provides a storage facility for metal ions, which maintain metal homeostasis (Giles et al., 2003). *P. perna* metal binding site prediction showed that cysteine residue binds with some transition metal ions such as manganese, copper, cobalt, cadmium, and nickel. These metals act as cofactors involved in structure stabilization and enzyme catalysis (Lukács et al., 2021). Mesterházy et al. (2018) demonstrate toxic Hg (II) ions intracellular concentration regulation by cysteine-rich proteins. Similarly, Chung et al. (2016) investigated the oxidation protection ability of cysteine-containing metal binding motifs. Toxic metal binding affinity to the thiol group of cysteine is involved in the metal detoxification mechanism, thereby reducing oxidative damage. The present study results concluded that two variants of *P. perna* foot protein 6 had an excellent metal binding activity which involved protein cross-linking and maintaining stability, structure and function. It also involved in reducing oxidative damage in soft tissue through metal detoxification mechanism.

CONCLUSION

The present chapter mainly focused on mussel foot protein gene sequencing and characterisation. The RNA is very sensitive and easily degraded by RNases. Hence, the best condition for RNA and cDNA storage was studied. The results highlighted that storage at -80°C was a more efficient and cost-effective strategy. The tissue for RNA extraction and extracted RNA was secured at -80°C with good quality and quantity. Two variants of mussel foot protein 6 namely Ppfp-6(1) and Ppfp-6(2) were obtained through sequencing and the consensus sequences were deposited in NCBI. Through insilico analysis, physico chemical characterisation of two variants was analysed. Similarly, functional role, antioxidant activity, metal binding ability, and phylogeny construction were obtained. The results highlighted that mussel foot protein 6 two variants act as protease inhibitors and had high antioxidant activity. This property of foot protein 6 helps to reduce DOPA oxidation. Hence, foot protein 6 acts as a guard of DOPA found in other adhesion proteins such as mfp-3 and mfp-5, facilitating strong adhesion. Furthermore, foot protein 6 had unusual excess cysteine content that provides thiol moiety for the metal binding and antioxidant activity. The antioxidant activity and metal binding results unveiled the scope of mussel foot protein 6 peptides as an excellent antioxidant. The present chapter results provide significant information for designing mussel-inspired recombinant adhesives and also for docking studies to prevent biofouling.

INTRODUCTION

All living organisms require essential nutrients for their growth and development. Plants acquire nutrients from the soil, and other living organisms gain them from plants through the food chain. In plants, changes in the mineral nutrients make alterations in morphological and physiological responses. Hence for better productivity, plants require availability of optimal essential minerals (Maathuis, 2009). There are 13 essential elements required for better growth in plants and they are categorized into two macro and micronutrients. As their name mentions macronutrients required in large quantities and they are subdivided into two, primary and secondary macronutrients. Nitrogen (N), phosphorous (P), and potassium (K) are primary macronutrients and secondary macronutrients include sulphur (S), magnesium and calcium (Ca). On the other hand, iron (Fe), zinc (Zn), copper (Cu), boron (B), manganese (Mn), molybdenum (Mo), and chlorine (Cl) are micronutrients and they are required in small quantities but their absence makes severe adverse effects (Kumar et al., 2021).

Nitrogen is essentially required during the synthesis of starch and amino acids and is involved in vegetative growth and yield of crops. Similarly, phosphorous is mainly involved in cellular processes like photosynthesis, carbohydrate metabolism, energy production, and signalling and in seeds, it helps for germination, embryo development and seedling growth (Maathuis, 2009). Potassium mainly acts as an enzyme activator and hence it is mainly involved in metabolic processes (Britto & Kronzucker, 2008). Sulphur is another

macronutrient mainly found in reduced form and involved in the synthesis of sulphur-containing amino acids such as cysteine and methionine. It also acts as a mobile carrier of glutathione and it is found as inorganic sulphate in the form of sulfolipids in chloroplast thylakoids (Ramani et al., 2004). Calcium act mainly as a second messenger and structural component of cell and magnesium function as a cofactor, involved in the stabilization of nucleotides and nucleic acids and also it is a central component of the chlorophyll molecule (Robinson et al., 2000; Axelsson et al., 2006; McAinsh & Pittman, 2009).

Even though the concentration of micronutrients is low but their essentiality of them is high. Zn is mainly involved in regulating enzyme activity, which is the only metal required in the activity of hydrolases, oxidoreductases, lyases, transferases, ligases, and isomerases (Kumar et al., 2021). Likewise, Fe, Cl and Mn are mainly involved in photosynthesis and carbohydrate synthesis and copper functions in protein and chlorophyll synthesis. The micronutrient Molybdenum engaged in nitrogen fixation and Nickel in nitrogen metabolism (Zewide & Sherefu, 2021). Nutrients are not only working independently. Mutual interactions between multiple nutrients are required in some physiological and cellular processes. For example, iron deficiency alters the transcription of phosphorous assimilation related genes and similarly, sufficient potassium concentration is needed for nitrogen metabolism (Ruiz & Romero, 2002; Zheng et al., 2009).

The studies are indicating that single nutrient deficiency affects not only single physiological and cellular processes of plants but affects whole biochemical and molecular processes. Fertilization provides essential plant nutrients for increasing crop yield and quality. During the 20^{th} century introduction of chemical fertilizers leads a 50% increase in crop yield (Fageria, 2005). The introduction of nitrogen and phosphorous chemical fertilizers is one of the key components of the Green revolution (Kumar, 2013). Nitrogen and phosphorous are irreplaceable nutrients for plant growth. Nitrogen is provided to plants in the form of urea synthesised by the Haber Bosh process. However, phosphorous availability is finite because it is obtained from phosphate rocks, which are prone to extinction. Hence, in the future phosphorous supply to plants will become a global challenge (Cordell et al., 2009; Dawson & Hilton, 2011). Continuous fertilization is required for increased crop production, even though increased use of mineral fertilizers harms the environment including the production of greenhouse gases, NH_3 volatilization, decreased water quality and eutrophication (Calabi-Floody et al., 2018). Fertilizer application must be done based on the soil type because some soils are deficient with only a few minerals. For example, cambisol is one of the major soil types used for agricultural purposes, which faces phosphorous deficiency. Hence, the application of the undesirable amount of other minerals in cambisols leads to acceleration of acidity and loss of organic matter (Tesfay & Gebresamuel, 2016).

The runoff of minerals from plant proximity through watering and rain, they are the major reason for eutrophication. Hence, the production of

a sustainable nutrient management system is essential in the agricultural field to maintain biogeochemical cycles. The slow-release fertilizers provide nutrients to plants for a period of time and hence reduce nutrient leaching from the soil. Nowadays, slow-release fertilizers are made by two methods. The first method uses substances that slow down the transformation of nitrogen forms in the soil and in the second method a physical barrier or coating material is made around the nutrients (Wesolowska et al., 2021). The major drawback of coating materials is the very slow biodegradation capacity and the production is much more expensive but its application reduces input cost and frequency of fertilization (Wang et al., 2021). In this circumstance, the introduction of inorganic, eco-friendly and cost-effective slow-release fertilizer reduces imperfections of slow-release fertilizers. The present study focused on the synthesis of slow-release fertilizer from waste materials like cow urine and mussel shell. Cow urine and mussel shell are animal origin waste materials and the waste mussel shell causes environmental pollution. Both raw materials are conventionally used in the agricultural field for different purposes. Hence, the synthesis of slow-release fertilizer from cow urine and mussel shell powder has a positive synergic effect in the agricultural field.

MATERIALS AND METHODS

4.2.1 Scanning electron microscopic analysis

Microstructural characterization of the *P. perna* mussel shell was done by using field emission scanning microscopy. Figure 1 represents the right and left halves of *P. perna* shell. Mussel shell was thoroughly cleaned and crushed into small pieces. The shell pieces were dried in a hot air oven at 60°C for one hour and kept in a desiccator. Properly dried threads were mounted on stub with conductive carbon tape and sputter-coated with gold particles for the 50s on Quorum SC 7620 sputter coater. Ultrastructure imaging was conducted using an FE-SEM microscope (ZEISS GeminiSEM 300) (Checa, 2018).

Figure 1: *P. perna* shell; (**A**) dorsal side, (**B**) ventral side

4.2.2 Fourier transform infrared spectroscopy (FTIR)

For FTIR analysis shell powder was grounded with KBr (Potassium bromide) and pelletized. The infrared examination was carried out using a spectrometer (Jasco-4100, Shanghai, China) in the spectral region of 500 to 4000^{cm-1}. Origin software has been used to process the unprocessed FT-IR data (Version OriginPro 9.0 64Bit). The interpretation of FTIR spectra was done based on the article "infrared spectroscopy of proteins" by Barth, (2007).

4.2.3 Thermogravimetric analysis (TGA)

The thermogravimetric analysis measures the material's thermal stability by analysing the weight changes when heating the sample at a constant rate (Gigante et al., 2020). Thermal stability of shell (6 mg) was carried out in an STA 8000 simultaneous thermal analyser under the temperature range 30-900°C with a heating rate of 10°C/min.

4.2.4 Mineral enrichment experiment

Thoroughly washed mussel shells were properly dried and crushed using an iron rod. Chopped shells were powdered in a mixer grinder and 45 micron particle size powder was separated using a brass frame sieve set. Similarly, cow urine was collected from cattle farm without contamination and filtered urine was used for the study. Two different protocols were done for obtaining the best nutrient-enriched slow-release fertilizer.

4.2.4a Shell saturation experiment

Here, the shell powder used in the experiment remains constant and the urine was changed on alternative days. In this experiment, add 25 g mussel shell powder and 75 ml cow urine to a beaker and gentle stirring was provided for one hour. After stirring the setup was stored at room temperature without disturbance. On every alternative day, existing urine was removed and added new sample and at the same time 1 g of shell powder was removed. Finally, the removed shell powder was gently washed in distilled water to remove excess urine content and dried well. The complete experiment extends up to 10 days.

4.2.4b Urine filtration experiment

In the urine filtration experiment, urine became constant and shell powder changed on alternate days. Here, mixed 75 ml urine with 25 g mussel shell powder and continuously stirred for one hour. After stirring the setup was kept without disturbance. On every alternate day, the shell powder was changed and the same procedure continued. Finally, the removed shell powder was washed gently for removing excess urine and dried for further examination. The complete experiment extends up to 10 days.

4.2.5 Shell leaching experiment

In this experiment, mixed 25 g shell powder collected from the shell saturation experiment and 75 ml distilled water in a beaker and it was kept without disturbance for 30 days. Every 10 days, one gram of shell

powder was collected from the experiment, dried well and used for further analysis.

4.2.6 XRF analysis

Nutrient enrichment in the shell was confirmed using X-Ray fluorescence spectroscopy. Elemental concentration variations in the shell saturation experiment, urine filtration experiment and shell leaching experiment were calculated by X-Ray fluorescence spectroscopy (Spectro-Ametek, SPECTRO XEPOS-XRF). The concentration variations of macroelements such as phosphorous, potassium, calcium, sulphur, and magnesium and microelements such as iron, zinc, copper, manganese, molybdenum, chlorine, and nickel were calculated.

4.2.7 BET analysis

Nutrient impregnation and leaching in shell powder were confirmed by Brunauer–Emmett–Teller (BET) analyser. The specific surface area and pore size distribution of normal mussel shell, nutrient impregnated shell powder, and 30 days nutrient leached shell powder was measured by BET analyser (BELSORP-max) with N_2 as the analysis gas. In BET analysis, the solid surface adsorbed specific pressure gas under constant temperature and equilibrium state. Therefore, the amount of adsorbed gas was determined by gas pressure (Zhang et al., 2013).

4.2.8 Statistical analysis

The experiments's results were statistically analysed using the programme IBM SPSS version 20.0. All data represented as mean ± standard deviation acquired by descriptive statistics and statistical significance was determined by Kruskal–Wallis one-way analysis. The results were considered statistically significant when $P<0.05$.

RESULTS

4.3.1 Shell structure

The microstructure of the *P. perna* shell revealed that it contains three distinct layers namely; the outer periostracum, middle prismatic layer and inner nacreous layer (Figure 2). Periostracum is brown and small ripples appear at regular intervals (Figure 2A & 2B). The gap between each ripple was around 1.539±0.075µm. The prismatic layer formed of microscopic calcite tablets arranged in a brick wall manner (Figure 2D). The height and width of bricks in the prismatic layer varied from near nacreous layer to near periostracum and the results were tabulated in Table 1. Bricks were more comprehensive near the nacreous layer and become compact when reaching the periostracum. In *P. perna*, the nacre layer (Figure 2E & 2F) is lustrous and aragonite built with thin layers of stable calcium carbonate lath arranged as superimposed sheets.

Table 1: Prismatic layer brick measurements

Region	Measurement (Mean ± SD)
Height of Brick near the periostarcum	0.834 ± 0.119
Width of Brick near the periostarcum	2.767 ± 0.158
Height of Brick at middle of prismatic layer	0.766 ± 0.062
Width of Brick at middle of prismatic layer	3.48 ± 0.08
Height of Brick near the nacreous layer	0.814 ± 0.079
Width of Brick near the nacreous layer	4.28 ±0.954

SD=Standard deviation

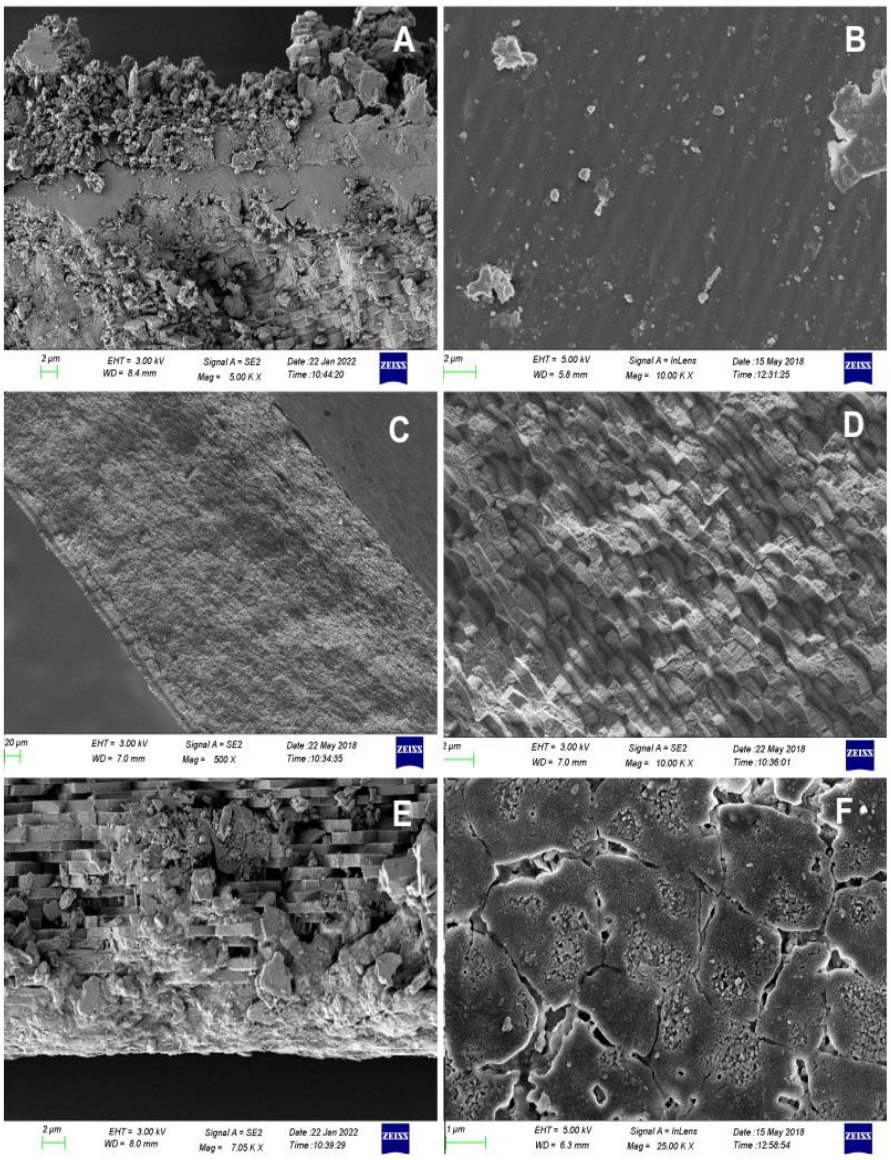

Figure 2: Microstructure of *P. perna* shell; (**A**) boundary between periostracum and prismatic layer, (**B**) Top view of periostracum, (**C**) cross section of shell, (**D**) prismatic layer, (**E**) boundary between prismatic layer and nacreous layer (**F**) Inner nacreous layer

4.3.2 FTIR analysis

FTIR spectra of the *P. perna* shell (Figure 3 & Table 2) show a total of 9 peaks. The large broad band observed at 3422 cm^{-1} represents the hydroxyl group of water. Between 2000 to 3000 cm^{-1} three bands were observed at wavelengths 2916 cm^{-1}, 2631 cm^{-1} and 2522 cm^{-1} corresponding to alkane, aldehyde and thiol. The peak at 1785 cm^{-1}, 860 cm^{-1} and 713 cm^{-1} represent the presence of carbonate minerals.

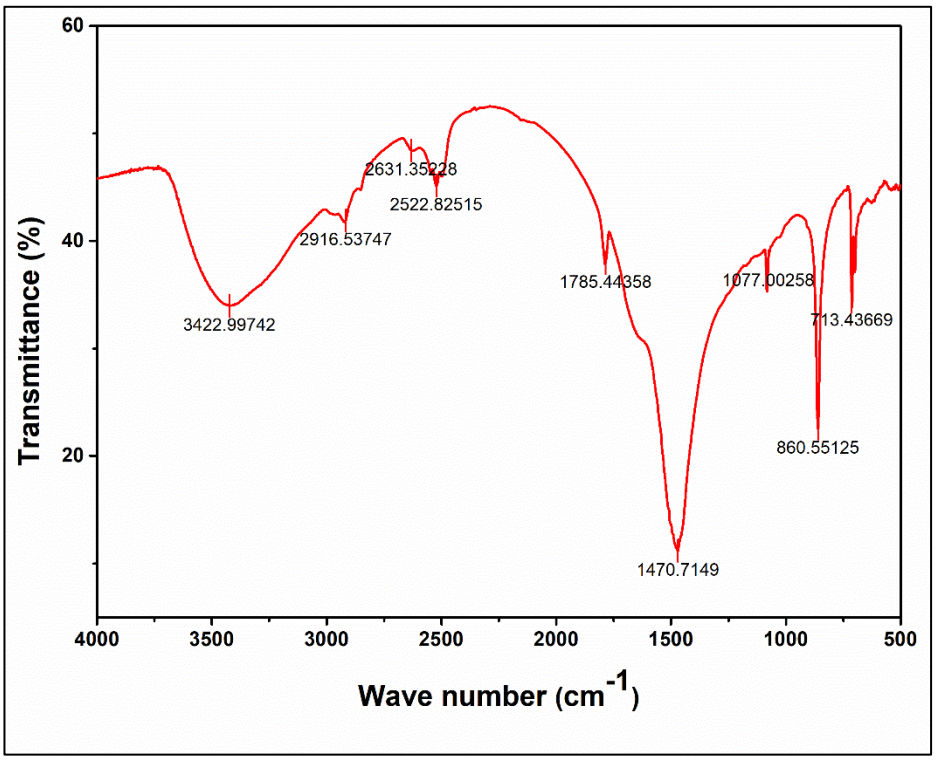

Figure 3: FTIR spectrum of *P. perna* shell

Table 2: IR interpretation of shell

Wavelength (cm^{-1})	**Group**	**Compound class**
3422.99	O-H Stretching	Water
2916.53	C-H Stretching	Alkane
2631.39	C-H Stretching	Aldehyde
2522.82	S-H Stretching	Thiol
1785.44	C=O Stretching	Conjugated acid halide
1470.71	C-H Stretching	Alkane
1077.00	C-O Stretching	Primary alcohol
860.55	C-H Stretching	Aromatic
713.43	C-H Bending	Benzene derivative

4.3.3 Thermogravimetric analysis (TGA)

The thermal stability of mussel shell was studied by thermogravimetric analysis and graph is represented in Figure 4. Two weight losses were observed in the graph. The initial 3 % weight loss observed between 250° C to 350° C and second major weight loss was observed between 620 to 850° C.

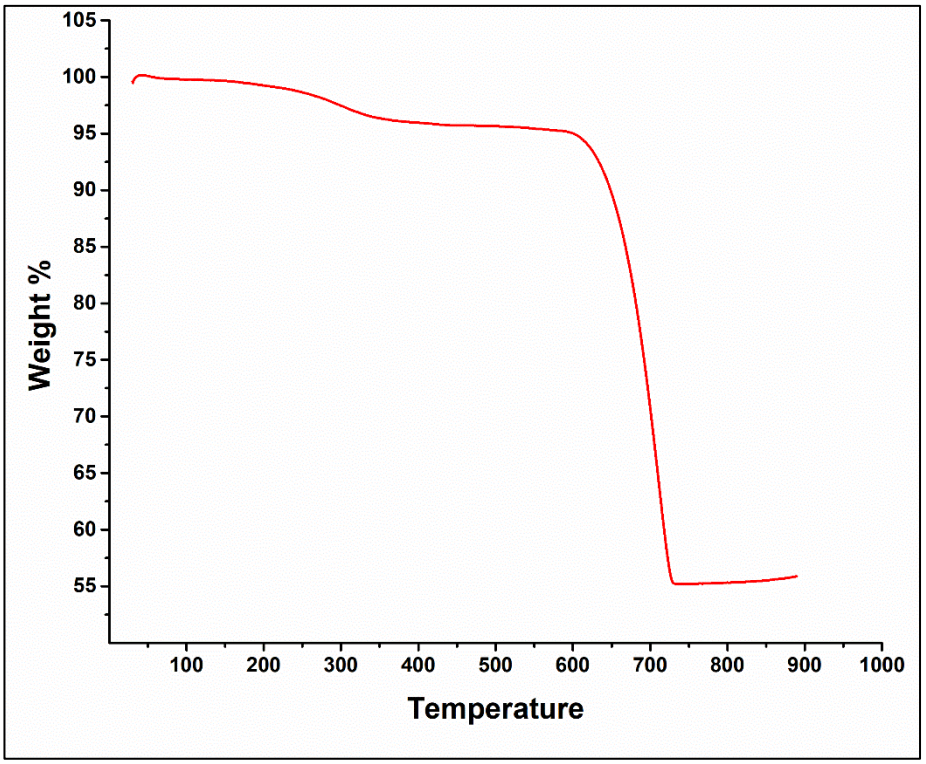

Figure 4: TGA analysis of *P. perna* shell

4.3.4 Mineral enrichment experiment

Essential nutrient impregnation is the major target of the mineral enrichment experiment. Hence, macro and micronutrients concentration in normal shell powder, raw cow urine, cow urine treated shell powder and nutrient leached shell powder were measured by XRF.

4.3.4a Shell saturation experiment

In the shell saturation experiment, all macronutrients concentration (Figure 5) was increased in nutrient impregnated shell except calcium.

Phosphorous, potassium and sulphur show a significant concentration ($P<0.05$) increase in the treated shell than in the untreated shell. Calcium concentration is exponentially high in shell powder; hence calcium level was decreased in the treated shell due to diffusion. Compared with cow urine magnesium concentration was high in the shell in but during nutrient impregnation, its concentration was also increased in treated shell powder. A significant concentration increase was not observed ($P>0.05$) in the case of micronutrients (Table 3). Iron and chlorine were more concentrated micronutrients in the treated shell. Zinc, copper and nickel had moderate concentrations and manganese and molybdenum had very feeble concentrations.

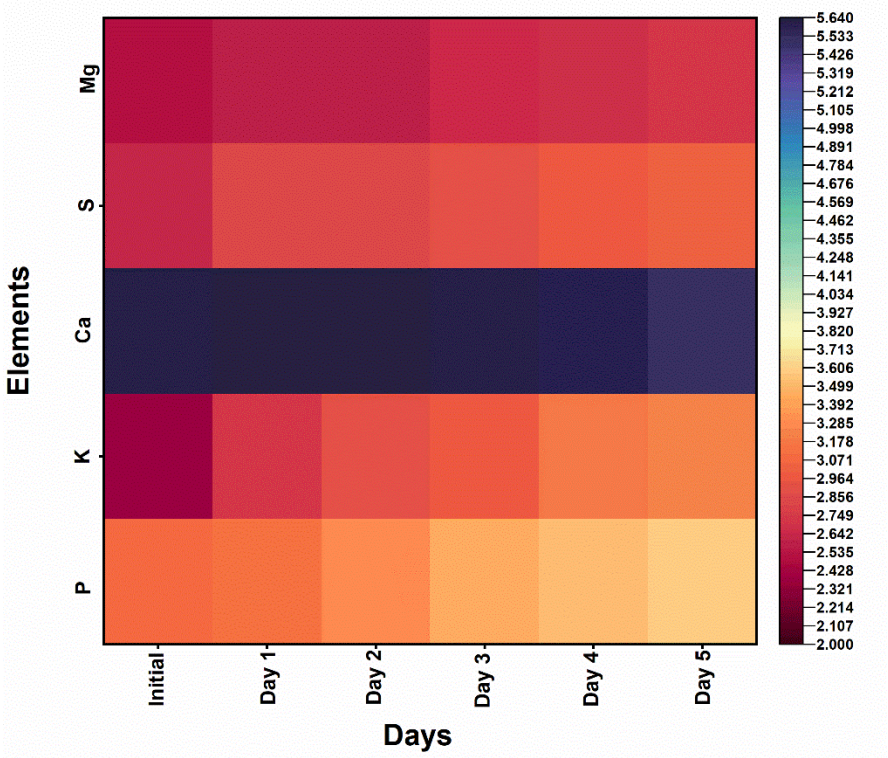

Figure 5: Macronutrients concentration in shell saturation experiment

Table 3: Micronutrients concentration in shell saturation experiment

Sample	**Fe (ppm)**	**Zn (ppm)**	**Cu (ppm)**	**Mn (ppm)**	**Mo (ppm)**	**Cl (ppm)**	**Ni (ppm)**
Raw cow urine	0.68± 0.02	0.52 ± 0.02	0.413 ± 0.15	3.64 ± 0.25	0.27 ± 0.029	1170.33 ± 250.52	0.62 ±0.006
Raw shell powder	56.76 ± 9.37	1.58 ± 0.23	1.77 ± 0.09	0.085 ±0	0.64±0.09	287.42±18.67	0.085 ±0
Day 1	56.59±2.10	1.33±0.35	1.50±0.15	0.085 ±0	0.58±0.14	227.79±4.42	0.085±0
Day 2	58.43 ± 9.9	1.44±0.30	1.66±0.26	0.085 ±0	0.53±0.16	239.96±1.70	2.91±0.29
Day 3	60.01 ± 3.45	1.47 ± 0.41	1.74 ±0.17	0.085 ±0	0.71 ± 0.17	289 ± 5.89	2.86 ± 0.15
Day 4	60.24±1.04	1.56±0.2	1.81±0.11	0.085 ±0	0.74±0.04	284.32±1.04	2.90±0.14
Day 5	60.45±3.17	1.62±0.71	1.92±0.3	0.085 ±0	0.68±0.11	295.17±2.47	2.91±0.2

Values are expressed in mean ± standard deviation

4.3.4b Urine filtration experiment

A significant increase in macronutrient concentration was not observed ($P>0.05$) in the urine filtration experiment. A slight increase in phosphorous, potassium and sulphur was noticed during the early days but eventually, its concentration was decreased (Figure 6). In the case of micronutrients, the concentrations were gradually decreased and Ni was completely absent in all samples (Table 4).

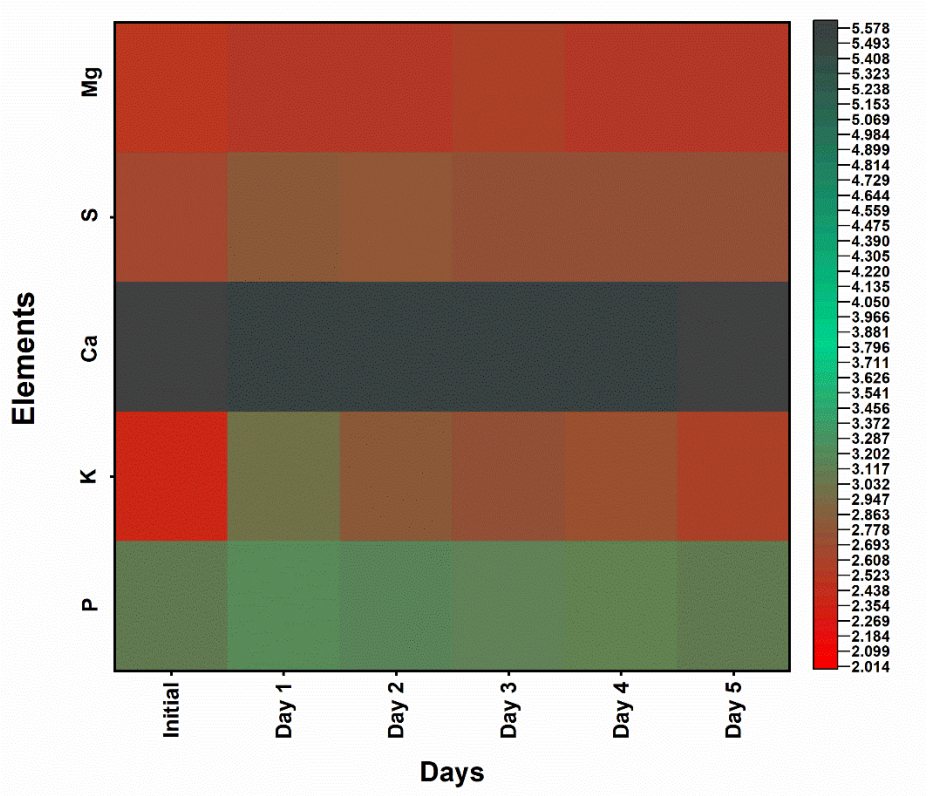

Figure 6: Macronutrients concentration in urine filtration experiment

Hence the results of two nutrient enrichment experiments concluded that mussel shell powder could use as a good adsorbent and the shell

saturation experiment was ideal for nutrient impregnation. Furthermore, the microscopic observation of nutrient impregnated shell samples from both experiments revealed the formation of struvite crystals (Figure 7). Struvite crystals are transparent crystals formed of equimolar concentrations of phosphorous, ammonium and magnesium or potassium, ammonium and magnesium.

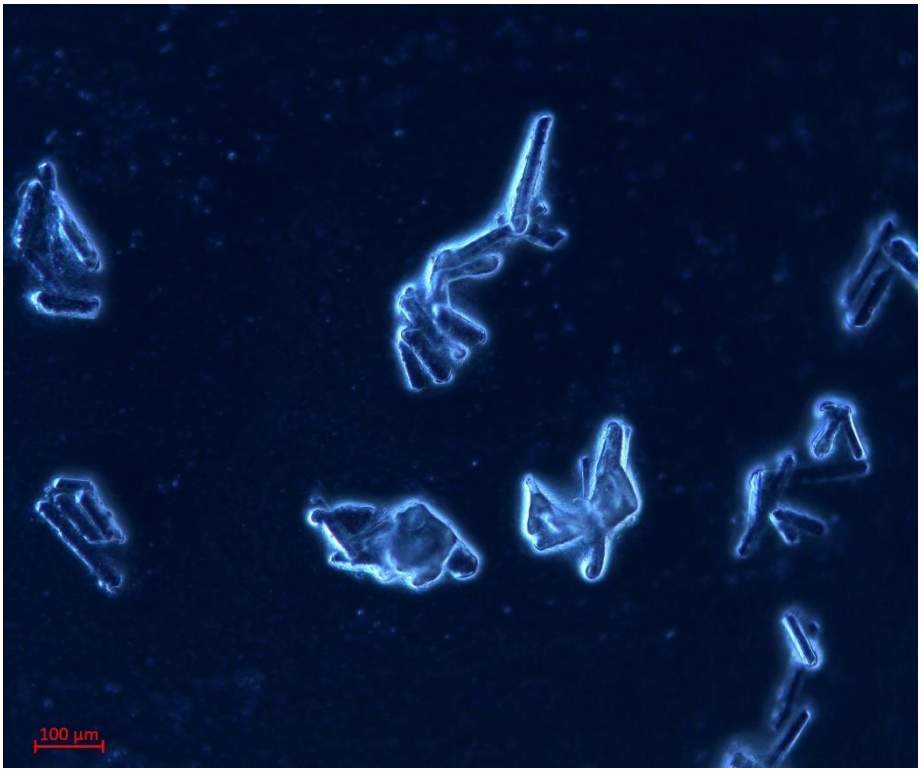

Figure 7: Struvite crystals

Table 4: Micronutrients concentration in urine filtration experiment

Sample	Fe (ppm)	Zn (ppm)	Cu (ppm)	Mn (ppm)	Mo (ppm)	Cl (ppm)	Ni (ppm)
Raw cow urine	0.68± 0.02	0.52 ± 0.02	0.413 ± 0.15	3.64 ± 0.25	0.27 ± 0.029	1170.33 ± 250.52	0.62 ± 0.006
Raw shell powder	56.76 ± 9.37	1.58 ± 0.23	1.77 ± 0.09	0.085 ±0	0.64±0.09	287.42±18.67	0.085 ± 0
Day 1	46.23±5.31	1.66±0.22	1.56±0.04	0.085 ±0	0.51±0.01	314.21±10.41	ND
Day 2	43.59±3.14	1.59±0.07	1.47±0.57	0.085 ±0	0.6±0.12	297±9.34	ND
Day 3	36.51±1.64	1.53±0.62	1.61±0.1	0.085 ±0	0.59±0.04	305±4.12	ND
Day 4	44.78±4.28	1.6±0.3	1.59±0.07	0.085 ±0	0.58±0.11	284±8.54	ND
Day 5	45.52±2.98	1.54±0.24	1.64±0.74	0.085 ±0	0.67±0.74	297±5	ND

Values are expressed in mean ± standard deviation

4.3.5 Shell leaching experiment

The results of shell leaching experiments imply that macronutrients were released from shell powder at a slow rate manner (Figure 8). Half of the nutrients were not released from the shell even 30th day of the experiment. In the case of micronutrients (Table 5), Fe shows slow release property but other elements concentration was very feeble except for chlorine. The results concluded that nutrient-impregnated shell powder could use as a slow-release fertilizer.

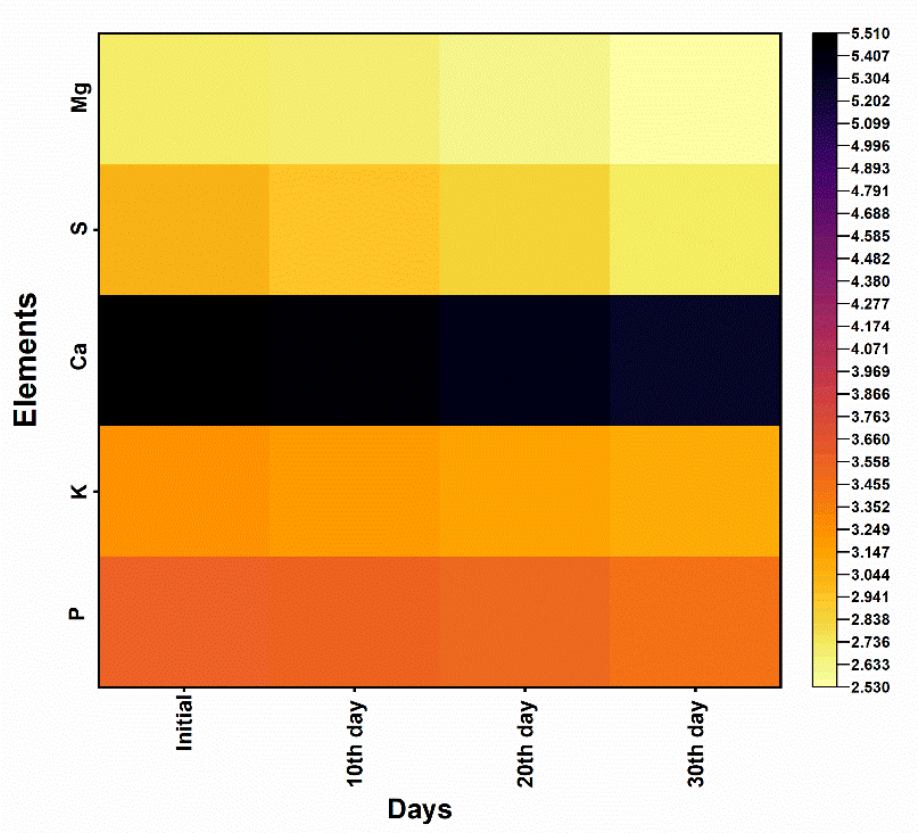

Figure 8: Macronutrients concentration after leaching

Table 5: Microelements concentration after leaching

Sample	**Fe (ppm)**	**Zn (ppm)**	**Cu (ppm)**	**Mn (ppm)**	**Mo (ppm)**	**Cl (ppm)**	**Ni (ppm)**
Initial	60.45±3.17	1.62±0.71	1.92±0.3	0.085 ±0	0.68±0.11	295.17±2.47	2.91±0.2
10^{th} day	49.31±2.41	0.77±0.01	0.89±0.04	0.085 ±0	0.14±0.005	164.34±2.11	1.03±0.07
20^{th} day	36.87±2.22	0.54±0.04	0.41±0.01	0.085 ±0	0.085 ±0	106.4±3.74	0.45±0.01
30^{th} day	29.45±4.14	0.37±0.02	0.085 ±0	0.085 ±0	0.085 ±0	56.45±1.89	0.085 ±0

Values are expressed in mean ± standard deviation

4.3.6 BET analysis

BET analysis was conducted to analyse the differences in surface area, pore size and pore volume of normal, nutrient impregnated and nutrient leached shell powder (Table 6). The surface area and pore volume were reduced in nutrient immobilized shell powder than in normal shell powder. But in nutrient leached shell both of these were increased than normal shell powder because of nutrient loss. The normal shell powder and nutrient immobilized shell powder had similar pore sizes but in the nutrient leached shell this was increased because nutrient loss makes more space.

Table 6: BET analysis

Measures	**Normal shell**	**Nutrient immobilized shell**	**Nutrient leached shell**
Surface area	0.70858 m^2/g	0.37814 m^2/g	2.2811 m^2/g
Pore diameter	1.26 nm	1.26 nm	1.74 nm
Pore volume	0.2246 m^3/g	-0.17186 m^3/g	1.0682 m^3/g

DISCUSSION

Mussel shell microstructure has highly ordered three-dimensional arrangements, which can resist habitat stress. The microstructural evaluation of mussel shells is highly beneficial in many fields of science including geology, palaeontology, medicine etc. Mussel shells have both organic and mineral parts hence they are called organo-mineral biomaterials. Nearly, 95-99% of shell weight constitutes mineral part and the organic part remains only 0.1-5% (Chateigner et al., 2000; Checa, 2018). *P. perna* mussel shell contains three distinct layers namely, outer periostracum, middle prismatic layer and inner nacreous layer. The outer periostracum is a brown-coloured, protein-containing, sclerous, protective, and entirely organic or sparsely mineralized layer. The shell secretion begins from the synthesis of the periostracum occurs in the periostracal groove found between the outer and middle mantle folds (Checa & Salas, 2017; Checa, 2018). Periostracum saves mussels from the attack of fouling and boring species and also protects them from hyper-osmotic surroundings. However, as the age of species increases the effectiveness of periostracum protection diminishes. Changing environmental factors also causes deterioration of this barrier (Watson et al., 2009). Proteins, acidic polysaccharides, glycoproteins and chitin are major organic compounds found in periostracum (Checa, 2018). In addition, periostracum contains a quinone-tanned protein called conchiolin or conchins which provides a microenvironment for the nucleation and growth of mineral crystals. Conchins also found in the nacreous layer

helps to provide stiffness by holding and binding crystals (Grégoire et al., 1961).

The prismatic and nacreous layers are typically mineral layers made up of calcium carbonate in the form of calcite and/or aragonite. The prismatic layer of the *P. perna* formed with microscopic calcite tablets arranged in a brick wall manner. Prismatic layer layer is synthesised by the epithelial cells located at the edge of the outer mantle and the nacreous layer formed from the pallium of the mantle (Funabara et al., 2014). *P. perna* nacreous layer is lustrous and aragonite which had sheet nacre arranged as broad, regularly formed parallel sheets. Sheet structured nacreous layer is mainly found in bivalves and nautilus (Chateigner et al., 2000). Depending upon the stacking mode of calcium carbonate tablets, two types of nacre were formed in mussels called columnar nacre and sheet nacre (Chateigner et al., 2000). The nacreous layer is the strongest part of the shell and is resistant to fracture and even if the shell's exterior layer cracks, the nacreous layer can maintain the shell's integrity and protect soft tissue (Checa, 2018). Nacreins and pearlins are the two proteins extracted from the nacreous layer, which are also found in the prismatic layer involved in calcium binding activity, carbonic anhydrase activity and also inhibit calcium carbonate precipitation. The studies revealed that these proteins are mainly involved in nucleation, growth, polymorphism, and orientation of mineral deposition (Funabara et al., 2014; Checa, 2018).

FTIR spectra of the *P. perna* mussel shell showed 9 prominent peaks. Among these, peaks such as 1785.44 cm^{-1}, 1077 cm^{-1}, 860.55 cm^{-1} and

713.43 cm^{-1} are indicating the presence of calcium carbonate. Gaffey, (1987), Legodi et al. (2001) and Gunasekaran et al. (2006) reported similar peaks of calcium carbonate. Nevertheless, slight variations were found in peak position in every study because of the contamination of trace metals and natural impurities. Parveen et al. (2020) studied three freshwater snail shell characterisations through FT-IR analysis and the results showed the presence of functional group C=C stretching and C-O stretching indicating the presence of CO_3^{2-} ions and glycosylated proteins. Similarly, peaks at 713 cm^{-1} and 865 cm^{-1} wavelength indicate the aragonite forms of calcium carbonate. *P. perna* also has C=C stretching and C-O stretching peaks at wavelengths 1785.44 cm^{-1} and 1077 cm^{-1} respectively and aragonite wavelength at 713.43 and 860.55. According to the study of Jovanovski et al. (2002), the peaks wavelength 1000-1100 cm^{-1} can be utilized to distinguish calcite and aragonite forms of calcium carbonate. These peaks are only found in aragonite form and aragonite has a higher value in the wavelength range 1400-1490 cm^{-1} and 830-850 cm^{-1}. Hence these peaks help to analyse the purity of calcium carbonate forms.

Thermogravimetric analysis indicated the extreme thermal stability of the *P. perna* mussel shell and this property was widely useful in the synthesis of many biocomposites. Felipe-Sesé et al. (2011) study revealed that an initial 0.4% weight loss of mussel shell between the temperatures 200° C and 356° C due to moisture release and a second 0.7% weight loss between the temperatures 356° C and 600° C because of volatile matter removal. The temperature beyond 600° C–850° C

causes drastic weight loss due to the decomposition of the shell. In the present study, an initial 3 % weight loss was observed between 250° C to 350° C due to water and organic compound loss and a second drastic weight loss was observed between 600° C to 850° C due to the decarbonisation of calcium carbonate. Gigante et al. (2020) studied *Mytilus edulis* shell thermal stability. According to their results, three weight loss peaks were observed including 2% weight loss up to 200° C due to water loss, 3% weight loss between temperatures 300° C to 400° C due to volatile content removal and drastic weight loss over 600° C due to shell decomposition. The thermal stability analysis of the mussel shell was also conducted by Martínez-García et al. (2017) and their result was similar to the present *P. perna* thermogravimetric analysis results. Similarly, Chiou et al. (2014) reported that oyster shell was completely decomposed at when the temperature of 760° C and Mohamed et al. (2012) revealed that, between the temperatures of 700° C to 900° C cockle shell undergo significant weight loss due to calcium carbonate decomposition. Hence, these TGA analysis results highlighted that when exceeding the temperature from 600° C causes calcination of the shell which produces CaO as a by-product (Mo et al., 2018).

The plant growth and crop productivity proportionally correlated with the availability of macro and micronutrients in the soil. Both cow urine and mussel shell powder was rich in essential nutrients. The present study results showed that significant macronutrient scrubbing occurred from cow urine to shell powder in the shell saturation experiment. Many studies demonstrate the efficiency of mussel shell powder as an

inexpensive natural adsorber. In the study of Wang et al. (2021) mussel shell was used for the adsorption of lead (Pb) from an aqueous solution. Similarly, the study of Papadimitriou et al. (2017) also demonstrates the efficiency of mussel shell powder as a dye and heavy metal adsorbent. Eutrophication is one of the major reasons for the excess accumulation of nutrients in water bodies. Nguyen et al. (2021) studied mussel shells using ammonium ion removal possibilities from an aqueous solution. The results provide a promising treatment for water contamination. Likewise, Zukri et al. (2018) used mussel shell powder as an adsorbent in their study for improving lake water quality. These study results suggested that mussel shell powder is a natural, agricultural waste and it can used as the best low-cost adsorbent for removing excess elements from lake water. The present study also proved that *P. perna* mussel shell powder can use as an excellent nutrient scrubbing agent.

The formation of struvite crystals is another highlight of the present study. The struvite crystals are formed with equimolar concentration of phosphorous, ammonium and magnesium or potassium, ammonium and magnesium. The struvites formed with phosphorous called phosphorous struvites and with potassium called potassium struvites (Zhang et al., 2017). In the present study, cow urine was rich with phosphorous and ammonium and shell powder had much more concentration of magnesium. The mid-alkaline condition was the optimum pH condition for struvite formation. Hence cow urine and shell powder mixing provide optimum pH environment and also raw materials for struvite synthesis. Phosphorous is a non-substitute

macronutrient essential for all life forms. Phosphate rocks are a source of phosphorous but they will run out in 50 years. Hence, phosphate recovery becomes an essential task for saving phosphate rocks. Struvite is considered an excellent technique to recover phosphate and can be used as slow release fertilizer (Hao et al., 2013). For phosphate removal and recovery, Ye et al. (2014) synthesised struvite crystals from wastewater. Similarly, Wang et al. (2019) attempted to recover phosphate from swine wastewater through struvite crystallization. These studies showed that struvite synthesis is a relatively simple process for phosphate recovery.

The components of struvites are considered macronutrients essential for the growth of plants. Hence, the use of struvite as fertilizer is highly recommended. Magnesium is another attractive component of struvite which is a critical element for many crops. Because of the slow-release nature of struvite crystals, it couldn't make any burning effects on roots or seeding. Similarly, it helps to reduce the frequency of fertilization leading to minimising eutrophication (Farooq & Ahmad, 2017). Ryu et al. (2012) compared the fertilizing efficiency of struvite crystals recovered from semiconductor wastewater with commercial fertilizer in cultivating Chinese cabbage. Their results concluded that struvite recovered from semiconductor wastewater was an effective multi-nutrient fertilizer for the production of Chinese cabbage. As a part of resource conservation and environmental protection, Rodrigues et al. (2019) attempted to recover phosphate as struvite from urban wastewater like urine diverting toilets and Szymańska et al. (2020) studied struvite recovery from anaerobic

digestate in a farm bio-refinery. All these kinds of studies concluded that the recovery of phosphate as struvite is an economic process which helps to reduce phosphorous leaching, minimize eutrophication and also the product can be used as an excellent slow-release fertilizer.

In the present study nutrient leaching experiment shows that nutrient impregnated shell had a slow releasing capacity and half of the nutrients were not released after 30 days of leaching. BET analysis was used to confirm the adsorption and leaching of nutrients in the shell. During the leaching surface area and pore diameter get increased because of the loss of nutrients and organic content in the shell. The leaching property of this nutrient-scrubbed shell powder showed that it could be used as an excellent slow-release fertilizer. Chemical fertilizers help to improve crop production but easily run off from plant proximity after rainfall or watering. This leads to serious environmental and economic issues including leaching, volatilization, increased unnecessary labour etc. (Wang et al., 2016). Use of slow-release fertilizers help to overcome this issue, which release nutrients for a period of time without washout. Hence, slow-release fertilizers maintain soil fertility in a reduced dosage which meets the nutrient requirements of plants (Wang et al., 2021). Mostly slow-released fertilizers are either super granules or coated condensation products of urea-aldehyde. The coating materials of slow-released fertilizers are either inorganic materials like sulphur, bentonite and phosphogypsum or organic materials such as biochar, resins and polyphenols. Slow-released fertilizers release nutrients either by microbial activity or by chemical decomposition (Lawrencia et al., 2021). Even though the

benefits of slow-release fertilizer are very high but its excess manufacturing cost restricts its widespread use in agriculture (Lubkowski & Grzmil, 2007).

Nutritional deficiencies compromise the quality and quantity of crop production. For example, nitrogen-limiting conditions directly affect yield because they promote leaf senescence due to a reduction in chlorophyll content and photosynthesis efficiency (Huang et al., 2020). Among macronutrients, phosphorous deficiency causes alteration in metabolism and translocation of carbohydrates in plants and also leads to increased production of free radicals as a by-product of photosynthesis (Meng et al., 2021). Similarly, potassium deficiency causes aberrant growth, decreased plant development and alteration in the expression of protein coding genes (Thornburg et al., 2020) and calcium deficiency leads to oxidative stress, stunted growth and curling (De Freitas et al., 2016). Sulphur and magnesium are the other two macronutrients. Sulphur deficiency also causes stunted growth and reduced yield quality and magnesium deficiency impairs photosynthetic electron transport (Ye et al., 2019; Narayan et al., 2022). The nutrient-impregnated new slow-released shell fertilizer is rich in all macronutrients; hence it provides nutrients to plants for their better growth and development.

Like macronutrients, micronutrients are essential for plants but their required quantity is low. Iron and chlorine are the most abundant micronutrients found in nutrient-impregnated shell powder. Zinc, copper, molybdenum, manganese, and nickel are the other

micronutrients detected. Each microelement critically plays role in physical and metabolic activities. For example, manganese deficiency negatively affects non-structural carbohydrates and root carbohydrates leading to reduced crop quality and quantity (Zewide et al., 2021). Zinc deficiency causes reduced fruit bud formation and iron and chlorine deficiency leads to severe chlorosis. Similarly, copper deficiency causes stunted growth and failure in flowering and fruiting and molybdenum deficiency symptoms are similar to nitrogen deficiency because it plays a critical role in nitrogen utilization (Rahman et al., 2020). The elemental composition analysis results suggested that the new slow-release nutrient-impregnated shell powder contains sufficient quantity of micronutrients for crops. The results highlighted that the product is a nutrient factory that can use as an economic nutrition source.

So, mussel shells are waste products originating from the fishery industry and they are dumped on lands without any eco-friendly reuse value. However, many tones of mussel shells were generated annually and their proper recycling is needed for reducing several environmental problems and public health. Even though they are waste materials, it is an excellent biocomposite material and has many industrial applications (Mo et al., 2018). Many studies were conducted for recycling mussel shell includes, studies for use as construction material (Yoon et al., 2004; Yang et al., 2005), some others investigated shells to use as a filler in the polymer (Chong et al., 2006; Hamester et al., 2012), and some other studies demonstrate the efficiency of the shell as supplementary feed (Fujita et al., 1990) and

also as an alternative liming material to reduce soil acidity (Lee et al., 2008). Similarly, cow urine is also an animal-origin waste product and it is also applied to soil in a dilute manner for nutrient supply. The present study demonstrates the use of mussel shell powder as a slow-release fertilizer. They leached to soil very slowly and hence they are economical and environment friendly with high nutritional value for the growth of plants.

CONCLUSION

The present study mainly focused on the structural, physical and chemical properties of mussel shells along with the development of slow-release natural fertilizer. Structural analysis revealed different layers and calcium carbonate arrangement patterns in the shell. FTIR analysis help to understand the calcite and aragonite composition of the shell and TGA analysis highlights the extreme thermal stability of the shell. The major focus of this chapter was the synthesis of natural slow-release mineral fertilizer from animal origins waste materials such as mussel shells and cow urine. The adsorption ability of mussel shell powder was confirmed by using BET analysis. The shell powder significantly adsorbed mineral nutrients from cow urine. The combination of cow urine and mussel shell powder facilitates the development of struvite crystals which are made up of phosphorous, ammonium and magnesium or potassium, ammonium and magnesium.

The nutrient immobilization study was analysed by XRF analysis and the results showed that significant macronutrient concentration improvement in nutrient-impregnated shell powder than in normal shell powder. Mussel shell is also rich with plant essential micronutrients. The nutrient leaching experiment reveals that half of the nutrient concentration was not released after 30 days of leaching. Struvite crystals also show controlled release properties. Runoff of minerals after rain and watering is the limitation of conventional chemical fertilizer and which leads to continuous use of such chemical fertilizers. Their continuous prolonged use causes several economic

and environmental issues. The present developed natural slow-release fertilizer is rich with plant essential macro and micronutrients and which have reduced leaching properties. Hence this can use as natural slow-release mineral fertilizer in the agricultural field, which can reduce the frequent application of fertilizer in the soil and help to reduce economic and environmental issues to some extent.

Mussels are always fascinating creatures in the research community. They are utilized in the research areas such as biofouling, environment pollution monitoring, adhesive protein research, biomimetic studies etc. *M. edulis* is the most studied mussel species and *P. perna* is the least studied mussel species. The first chapter of the present study mainly focused on *P. perna* adhesive system. The byssus and foot are the two main parts involved in the adhesion of mussels. This chapter demonstrates the structural organization and chemical composition of the byssus and foot of the *P. perna.* Histological imaging of foot tissue exhibits glandular organisation and the foot tissue comprises four glands namely the core gland or collagen gland, accessory gland or cuticle gland, phenol gland or plaque gland and mucous gland. Byssus thread imaging help to understand the different regions of the byssus thread. In *P. perna,* the byssus thread contains three regions proximal thread, distal thread and plaque. The studies revealed that each region shows gradients in protein composition. Anatomically, byssus thread divide into two regions namely cuticle and core and the protein composition in both regions are different. The strength and stability of the byssus thread were exhibited by functional group study and thermal stability analysis. The elemental composition analysis provides insight into the importance of mussel thread in environmental pollution studies. The mussel foot and threads structural and chemical studies help to make new strategies for preventing biofouling.

The second chapter highlights the importance of the natural extraction of mussel adhesive proteins. Several natural extraction methods are available but the yield of protein is the main hindrance in this research.

Cell-TakTM and MAP™ are two commercially available naturally extracted mussel adhesives. The adhesive protein extraction from *P. perna* is not studied yet. In this chapter new natural extraction protocol was developed and it provides high extraction yield. The result concluded that Na_2SO_4-mediated salting out was excellent and efficient for native adhesive protein extraction. Polyacrylamide gel analysis results showed the presence of a single polyphenolic protein found in extract, which is foot protein 1 and it confirmed by previous studies. Foot protein 1 is the most abundant polyphenolic protein secreted by the foot; hence its concentration is high in the extract. All commercially available natural mussel adhesives contain foot protein1 because of its abundance. The extracted proteins surface topography and roughness were measured by atomic force microscopy. The result implies that iron treatment enhances adhesive strength because it reduces the roughness of protein samples. Similarly, contact angle measurement result exhibited that extracted protein samples have hydrophilic nature and the adhesion strength was low in the hydrophilic substrate. This chapter results provide a track to the commercial synthesis of natural adhesive protein from *P. perna.*

The third chapter concentrated on mussel foot protein gene sequencing and characterisation. Two variants of mussel foot protein 6 namely Ppfp-6(1) and Ppfp-6(2) were obtained through sequencing and the consensus sequences were deposited in NCBI. Physico-chemical characterisation, functional role, antioxidant activity, metal binding ability, and phylogeny construction of two variants were done by insilico analysis. The findings showed that the two variants of mussel

foot protein 6 had strong antioxidant activity and serve as protease inhibitors. The findings of this chapter offer important guidance for creating recombinant adhesives inspired by mussels as well as docking studies for reducing biofouling.

The fourth chapter of this research provides the structural, physical and chemical properties of mussel shells along with the development of slow-release natural fertilizer. Nutrient deficiency is the key factor in crop production. The present work developed a natural slow-release fertilizer by using cow urine and mussel shell powder, which is rich with plant's essential macro and micronutrients and also, has slow-release leaching properties. The formation of struvite crystals is the attraction of this slow-release fertilizer. Because of its slow-leaching property, this fertilizer helps to decrease the frequent application of fertilizer in the soil and helps to reduce economic and environmental issues to some extent.

In India, the two most available species of mussels are *P. perna* and *P. viridis*. Research in *P. perna* is not well progressed and limited to ecology, life history, and distribution. On the other hand, mussel adhesive proteins have high commercial value and are less explored area. Hence, research in both natural and recombinant extraction of mussels adhesives has high scientific attention. The present study developed a new protocol for the natural extraction of mussel adhesive protein. The development of a novel commercially viable bioadhesive from *P. perna* is aided by further purification and adhesive performance assessment. Similarly, adhesive protein gene sequencing is important for the development of new recombinant proteins, and biomimetic materials development. In the present study, sequencing of

foot protein 6 was carried out and deposited in NCBI. In mussels, foot protein 6 rescues the DOPA from oxidation. The insilico analysis proved that foot protein 6 of *P. perna* is an excellent antioxidant. Hence researches in the area of synthesis of antioxidant peptides from foot protein 6 of *P. perna* are very promising. Similarly, instead of foot protein 6, *P. perna* has five other adhesive proteins. Therefore, the sequencing of remaining proteins from *P. perna* has high scientific value. Likewise, an eco-friendly slow-release fertilizer from waste materials such as mussel shells and cow urine is a new approach in the field of agriculture to maintain a steady nutrient concentration. The further field application of the current new slow-release fertilizer make significant impact on agricultural field.

Future Scope:

- De novo transcriptome assembly and annotation analysis of *P. perna* to explore adhesive foot proteins and their functional variants for biomedical and industrial application.
- Expression and immunogenicity analysis of adhesive proteins in a different expression model system.
- Explore abiotic stress influences the expression of functional adhesive foot proteins variants.
- Pathway analysis of natural degradation of adhesive foot proteins variants.

Agnihotry, S., Pathak, R. K., Singh, D. B., Tiwari, A., & Hussain, I. (2022). Bioinformatics. In D. B. Singh & R. K. Pathak (Eds.), *Protein structure prediction*. Academic Press.

Akemi Ooka, A., & Garrell, R. L. (2000). Surface-enhanced Raman spectroscopy of DOPA-containing peptides related to adhesive protein of marine mussel, *Mytilus edulis*. *Biopolymers: Original Research on Biomolecules*, *57*(2), 92-102.

Aldred, N., Wills, T., Williams, D., & Clare, A. (2007b). Tensile and dynamic mechanical analysis of the distal portion of mussel (*Mytilus edulis*) byssal threads. *Journal of the Royal Society Interface*, *4*(17), 1159–1167.

Algrain, M., Hennebert, E., Bertemes, P., Wattiez, R., Flammang, P., & Lengerer, B. (2022). In the footsteps of sea stars: deciphering the catalogue of proteins involved in underwater temporary adhesion. *Open Biology*, *12*(8), 220103.

Anand, P. P., & Shibu Vardhanan, Y. (2021). Dye and metal ion adsorption ability of Asian green mussel byssus thread complex; their microscopic and thermal property characterization. *Environmental Technology*, 1–17.

Anand, P. P., & Vardhanan, Y. S. (2020). Computational modelling of wet adhesive mussel foot proteins (Bivalvia): insights into the evolutionary convolution in diverse perspectives. *Scientific reports*, *10*(1), 1-24.

Anderson, K. E., & Waite, J. H. (2002). Biochemical characterization of a byssal protein from *Dreissena bugensis* (Andrusov). *Biofouling*, *18*(1), 37-45.

Andrade, G. R., Araújo, J. L. F. D., Nakamura Filho, A., Guañabens, A. C. P., Carvalho, M. D. D., & Cardoso, A. V. (2015). Functional Surface of the golden mussel's foot: morphology, structures and the role of cilia on underwater adhesion. *Materials Science and Engineering: C*, *54*, 32–42.

Andreasson, A., Kiss, N. B., Juhlin, C. C., & Höög, A. (2013). Long-term storage of endocrine tissues at− 80 C does not adversely affect RNA quality or overall histomorphology. *Biopreservation and biobanking*, *11*(6), 366-370.

Ardito, F., Giuliani, M., Perrone, D., Troiano, G., & Lo Muzio, L. (2017). The crucial role of protein phosphorylation in cell signaling and its use as targeted therapy. *International journal of molecular medicine*, *40*(2), 271-280.

Atasaral, E., Khan, U., Terzi, Y., & Seyhan, K. (2020). Mussel: a potential pollution indicator in the aquatic ecosystem and effect of climate change. *International Journal of Environment and Geoinformatics*, *7*(3), 300–304.

Auer, H., Mobley, J. A., Ayers, L. W., Bowen, J., Chuaqui, R. F., Johnson, L. A., ... & Ramirez, N. C. (2014). The effects of frozen tissue storage conditions on the integrity of RNA and protein. *Biotechnic & Histochemistry*, *89*(7), 518-528.

Axelsson, E., Lundqvist, J., Sawicki, A., Nilsson, S., Schröder, I., Al-Karadaghi, S., ... & Hansson, M. (2006). Recessiveness and dominance in barley mutants deficient in Mg-chelatase subunit D, an AAA protein involved in chlorophyll biosynthesis. *The Plant Cell*, *18*(12), 3606-3616.

Bandara, N., Zeng, H., & Wu, J. (2013). Marine mussel adhesion: biochemistry, mechanisms, and biomimetics. *Journal of Adhesion Science and Technology*, *27*(18–19), 2139–2162.

Barth, A. (2007). Infrared spectroscopy of proteins. *Biochimica Et Biophysica Acta (BBA) - Bioenergetics*, *1767*(9), 1073–1101.

Baty, A. M., Leavitt, P. K., Siedlecki, C. A., Tyler, B. J., Suci, P. A., Marchant, R. E., & Geesey, G. G. (1997). Adsorption of adhesive proteins from the marine mussel, *Mytilus edulis*, on polymer films in the hydrated state using angle dependent X-ray photoelectron spectroscopy and atomic force microscopy. *Langmuir*, *13*(21), 5702-5710.

Benaltabet, T., Gutner-Hoch, E., & Torfstein, A. (2021). Heavy metal, rare earth element and Pb isotope dynamics in mussels during a depuration experiment in the Gulf of Aqaba, Northern Red Sea. *Frontiers in Marine Science*, *8*.

Benkert, P., Tosatto, S. C., & Schomburg, D. (2008). QMEAN: A comprehensive scoring function for model quality assessment. *Proteins: Structure, Function, and Bioinformatics*, *71*(1), 261-277.

Blom, N., Gammeltoft, S., & Brunak, S. (1999). Sequence and structure-based prediction of eukaryotic protein phosphorylation sites. *Journal of molecular biology*, *294*(5), 1351-1362.

Blum, M., Chang, H. Y., Chuguransky, S., Grego, T., Kandasaamy, S., Mitchell, A., ... & Finn, R. D. (2021). The InterPro protein families and domains database: 20 years on. *Nucleic acids research*, *49*(D1), D344-D354.

Botling, J., & Micke, P. (2010). Fresh Frozen Tissue: RNA Extraction and Quality Control. *Methods in Molecular Biology*, 405–413.

Bozec, L., & Odlyha, M. (2011). Thermal Denaturation Studies of Collagen by Microthermal Analysis and Atomic Force Microscopy. *Biophysical Journal*, *101*(1), 228–236.

Bradford, M. M. (1976). A rapid and sensitive method for the quantitation of microgram quantities of protein utilizing the principle of protein-dye binding. *Analytical biochemistry*, *72*(1-2), 248-254.

Brazee, S. L., & Carrington, E. (2006). Interspecific comparison of the mechanical properties of mussel byssus. *The Biological Bulletin*, *211*(3), 263-274.

Britto, D. T., & Kronzucker, H. J. (2008). Cellular mechanisms of potassium transport in plants. *Physiologia Plantarum*, *133*(4), 637-650.

Burkett, J. R., Wojtas, J. L., Cloud, J. L., & Wilker, J. J. (2009). A method for measuring the adhesion strength of marine mussels. *The Journal of Adhesion*, *85*(9), 601-615.

Burns, A., Olszowy, P., & Ciborowski, P. (2016). Proteomic profiling and analytical chemistry: The crossroads. In P. Ciborowski & J. Silberring (Eds.), *Biomolecules* (2nd ed.). Elsevier.

Burzio, L. A., & Waite, J. H. (2000). Cross-linking in adhesive quinoproteins: studies with model decapeptides. *Biochemistry*, *39*(36), 11147-11153.

Burzio, L. A., & Waite, J. H. (2002). The other Topa: formation of 3, 4, 5-trihydroxyphenylalanine in peptides. *Analytical biochemistry*, *306*(1), 108-114.

Calabi-Floody, M., Medina, J., Rumpel, C., Condron, L. M., Hernandez, M., Dumont, M., & de La Luz Mora, M. (2018). Smart fertilizers as a

strategy for sustainable agriculture. *Advances in agronomy*, *147*, 119-157.

Camilloni, C., Rocco, A. G., Eberini, I., Gianazza, E. L. I. S. A. B. E. T. T. A., Broglia, R. A., & Tiana, G. (2008). Urea and guanidinium chloride denature protein L in different ways in molecular dynamics simulations. *Biophysical journal*, *94*(12), 4654-4661.

Carrington, E. (2002). Seasonal variation in the attachment strength of blue mussels: Causes and consequences. *Limnology and Oceanography*, *47*(6), 1723–1733.

Castillo, J. J., Shanbhag, B. K., & He, L. (2017). Comparison of natural extraction and recombinant mussel adhesive proteins approaches. *Food Bioactives*, 111–135.

Cha, H. J., Hwang, D. S., & Lim, S. (2008). Development of bioadhesives from marine mussels. *Biotechnology Journal: Healthcare Nutrition Technology*, *3*(5), 631-638.

Cha, H. J., Hwang, D. S., Lim, S., White, J. D., Matos-Perez, C. R., & Wilker, J. J. (2009). Bulk adhesive strength of recombinant hybrid mussel adhesive protein. *Biofouling*, *25*(2), 99-107.

Chakraborty, A., Parveen, S., Chanda, D. K., & Aditya, G. (2020). An insight into the structure, composition and hardness of a biological material: the shell of freshwater mussels. *RSC advances*, *10*(49), 29543-29554.

Chateigner, D., Hedegaard, C., & Wenk, H. R. (2000). Mollusc shell microstructures and crystallographic textures. *Journal of Structural Geology*, *22*(11-12), 1723-1735.

Checa, A. G. (2018). Physical and biological determinants of the fabrication of molluscan shell microstructures. *Frontiers in Marine Science*, *5*, 353.

Checa, A. G., & Salas, C. (2017). Periostracum and shell formation in the Bivalvia: Treatise Online, part N, Revised, Vol. 1, Chap. 3. Lawrence, K: Kansas University Paleontological Institute, 1-51.

Chiou, I. J., Chen, C. H., & Li, Y. H. (2014). Using oyster-shell foamed bricks to neutralize the acidity of recycled rainwater. *Construction and Building Materials*, *64*, 480-487.

Chong, M. H., Chun, B. C., Chung, Y. C., & Cho, B. G. (2006). Fire-retardant plastic material from oyster-shell powder and recycled polyethylene. *Journal of Applied Polymer Science*, *99*(4), 1583-1589.

Chung, H. S., Lee, S., & Park, S. J. (2016). Oxidation protection in metal-binding peptide motif and its application to antibody for site-selective conjugation. *Plos one*, *11*(7), e0159451.

Cieśla, J., Frączyk, T., & Rode, W. (2011). Phosphorylation of basic amino acid residues in proteins: important but easily missed. *Acta Biochimica Polonica*, *58*(2), 137-48.

Colovos, C., & Yeates, T. O. (1993). Verification of protein structures: patterns of nonbonded atomic interactions. *Protein science*, *2*(9), 1511-1519.

Cordell, D., Drangert, J. O., & White, S. (2009). The story of phosphorus: global food security and food for thought. *Global environmental change*, *19*(2), 292-305.

Coyne, K. J., Qin, X. X., & Waite, J. H. (1997). Extensible collagen in mussel byssus: A natural block copolymer. *Science*, *277*(5333), 1830–1832.

Creuzenet, C., Korshunova, G., Naharisoa, H., Nedev, H., & Haertlé, T. (1993). Synthesis, purification and interactions of casein signal peptides. In *Techniques in protein chemistry IV* (pp. 239-248). Academic Press.

Das, A., & Mukhopadhyay, C. (2009). Urea-mediated protein denaturation: a consensus view. *The Journal of Physical Chemistry B*, *113*(38), 12816-12824.

Dawson, C. J., & Hilton, J. (2011). Fertiliser availability in a resource-limited world: Production and recycling of nitrogen and phosphorus. *Food Policy*, *36*, S14-S22.

de Fouw, J., van der Zee, E. M., van Gils, J. A., Eriksson, B. K., Weerman, E. J., Donadi, S., ... & van der Heide, T. (2020). The interactive role of predation, competition and habitat conditions in structuring an intertidal bivalve population. *Journal of Experimental Marine Biology and Ecology*, *523*, 151267.

De Freitas, S. T., Amarante, C. D., & Mitcham, E. J. (2016). Calcium deficiency disorders in plants. *Postharvest ripening physiology of crops*, 477-502.

Desjardins, P., & Conklin, D. (2010). NanoDrop microvolume quantitation of nucleic acids. *Journal of Visualized Experiments*, (45), e2565.

Douek, J., Paz, G., Gayer, K., Mendelson, M., Rinkevich, B., & Galil, B. (2021). An outbreak of *Perna perna* (Linnaeus, 1758) (Mollusca, Bivalvia, Mytilidae) in the Eastern Mediterranean. *BioInvasions Records*, *10*(1), 136–148.

Elsliger, M. A., & Wilson, I. A. (2012). Comprehensive biophysics. In E. H. Egelman (Ed.), *Structure Validation and Analysis*. Elsevier, 312–36.

Engel, F. G., Alegria, J., Andriana, R., Donadi, S., Gusmao, J. B., van Leeuwe, M. A., ... & Eriksson, B. K. (2017). Mussel beds are biological power stations on intertidal flats. *Estuarine, Coastal and Shelf Science*, *191*, 21-27.

Even, M. A., Wang, J., & Chen, Z. (2008). Structural information of mussel adhesive protein Mefp-3 acquired at various polymer/Mefp-3 solution interfaces. *Langmuir*, *24*(11), 5795-5801.

Fabre, A. L., Colotte, M., Luis, A., Tuffet, S., & Bonnet, J. (2014). An efficient method for long-term room temperature storage of RNA. *European Journal of Human Genetics*, *22*(3), 379-385.

Fageria, N. K. (2005). Soil fertility and plant nutrition research under controlled conditions: Basic principles and methodology. *Journal of plant nutrition*, *28*(11), 1975-1999.

Fan, F., Liu, M., Shi, P., Xu, X., Lu, W., Wang, Z., & Du, M. (2018). Protein cross- linking and the Maillard reaction decrease the solubility of milk protein concentrates. *Food Science & Nutrition*, *6*(5), 1196-1203.

Farooq, R., & Ahmad, Z. (2017). *Physico-Chemical Wastewater Treatment and Resource Recovery*. InTechOpen, 1-9.

Farsad, N., & Sone, E. D. (2012). Zebra mussel adhesion: Structure of the byssal adhesive apparatus in the freshwater mussel, Dreissena polymorpha. *Journal of Structural Biology*, *177*(3), 613–620.

Feldman, A. T., & Wolfe, D. (2014). Tissue Processing and Hematoxylin and Eosin Staining. *Histopathology*, 31–43.

Felipe-Sesé, M., Eliche-Quesada, D., & Corpas-Iglesias, F. A. (2011). The use of solid residues derived from different industrial activities to obtain calcium silicates for use as insulating construction materials. *Ceramics International*, *37*(8), 3019-3028.

Filpula, D. R., Lee, S. M., Link, R. P., Strausberg, S. L., & Strausberg, R. L. (1990). Structural and functional repetition in a marine mussel adhesive protein. *Biotechnology progress*, *6*(3), 171-177.

Fleige, S., & Pfaffl, M. W. (2006). RNA integrity and the effect on the real-time qRT-PCR performance. *Molecular aspects of medicine*, *27*(2-3), 126-139.

Frank, B. P., & Belfort, G. (2002). Adhesion of *Mytilus edulis* foot protein 1 on silica: ionic effects on biofouling. *Biotechnology progress*, *18*(3), 580-586.

Freudl, R. (2018). Signal peptides for recombinant protein secretion in bacterial expression systems. *Microbial cell factories*, *17*(1), 1-10.

Fujita, T., Fukase, M., Miyamoto, H., Matsumoto, T., & Ohue, T. (1990). Increase of bone mineral density by calcium supplement with oyster shell electrolysate. *Bone and Mineral*, *11*(1), 85-91.

Funabara, D., Ohmori, F., Kinoshita, S., Koyama, H., Mizutani, S., Ota, A., ... & Watabe, S. (2014). Novel genes participating in the formation of prismatic and nacreous layers in the pearl oyster as revealed by their tissue distribution and RNA interference knockdown. *PLoS One*, *9*(1), e84706.

Gaffey, S. J. (1987). Spectral reflectance of carbonate minerals in the visible and near infrared (0.35–2.55 um): Anhydrous carbonate minerals. *Journal of Geophysical Research: Solid Earth*, *92*(B2), 1429-1440.

Gantayet, A., Ohana, L., & Sone, E. D. (2013). Byssal proteins of the freshwater zebra mussel, *Dreissena polymorpha*. *Biofouling*, *29*(1), 77-85.

Gargaud, M., Irvine, W. M., Amils, R., Ii, C. H. J., Pinti, D., Quintanilla, C. J., Rouan, D., Spohn, T., Tirard, S., & Viso, M. (2015). *Encyclopedia of Astrobiology* (2nd ed. 2015). Springer, 138-157.

Gasteiger, E., Hoogland, C., Gattiker, A., Wilkins, M. R., Appel, R. D., & Bairoch, A. (2005). Protein identification and analysis tools on the ExPASy server. *The proteomics protocols handbook*, 571-607.

Geourjon, C., & Deleage, G. (1994). SOPM: a self-optimized method for protein secondary structure prediction. *Protein Engineering, Design and Selection*, *7*(2), 157-164.

Gigante, V., Cinelli, P., Righetti, M. C., Sandroni, M., Tognotti, L., Seggiani, M., & Lazzeri, A. (2020). Evaluation of mussel shells powder as reinforcement for PLA-based biocomposites. *International journal of molecular sciences*, *21*(15), 5364.

Giles, N. M., Watts, A. B., Giles, G. I., Fry, F. H., Littlechild, J. A., & Jacob, C. (2003). Metal and redox modulation of cysteine protein function. *Chemistry & biology*, *10*(8), 677-693.

Gim, Y., Hwang, D. S., Lim, S., Song, Y. H., & Cha, H. J. (2008). Production of fusion mussel adhesive fp-353 in *Escherichia coli*. *Biotechnology progress*, *24*(6), 1272-1277.

Goldberg ED (1975) The mussel watch: a frst step in global marine monitoring. *Marine Pollution Bulletin, 6*, 111–114.

Goldman, N. (1990). Maximum likelihood inference of phylogenetic trees, with special reference to a Poisson process model of DNA substitution and to parsimony analyses. *Systematic Zoology*, *39*(4), 345-361.

Grégoire, C. (1961). Structure of the conchiolin cases of the prisms in *Mytilus edulis* Linne. *The Journal of Cell Biology*, *9*(2), 395-400.

Gunasekaran, S., Anbalagan, G., & Pandi, S. (2006). Raman and infrared spectra of carbonates of calcite structure. *Journal of Raman Spectroscopy*, *37*(9), 892-899.

Gupta, A., & Denis, Y. (Eds.). (2016). Flotation. In *Mineral Processing Design and Operations* (2nd ed., pp. 689–741). Elsevier.

Guvendiren, M., Brass, D. A., Messersmith, P. B., & Shull, K. R. (2009). Adhesion of DOPA-functionalized model membranes to hard and soft surfaces. *The Journal of adhesion*, *85*(9), 631-645.

Haemers, S., Koper, G. J., & Frens, G. (2003). Effect of oxidation rate on cross-linking of mussel adhesive proteins. *Biomacromolecules*, *4*(3), 632-640.

Haemers, S., van der Leeden, M. C., & Frens, G. (2005). Coil dimensions of the mussel adhesive protein Mefp-1. *Biomaterials*, *26*(11), 1231-1236.

Hagenau, A., Scheidt, H. A., Serpell, L., Huster, D., & Scheibel, T. (2009). Structural analysis of proteinaceous components in byssal threads of the mussel*Mytilus galloprovincialis*. *Macromolecular Bioscience*, *9*(2), 162–168.

Hamby, S. E., & Hirst, J. D. (2008). Prediction of glycosylation sites using random forests. *BMC bioinformatics*, *9*(1), 1-13.

Hamester, M. R. R., Balzer, P. S., & Becker, D. (2012). Characterization of calcium carbonate obtained from oyster and mussel shells and incorporation in polypropylene. *Materials Research*, *15*, 204-208.

Hani, F. M., Cole, A. E., & Altman, E. (2019). The ability of salts to stabilize proteins in vivo or intracellularly correlates with the Hofmeister series of ions. *International Journal of Biochemistry and Molecular Biology*, *10*(3), 23.

Hao, X., Wang, C., van Loosdrecht, M. C. M., & Hu, Y. (2013). Looking Beyond Struvite for P-Recovery. *Environmental Science &Amp; Technology*, *47*(10), 4965–4966.

Harrington, M. J., & Waite, J. H. (2007). Holdfast heroics: comparing the molecular and mechanical properties of *Mytilus californianus* byssal threads. *Journal of Experimental Biology*, *210*(24), 4307–4318.

Harrington, M. J., Masic, A., Holten-Andersen, N., Waite, J. H., & Fratzl, P. (2010). Iron-clad fibers: a metal-based biological strategy for hard flexible coatings. *Science*, *328*(5975), 216-220.

Hedlund, J., Andersson, M., Fant, C., Bitton, R., Bianco-Peled, H., Elwing, H., & Berglin, M. (2009). Change of colloidal and surface properties of *Mytilus edulis* foot protein 1 in the presence of an oxidation ($NaIO_4$) or a complex-binding (Cu^{2+}) agent. *Biomacromolecules*, *10*(4), 845-849.

Hellio, C., Thomas-Guyon, H., Culioli, G., Piovettt, L., Bourgougnon, N., & le Gal, Y. (2001). Marine antifoulants from *Bifurcaria bifurcata* (Phaeophyceae, Cystoseiraceae) and other brown macroalgae. *Biofouling*, *17*(3), 189-201.

Hennebert, E., Gregorowicz, E., & Flammang, P. (2018). Involvement of sulfated biopolymers in adhesive secretions produced by marine invertebrates. *Biology Open*, *7*(11), bio037358.

Hicks, D. W. (1993). Invasion of the south Texas coast by the edible brown mussel *Perna perna* (Linnaeus, 1758). *Veliger*, *36*(1), 92-94.

Hicks, D. W., & McMahon, R. (2002). Temperature acclimation of upper and lower thermal limits and freeze resistance in the nonindigenous brown mussel, *Perna perna* (L.), from the Gulf of Mexico. *Marine Biology*, *140*(6), 1167–1179.

Hicks, D. W., Hawkins, D. L., & McMahon, R. F. (2000). Salinity tolerance of brown mussel *Perna perna* (L.) from the Gulf of Mexico: An extension of life table analysis to estimate median survival time in the presence of regressor variables. *Journal of Shellfish Research*, *19*(1), 203–212.

Hight, L. M., & Wilker, J. J. (2007). Synergistic effects of metals and oxidants in the curing of marine mussel adhesive. *Journal of materials science*, *42*(21), 8934-8942.

Hollingsworth, S. A., & Karplus, P. A. (2010). A fresh look at the Ramachandran plot and the occurrence of standard structures in proteins. *BioMolecular Concepts*, *1*(3–4), 271–283.

Holten-Andersen, N., Fantner, G. E., Hohlbauch, S., Waite, J. H., & Zok, F. W. (2007). Protective coatings on extensible biofibres. *Nature Materials*, *6*(9), 669–672.

Holten-Andersen, N., Mates, T. E., Toprak, M. S., Stucky, G. D., Zok, F. W., & Waite, J. H. (2009). Metals and the integrity of a biological coating: the cuticle of mussel byssus. *Langmuir*, *25*(6), 3323-3326.

Holten-Andersen, N., Slack, N., Zok, F., & Herbert Waite, J. (2004). Nano-Mechanical Investigation of the Byssal Cuticle, a Protective Coating of a Bio-Elastomer. *MRS Proceedings*, *841*.

Holten-Andersen, N., Zhao, H., & Waite, J. H. (2009). Stiff coatings on compliant biofibers: the cuticle of *Mytilus californianus* byssal threads. *Biochemistry*, *48*(12), 2752-2759.

Hu, S., Wang, Y., & Han, H. (2011). Utilization of waste freshwater mussel shell as an economic catalyst for biodiesel production. *biomass and bioenergy*, *35*(8), 3627-3635.

Huang, C. H., Singh, G. P., Park, S. H., Chua, N. H., Ram, R. J., & Park, B. S. (2020). Early diagnosis and management of nitrogen deficiency in plants utilizing Raman spectroscopy. *Frontiers in plant science*, *11*, 663.

Huang, L. H., Lin, P. H., Tsai, K. W., Wang, L. J., Huang, Y. H., Kuo, H. C., & Li, S. C. (2017). The effects of storage temperature and duration of blood samples on DNA and RNA qualities. *Plos one*, *12*(9), e0184692.

Hwang, D. S., Gim, Y., & Cha, H. J. (2005). Expression of functional recombinant mussel adhesive protein type 3A in *Escherichia coli*. *Biotechnology progress*, *21*(3), 965-970.

Hwang, D. S., Gim, Y., Kang, D. G., Kim, Y. K., & Cha, H. J. (2007a). Recombinant mussel adhesive protein Mgfp-5 as cell adhesion biomaterial. *Journal of biotechnology*, *127*(4), 727-735.

Hwang, D. S., Gim, Y., Yoo, H. J., & Cha, H. J. (2007b). Practical recombinant hybrid mussel bioadhesive fp-151. *Biomaterials*, *28*(24), 3560-3568.

Hwang, D. S., Kim, K. R., Lim, S., Choi, Y. S., & Cha, H. J. (2009). Recombinant mussel adhesive protein as a gene delivery material. *Biotechnology and Bioengineering*, *102*(2), 616–623. https://doi.org/10.1002/bit.22086

Hwang, D. S., Sim, S. B., & Cha, H. J. (2007c). Cell adhesion biomaterial based on mussel adhesive protein fused with RGD peptide. *Biomaterials*, *28*(28), 4039-4046.

Hwang, D. S., Yoo, H. J., Jun, J. H., Moon, W. K., & Cha, H. J. (2004). Expression of functional recombinant mussel adhesive protein Mgfp-5 in Escherichia coli. *Applied and environmental microbiology*, *70*(6), 3352-3359.

Hwang, D. S., Zeng, H., Masic, A., Harrington, M. J., Israelachvili, J. N., & Waite, J. H. (2010). Protein- and metal-dependent interactions of a prominent protein in mussel adhesive plaques. *Journal of Biological Chemistry*, *285*(33), 25850–25858.

Hyde, A. M., Zultanski, S. L., Waldman, J. H., Zhong, Y. L., Shevlin, M., & Peng, F. (2017). General principles and strategies for Salting-Out informed by the hofmeister series. *Organic Process Research &Amp; Development*, *21*(9), 1355–1370.

Imperiali, B., & Hendrickson, T. L. (1995). Asparagine-linked glycosylation: specificity and function of oligosaccharyl transferase. *Bioorganic & medicinal chemistry*, *3*(12), 1565-1578.

Inoue, K., Onitsuka, Y., & Koito, T. (2021). Mussel biology: from the byssus to ecology and physiology, including microplastic ingestion and deep-sea adaptations. *Fisheries science*, *87*(6), 761-771.

Inoue, K., Takeuchi, Y., Miki, D., & Odo, S. (1995). Mussel adhesive plaque protein gene is a novel member of epidermal growth factor-like gene family. *Journal of Biological Chemistry*, *270*(12), 6698-6701.

Inoue, K., Yoshioka, Y., Tanaka, H., Kinjo, A., Sassa, M., Ueda, I., ... & Itoh, T. (2021). Genomics and transcriptomics of the green mussel explain the durability of its byssus. *Scientific reports*, *11*(1), 1-11.

Jentoft, N. (1990). Why are proteins O-glycosylated?. *Trends in biochemical sciences*, *15*(8), 291-294.

Jeyachandran, Y. L., Mielczarski, E., Rai, B., & Mielczarski, J. A. (2009). Quantitative and qualitative evaluation of adsorption/desorption of bovine serum albumin on hydrophilic and hydrophobic surfaces. *Langmuir*, *25*(19), 11614-11620.

Jones, M. I., Wang, L. Y., Abeynaike, A., & Patterson, D. A. (2011). Utilisation of waste material for environmental applications: calcination of mussel shells for waste water treatment. *Advances in applied ceramics*, *110*(5), 280-286.

Jovanovski, G., Stefov, V., Shoptrajanov, B., & Boev, B. (2002). Minerals from Macedonia IV. Discrimination between some carbonate minerals by FTIR spectroscopy. *Min. Abh*, (404), 1-13.

Kapp, K., Schrempf, S., Lemberg, M. K., & Dobberstein, B. (2009). Post-targeting functions of signal peptides. *Protein transport into the endoplasmic reticulum*, 1-16.

Kaushik, N. K., Kaushik, N., Pardeshi, S., Sharma, J. G., Lee, S. H., & Choi, E. H. (2015). Biomedical and clinical importance of mussel-inspired polymers and materials. *Marine drugs*, *13*(11), 6792-6817.

Kitamura, M., Kawakami, K., Nakamura, N., Tsumoto, K., Uchiyama, H., Ueda, Y., ... & Nakaya, T. (1999). Expression of a model peptide of a marine mussel adhesive protein in *Escherichia coli* and characterization of its structural and functional properties. *Journal of Polymer Science Part A: Polymer Chemistry*, *37*(6), 729-736.

Ku, S. H., Lee, J. S., & Park, C. B. (2010). Spatial control of cell adhesion and patterning through mussel-inspired surface modification by polydopamine. *Langmuir*, *26*(19), 15104-15108.

Kumar, B.R. and Rao, T.S. (2012) AFM Studies on surface morphology, topography and texture of nanostructured zinc aluminum oxide thin films. *Digest Journal of Nano-materials and Biostructures*, *7*, 1881-1889.

Kumar, P., Halder, S., & Bansal, M. (2019). Biomolecular structures: prediction, identification and analyses. *Encyclopedia of Bioinformatics and Computational Biology*, 504–534.

Kumar, S. (2013). The role of biopesticides in sustainably feeding the nine billion global populations. *Journal of Biofertilizers & Biopesticides*, *4*, e114.

Kumar, S., Kumar, S., & Mohapatra, T. (2021). Interaction between macro-and micro-nutrients in plants. *Frontiers in Plant Science*, *12*, 665583.

Kuriakose, P. S., & Nair, N. B. (1976). Genus perna along the coasts of India with the description of a new species *perna indica*. *Aquatic Biology*, *1*, 25–36.

Lane, D. J. W., Nott, J. A., & Crisp, D. J. (1982b). Enlarged stem glands in the foot of the post-larval mussel, *Mytilus Edulis*: adaptation for bysso-pelagic migration. *Journal of the Marine Biological Association of the United Kingdom*, *62*(4), 809–818.

Laskowski, R. A., MacArthur, M. W., Moss, D. S., & Thornton, J. M. (1993). PROCHECK: a program to check the stereochemical quality of protein structures. *Journal of applied crystallography*, *26*(2), 283-291.

Lawrencia, D., Wong, S. K., Low, D. Y. S., Goh, B. H., Goh, J. K., Ruktanonchai, U. R., ... & Tang, S. Y. (2021). Controlled release fertilizers: A review on coating materials and mechanism of release. *Plants*, *10*(2), 238.

Lee, B. P., Dalsin, J. L., & Messersmith, P. B. (2002). Synthesis and gelation of DOPA-modified poly (ethylene glycol) hydrogels. *Biomacromolecules*, *3*(5), 1038-1047.

Lee, B. P., Messersmith, P. B., Israelachvili, J. N., & Waite, J. H. (2011). Mussel-inspired adhesives and coatings. *Annual review of materials research*, *41*, 99.

Lee, C. H., Lee, D. K., Ali, M. A., & Kim, P. J. (2008). Effects of oyster shell on soil chemical and biological properties and cabbage productivity as a liming materials. *Waste Management*, *28*(12), 2702-2708.

Lee, H., Scherer, N. F., & Messersmith, P. B. (2006). Single-molecule mechanics of mussel adhesion. *Proceedings of the National Academy of Sciences*, *103*(35), 12999-13003.

Lee, J. S., Lee, Y. G., Park, J. J., & Shin, Y. K. (2012). Microanatomy and ultrastructure of the foot of the infaunal bivalve *Tegillarca granosa* (Bivalvia: Arcidae). *Tissue and Cell*, *44*(5), 316–324.

Legodi, M. A., De Waal, D., & Potgieter, J. H. (2001). Quantitative determination of CaCO 3 in cement blends by FT-IR. *Applied Spectroscopy*, *55*(3), 361-365.

Li, N. N., Shi, G., Yang, X. X., Wang, Z. P., & Liao, Z. (2011). Detection of Dihydroxyphenylalanine in native foot proteins from *Mytilus coruscus* Byssus. *Chinese Journal of Biochemistry and Molecular Biology*, *27*, 148-153.

Li, S., Chen, J., Wang, J., & Zeng, H. (2021). Anti-biofouling materials and surfaces based on mussel-inspired chemistry. *Materials Advances*, *2*(7), 2216–2230.

Li, S., Xia, Z., Chen, Y., Gao, Y., & Zhan, A. (2018). Byssus structure and protein composition in the highly invasive fouling mussel *Limnoperna fortunei*. *Frontiers in Physiology*, *9*.

Lin, Q., Zhang, F., Han, F., Zhao, M., & Jiang, Z. (2019). Influence of surface roughness on the adhesion hysteresis of nano thin film. *Micro &Amp; Nano Letters*, *14*(12), 1278–1281.

Liu, X. X., Li, Y., & Bai, Z. H. (2021). Corynebacterium glutamicum as a robust microbial factory for production of value-added proteins and small molecules: fundamentals and applications. In *Microbial Cell Factories Engineering for Production of Biomolecules* (pp. 235-263). Academic Press.

Lu, C. H., Chen, C. C., Yu, C. S., Liu, Y. Y., Liu, J. J., Wei, S. T., & Lin, Y. F. (2022). MIB2: metal ion-binding site prediction and modeling server. *Bioinformatics*, *38*(18), 4428-4429.

Lu, Q., Danner, E., Waite, J. H., Israelachvili, J. N., Zeng, H., & Hwang, D. S. (2013). Adhesion of mussel foot proteins to different substrate surfaces. *Journal of The Royal Society Interface*, *10*(79), 20120759.

Lu, Q., Hwang, D. S., Liu, Y., & Zeng, H. (2012). Molecular interactions of mussel protective coating protein, mcfp-1, from Mytilus californianus. *Biomaterials*, *33*(6), 1903-1911.

Lubkowski, K., & Grzmil, B. (2007). Controlled release fertilizers. *Polish Journal of Chemical Technology*, *9*(4), 81-84.

Lukács, M., Csilla Pálinkás, D., Szunyog, G., & Várnagy, K. (2021). Metal binding ability of small peptides containing cysteine residues. *ChemistryOpen*, *10*(4), 451-463.

Lyu, Z., Wang, Z., Luo, F., Shuai, J., & Huang, Y. (2021). Protein secondary structure prediction with a reductive deep learning method. *Frontiers in Bioengineering and Biotechnology*, 404.

Maathuis, F. J. (2009). Physiological functions of mineral macronutrients. *Current opinion in plant biology*, *12*(3), 250-258.

Martinez Rodriguez, N. R., Das, S., Kaufman, Y., Israelachvili, J. N., & Waite, J. H. (2015). Interfacial pH during mussel adhesive plaque formation. *Biofouling*, *31*(2), 221-227.

Martínez-García, C., González-Fonteboa, B., Martínez-Abella, F., & Carro-López, D. (2017). Performance of mussel shell as aggregate in plain concrete. *Construction and Building Materials*, *139*, 570-583.

McAinsh, M. R., & Pittman, J. K. (2009). Shaping the calcium signature. *New Phytologist*, *181*(2), 275-294.

Meng, X., Chen, W. W., Wang, Y. Y., Huang, Z. R., Ye, X., Chen, L. S., & Yang, L. T. (2021). Effects of phosphorus deficiency on the absorption of mineral nutrients, photosynthetic system performance and antioxidant metabolism in *Citrus grandis*. *Plos One*, *16*(2), e0246944.

Mesterházy, E., Lebrun, C., Crouzy, S., Jancsó, A., & Delangle, P. (2018). Short oligopeptides with three cysteine residues as models of sulphur-rich Cu (i)-and Hg (ii)-binding sites in proteins. *Metallomics*, *10*(9), 1232-1244.

Mirshafian, R., Wei, W., Israelachvili, J. N., & Waite, J. H. (2016). α, β-dehydro-Dopa: A hidden participant in mussel adhesion. *Biochemistry*, *55*(5), 743-750.

Mititelu, M., Stanciu, G., Drăgănescu, D., Ioniță, A. C., Neacșu, S. M., Dinu, M., ... & Moroșan, E. (2021). Mussel Shells, a Valuable Calcium Resource for the Pharmaceutical Industry. *Marine Drugs*, *20*(1), 25.

Mo, K. H., Alengaram, U. J., Jumaat, M. Z., Lee, S. C., Goh, W. I., & Yuen, C. W. (2018). Recycling of seashell waste in concrete: A review. *Construction and Building Materials*, *162*, 751-764.

Mohamed, M., Yusup, S., & Maitra, S. (2012). Decomposition study of calcium carbonate in cockle shell. *Journal of Engineering Science and Technology*, 7(1), 1-10.

Monahan, J., & Wilker, J. J. (2003). Specificity of metal ion cross-linking in marine mussel adhesives. *Chemical Communications*, (14), 1672-1673.

Monahan, J., & Wilker, J. J. (2004). Cross-linking the protein precursor of marine mussel adhesives: bulk measurements and reagents for curing. *Langmuir*, *20*(9), 3724-3729.

Montroni, D., Giusti, G., Simoni, A., Cau, G., Ciavatta, C., Marzadori, C., & Falini, G. (2020). Metal ion removal using waste byssus from aquaculture. *Scientific Reports*, *10*(1).

Mutter, G. L., Zahrieh, D., Liu, C., Neuberg, D., Finkelstein, D., Baker, H. E., & Warrington, J. A. (2004). Comparison of frozen and RNALater solid tissue storage methods for use in RNA expression microarrays. *BMC Genomics*, *5*(1).

Narayan, O. P., Kumar, P., Yadav, B., Dua, M., & Johri, A. K. (2022). Sulfur nutrition and its role in plant growth and development. *Plant Signaling & Behavior*, 2030082.

Nguyen, V. Q., Van, H. T., Sy, H. L., Nguyen, T. M. L., & Nguyen, D. K. (2021). Application of Mussell-derived biosorbent to remove NH4+ from aqueous solution: Equilibrium and Kinetics. *SN Applied Sciences*, *3*(4), 1-12.

Nicklisch, S. C., Das, S., Martinez Rodriguez, N. R., Waite, J. H., & Israelachvili, J. N. (2013). Antioxidant efficacy and adhesion rescue by a recombinant mussel foot protein-6. *Biotechnology progress*, *29*(6), 1587-1593.

Ninan, L., Monahan, J., Stroshine, R. L., Wilker, J. J., & Shi, R. (2003). Adhesive strength of marine mussel extracts on porcine skin. *Biomaterials*, *24*(22), 4091-4099.

Nwachukwu, I. D., & Aluko, R. E. (2019). Structural and functional properties of food protein-derived antioxidant peptides. *Journal of Food Biochemistry*, *43*(1), e12761.

Ohkawa, K., Nagai, T., Nishida, A., & Yamomoto, H. (2009b). Purification of DOPA-Containing foot proteins from green mussel,*Perna viridis*, and adhesive properties of synthetic model copolypeptides. *The Journal of Adhesion*, *85*(11), 770–791.

Ohkawa, K., Nishida, A., Yamamoto, H., & Waite, J. H. (2004). A glycosylated byssal precursor protein from the green mussel *Perna viridis* with modified dopa side-chains. *Biofouling*, *20*(2), 101-115.

Ohtsubo, K., & Marth, J. D. (2006). Glycosylation in cellular mechanisms of health and disease. *Cell*, *126*(5), 855-867.

Olsen, T. H., Yesiltas, B., Marin, F. I., Pertseva, M., García-Moreno, P. J., Gregersen, S., ... & Marcatili, P. (2020). AnOxPePred: using deep learning for the prediction of antioxidative properties of peptides. *Scientific Reports*, *10*(1), 1-10.

Papadimitriou, C. A., Krey, G., Stamatis, N., & Kallianiotis, A. (2017). The use of waste mussel shells for the adsorption of dyes and heavy metals. *Journal of Chemical Technology & Biotechnology*, *92*(8), 1943-1947.

Papov, V. V., Diamond, T. V., Biemann, K., & Waite, J. H. (1995). Hydroxyarginine-containing polyphenolic proteins in the adhesive plaques of the marine mussel *Mytilus edulis*. *Journal of Biological Chemistry*, *270*(34), 20183-20192.

Parveen, S., Chakraborty, A., Chanda, D. K., Pramanik, S., Barik, A., & Aditya, G. (2020). Microstructure analysis and chemical and mechanical characterization of the shells of three freshwater snails. *ACS omega*, *5*(40), 25757-25771.

Paz, M. A., Flückiger, R., Boak, A., Kagan, H. M., & Gallop, P. M. (1991). Specific detection of quinoproteins by redox-cycling staining. *Journal of Biological Chemistry*, *266*(2), 689-692.

Pearce, L. R., Komander, D., & Alessi, D. R. (2010). The nuts and bolts of AGC protein kinases. *Nature reviews Molecular cell biology*, *11*(1), 9-22.

Piferrer, F., Beaumont, A., Falguière, J. C., Flajšhans, M., Haffray, P., & Colombo, L. (2009). Polyploid fish and shellfish: production, biology and applications to aquaculture for performance improvement and genetic containment. *Aquaculture*, *293*(3-4), 125-156.

Priemel, T., Degtyar, E., Dean, M. N., & Harrington, M. J. (2017). Rapid self-assembly of complex biomolecular architectures during mussel byssus biofabrication. *Nature Communications*, *8*(1).

Priemel, T., Palia, R., Babych, M., Thibodeaux, C. J., Bourgault, S., & Harrington, M. J. (2020). Compartmentalized processing of catechols during mussel byssus fabrication determines the destiny of DOPA. *Proceedings of the National Academy of Sciences*, *117*(14), 7613-7621.

Qin, C. L., Pan, Q. D., Qi, Q., Fan, M. H., Sun, J. J., Li, N. N., & Liao, Z. (2016). In-depth proteomic analysis of the byssus from marine mussel Mytilus coruscus. *Journal of Proteomics*, *144*, 87–98.

Qin, X. X., & Waite, J. H. (1998). A potential mediator of collagenous block copolymer gradients in mussel byssal threads. *Proceedings of the National Academy of Sciences*, *95*(18), 10517–10522.

Qvist, M. (2002). U.S. Patent No. 6,335,430. Washington, DC: U.S. Patent and Trademark Office.

Rahman, R., Sofi, J. A., Javeed, I., Malik, T. H., & Nisar, S. (2020). Role of micronutrients in crop production. *International Journal of Current Microbiology and Applied Sciences*, *11*, 2265-2287.

Ramani, B., Zorn, H., & Papenbrock, J. (2004). Quantification and fatty acid profiles of sulfolipids in two halophytes and a glycophyte grown under different salt concentrations. *Zeitschrift für Naturforschung C*, *59*(11-12), 835-842.

Ramazi, S., & Zahiri, J. (2021). Post-translational modifications in proteins: resources, tools and prediction methods. *Database*, *2021*.

Rio, D. C., Ares, M., Hannon, G. J., & Nilsen, T. W. (2010). Purification of RNA Using TRIzol (TRI Reagent). *Cold Spring Harbor Protocols*, *2010*(6), pdb.prot5439.

Rius, M., & McQuaid, C. D. (2006). Wave action and competitive interaction between the invasive mussel Mytilus galloprovincialis and the indigenous *Perna perna* in South Africa. *Marine Biology*, *150*(1), 69–78.

Robinson, H., Gao, Y. G., Sanishvili, R., Joachimiak, A., & Wang, A. H. J. (2000). Hexahydrated magnesium ions bind in the deep major groove and at the outer mouth of A-form nucleic acid duplexes. *Nucleic acids research*, *28*(8), 1760-1766.

Rodrigues, D. M., do Amaral Fragoso, R., Carvalho, A. P., Hein, T., & Guerreiro de Brito, A. (2019). Recovery of phosphates as struvite from urine-diverting toilets: optimization of pH, Mg: PO4 ratio and contact time to improve precipitation yield and crystal morphology. *Water Science and Technology*, *80*(7), 1276-1286.

Rola, R. C., Souza, M. M., & Sandrini, J. Z. (2017). Hypoosmotic stress in the mussel *Perna perna* (Linnaeus, 1758): Is ecological history a determinant for organismal responses?. *Estuarine, Coastal and Shelf Science*, *189*, 216-223.

Rolla, M., Consuegra, S., Hall, D. J., & Garcia de Leaniz, C. (2020). Seasonal and spatial variation in growth and abundance of zebra mussel (*Dreissena polymorpha*) in a recently invaded artificial lake: Implications for management. *Frontiers in Ecology and Evolution*, *8*, 159.

Ruiz, J. M., & Romero, L. (2002). Relationship between potassium fertilisation and nitrate assimilation in leaves and fruits of cucumber (*Cucumis sativus*) plants. *Annals of applied Biology*, *140*(3), 241-245.

Ryšlavá, H., Doubnerová, V., Kavan, D., & Vaněk, O. (2013). Effect of posttranslational modifications on enzyme function and assembly. *Journal of proteomics*, *92*, 80-109.

Ryu, H. D., Lim, C. S., Kang, M. K., & Lee, S. I. (2012). Evaluation of struvite obtained from semiconductor wastewater as a fertilizer in cultivating Chinese cabbage. *Journal of hazardous materials*, *221*, 248-255.

Rzepecki, L. M., Hansen, K. M., & Waite, J. H. (1992). Characterization of a cystine-rich polyphenolic protein family from the blue mussel *Mytilus edulis* L. *The Biological Bulletin*, *183*(1), 123-137.

Sáez, C., Pardo, J., Gutierrez, E., Brito, M., & Burzio, L. O. (1991). Immunological studies of the polyphenolic proteins of mussels. *Comparative Biochemistry and Physiology--Part B: Biochemistry*, *98*(4), 569-572.

Sagert, J., & Waite, J. H. (2009). Hyperunstable matrix proteins in the byssus of *Mytilus galloprovincialis*. *Journal of Experimental Biology*, *212*(14), 2224–2236.

Sanger, F., & Coulson, A. R. (1975). A rapid method for determining sequences in DNA by primed synthesis with DNA polymerase. *Journal of molecular biology*, *94*(3), 441-448.

Sarmadi, B. H., & Ismail, A. (2010). Antioxidative peptides from food proteins: A review. *Peptides*, *31*(10), 1949-1956.

Schmitt, C. N. Z., Winter, A., Bertinetti, L., Masic, A., Strauch, P., & Harrington, M. J. (2015). Mechanical homeostasis of a DOPA-enriched biological coating from mussels in response to metal variation. *Journal of the Royal Society Interface*, *12*(110), 20150466.

Seguin-Heine, M. O., Lachance, A. A., Genard, B., Myrand, B., Pellerin, C., Marcotte, I., & Tremblay, R. (2014). Impact of open sea habitat on byssus attachment of suspension-cultured blue mussels (*Mytilus edulis*). *Aquaculture*, *426–427*, 189–196.

Sever, M. J., Weisser, J. T., Monahan, J., Srinivasan, S., & Wilker, J. J. (2004). Metal-mediated cross-linking in the generation of a marine-mussel adhesive. *Angewandte Chemie International Edition*, *43*(4), 448-450.

Sherman, S. D., Quist, A., & Hansma, P. (2009). Relationship between stickiness and surface roughness Of composite materials: atomic force microscopy and intermolecular adhesion force measurement. *Journal of Nano Research*, *6*, 225–235.

Shimazaki, Y., Takani, M., & Yamauchi, O. (2009). Metal complexes of amino acids and amino acid side chain groups: Structures and properties. *Dalton Transactions*, (38), 7854-7869.

Silverman, H. G., & Roberto, F. F. (2006a). *Cloning and expression of recombinant adhesive protein Mefp-1 of the Blue Mussel, Mytilus edulis* (No. US6987170B). Idaho National Lab.(INL), Idaho Falls, ID (United States).

Silverman, H. G., & Roberto, F. F. (2006b). *Cloning and expression of recombinant adhesive protein Mefp-2 of the Blue Mussel, Mytilus edulis* (No. US6995012B1).). Idaho National Lab.(INL), Idaho Falls, ID (United States).

Silverman, H. G., & Roberto, F. F. (2007). Understanding Marine Mussel Adhesion. *Marine Biotechnology*, *9*(6), 661–681.

Smith, B. J. (1984). Acetic Acid-Urea polyacrylamide gel electrophoresis of proteins. *Proteins*, 63–74.

Smith, V. J. (2011). Phylogeny of whey acidic protein (WAP) four-disulfide core proteins and their role in lower vertebrates and invertebrates. *Biochemical Society Transactions*, *39*(5), 1403-1408.

Sneha, P., & Doss, C. G. P. (2016). Molecular dynamics: new frontier in personalized medicine. *Advances in protein chemistry and structural biology*, *102*, 181-224.

Stewart, R. J., Ransom, T. C., & Hlady, V. (2011). Natural underwater adhesives. *Journal of Polymer Science Part B: Polymer Physics*, *49*(11), 757-771.

Suci, P. A., & Geesey, G. G. (2000). Influence of sodium periodate and tyrosinase on binding of alginate to adlayers of *Mytilus edulis* foot protein 1. *Journal of colloid and interface science*, *230*(2), 340-348.

Suci, P. A., & Geesey, G. G. (2000). Influence of sodium periodate and tyrosinase on binding of alginate to adlayers of *Mytilus edulis* foot protein 1. *Journal of colloid and interface science*, *230*(2), 340-348.

Sun, C., Lucas, J. M., & Waite, J. H. (2002). Collagen-binding matrix proteins from elastomeric extraorganismic byssal fibers. *Biomacromolecules*, *3*(6), 1240–1248.

Swann, C. P., Adewole, T., & Waite, J. (1998). Preferential manganese accumulation in dreissenid byssal threads. *Comparative Biochemistry and Physiology Part B: Biochemistry and Molecular Biology*, *119*(4), 755–759.

Szefer, P., Frelek, K., Szefer, K., Lee, C. B., Kim, B. S., Warzocha, J., Zdrojewska, I., & Ciesielski, T. (2002). Distribution and relationships of trace metals in soft tissue, byssus and shells of *Mytilus edulis* trossulus from the southern Baltic. *Environmental Pollution*, *120*(2), 423–444.

Szymańska, M., Sosulski, T., Bożętka, A., Dawidowicz, U., Wąs, A., Szara, E., ... & Cornelissen, R. L. (2020). Evaluating the struvite recovered from anaerobic digestate in a farm bio-refinery as a slow-release fertiliser. *Energies*, *13*(20), 5342.

Takeuchi, Y., Inoue, K., Miki, D., Odo, S., & Harayama, S. (1999). Cultured mussel foot cells expressing byssal protein genes. *Journal of Experimental Zoology*, *283*(2), 131-136.

Tamura, K., Stecher, G., Peterson, D., Filipski, A., & Kumar, S. (2013). MEGA6: molecular evolutionary genetics analysis version 6.0. *Molecular biology and evolution*, *30*(12), 2725-2729.

Taylor, S. W., Chase, D. B., Emptage, M. H., Nelson, M. J., & Waite, J. H. (1996). Ferric ion complexes of a DOPA-containing adhesive Protein from *Mytilus edulis*. *Inorganic Chemistry*, *35*(26), 7572–7577.

Tesfay, T., & Gebresamuel, G. (2016). Agronomic and economic evaluations of compound fertilizer applications under different planting methods and seed rates of tef [Eragrostis tef (Zucc.) Trotter] in Northern Ethiopia. *Journal of Drylands*, *6*(1), 409-422.

Teufel, F., Almagro Armenteros, J. J., Johansen, A. R., Gíslason, M. H., Pihl, S. I., Tsirigos, K. D., ... & Nielsen, H. (2022). SignalP 6.0 predicts all five types of signal peptides using protein language models. *Nature biotechnology*, 1-3.

Thaha, A., Wang, B. S., Chang, Y. W., Hsia, S. M., Huang, T. C., Shiau, C. Y., ... & Chen, T. Y. (2021). Food-derived bioactive peptides with antioxidative capacity, xanthine oxidase and tyrosinase inhibitory activity. *Processes*, *9*(5), 747.

Thompson, J. D., Higgins, D. G., & Gibson, T. J. (1994). CLUSTAL W: improving the sensitivity of progressive multiple sequence alignment through sequence weighting, position-specific gap penalties and weight matrix choice. *Nucleic acids research*, *22*(22), 4673-4680.

Thornburg, T. E., Liu, J., Li, Q., Xue, H., Wang, G., Li, L., ... & Pan, X. (2020). Potassium deficiency significantly affected plant growth and development as well as microRNA-mediated mechanism in wheat (*Triticum aestivum* L.). *Frontiers in Plant Science*, *11*, 1219.

Torres, F. G., Troncoso, O. P., & Ruiz, V. (2013). A thermomechanical study of elastomeric collagen-based fibers in the wet state. *Bioinspired, Biomimetic and Nanobiomaterials*, *2*(2), 93–97.

Torres, F.G., Troncoso, O.P., Torres, C.E., 2012. Mussel byssus fibres: A tough biopolymer, In John, M.J., Sabu, T. (Eds.), *Natural polymers* (pp. 305–329). Royal Society of Chemistry.

Uster, B., O'Sullivan, A. D., Ko, S. Y., Evans, A., Pope, J., Trumm, D., & Caruso, B. (2015). The use of mussel shells in upward-flow sulfate-reducing bioreactors treating acid mine drainage. *Mine Water and the Environment*, *34*(4), 442-454.

Vaccaro, E., & Waite, J. H. (2001). Yield and post-yield behavior of mussel byssal thread: A self-healing biomolecular material. *Biomacromolecules*, *2*(3), 906–911.

Vehniäinen, E. R., Ruusunen, M., Vuorinen, P. J., Keinänen, M., Oikari, A. O., & Kukkonen, J. V. (2019). How to preserve and handle fish liver samples to conserve RNA integrity. *Environmental Science and Pollution Research*, *26*(17), 17204-17213.

Vnučec, D., Kutnar, A., & Goršek, A. (2017). Soy-based adhesives for wood-bonding–a review. *Journal of adhesion science and Technology*, *31*(8), 910-931.

Waite, J. H. (1992). The formation of mussel byssus: anatomy of a natural manufacturing process. *Results and Problems in Cell Differentiation*, 27–54.

Waite, J. H. (2002). Adhesion a la moule. *Integrative and comparative biology*, *42*(6), 1172-1180.

Waite, J. H. (2017). Mussel adhesion – essential footwork. *Journal of Experimental Biology*, *220*(4), 517–530.

Waite, J. H., & Qin, X. (2001). Polyphosphoprotein from the adhesive pads of *Mytilus edulis*. *Biochemistry*, *40*(9), 2887-2893.

Waite, J. H., Hansen, D. C., & Little, K. T. (1989). The glue protein of ribbed mussels (*Geukensia demissa*): a natural adhesive with some features of collagen. *Journal of Comparative Physiology B*, *159*(5), 517-525.

Waite, J., Qin, X. X., & Coyne, K. J. (1998). The peculiar collagens of mussel byssus. *Matrix Biology*, *17*(2), 93–106.

Wang, C., Lv, J., Xie, J., Yu, J., Li, J., Zhang, J., ... & Patience, B. E. (2021). Effect of slow-release fertilizer on soil fertility and growth and quality of wintering Chinese chives (Allium tuberm Rottler ex Spreng.) in greenhouses. *Scientific Reports*, *11*(1), 1-14.

Wang, F., Fu, R., Lv, H., Zhu, G., Lu, B., Zhou, Z., ... & Chen, H. (2019). Phosphate recovery from swine wastewater by a struvite precipitation electrolyzer. *Scientific reports*, *9*(1), 1-10.

Wang, Q., Jiang, F., Ouyang, X. K., Yang, L. Y., & Wang, Y. (2021). Adsorption of Pb (II) from aqueous solution by mussel shell-based

adsorbent: Preparation, characterization, and adsorption performance. *Materials*, *14*(4), 741.

Wang, S., Luo, S., Yue, S., Shen, Y., & Li, S. (2016). Fate of 15N fertilizer under different nitrogen split applications to plastic mulched maize in semiarid farmland. *Nutrient cycling in agroecosystems*, *105*(2), 129-140.

Wang, X., Huang, Y., Sheng, Y., Su, P., Qiu, Y., Ke, C., & Feng, D. (2017). Antifouling activity towards mussel by small-molecule compounds from a strain of *Vibrio alginolyticus* bacterium associated with sea anemone *Haliplanella sp*. *Journal of Microbiology and Biotechnology*, *27*(3), 460–470.

Wang, Y. C., Peterson, S. E., & Loring, J. F. (2014). Protein post-translational modifications and regulation of pluripotency in human stem cells. *Cell research*, *24*(2), 143-160.

Warner, S. C., & Waite, J. H. (1999). Expression of multiple forms of an adhesive plaque protein in an individual mussel, *Mytilus edulis*. *Marine Biology*, *134*(4), 729–734.

Waterhouse, A., Bertoni, M., Bienert, S., Studer, G., Tauriello, G., Gumienny, R., ... & Schwede, T. (2018). SWISS-MODEL: homology modelling of protein structures and complexes. *Nucleic acids research*, *46*(W1), W296-W303.

Watson, D. I., Shumway, S. E., & Whitlatch, R. B. (2009). Biofouling and the shellfish industry. In *Shellfish Safety and quality* (pp. 317-337). Woodhead Publishing.

Wei, W., Yu, J., Broomell, C., Israelachvili, J. N., & Waite, J. H. (2013). Hydrophobic enhancement of dopa-mediated adhesion in a mussel foot protein. *Journal of the American Chemical Society*, *135*(1), 377-383.

Wesolowska, M., Rymarczyk, J., Góra, R., Baranowski, P., Slawinski, C., Klimczyk, M., ... & Schimmelpfennig, L. (2021). New slow-release fertilizers-economic, legal and practical aspects: a Review. *International Agrophysics*, *35*(1).

Wiegemann, M. (2005). Adhesion in blue mussels (Mytilus edulis) and barnacles (genus *Balanus*): mechanisms and technical applications. *Aquatic Sciences*, *67*(2), 166-176.

Wilker, J. J. (2010). Marine bioinorganic materials: mussels pumping iron. *Current opinion in chemical biology*, *14*(2), 276-283.

Wong, T. S., Kang, S. H., Tang, S. K. Y., Smythe, E. J., Hatton, B. D., Grinthal, A., & Aizenberg, J. (2011). Bioinspired self-repairing slippery surfaces with pressure-stable omniphobicity. *Nature*, *477*(7365), 443–447.

Wu, J., Mao, C., Zhang, W., & Cheng, Y. (2020). Prediction and identification of antioxidant peptides in potato protein hydrolysate. *Journal of Food Quality*, 2020.

Xiong, J. (2006). Protein motifs and domain prediction. In *Essential Bioinformatics* (pp. 85-94). Cambridge: Cambridge University Press.

Xu, Y., Zhang, H., Jiang, Q., & Xia, W. (2014). Preliminary purification and characterization of adhesive proteins from freshwater mussels. *The Journal of Adhesion*, *90*(7), 607-617.

Yamada, K., Chen, T., Kumar, G., Vesnovsky, O., Topoleski, L. T., & Payne, G. F. (2000). Chitosan based water-resistant adhesive. Analogy to mussel glue. *Biomacromolecules*, *1*(2), 252-258.

Yang, E. I., Yi, S. T., & Leem, Y. M. (2005). Effect of oyster shell substituted for fine aggregate on concrete characteristics: Part I. Fundamental properties. *Cement and Concrete Research*, *35*(11), 2175-2182.

Yap, C. K., Ismail, A., Tan, S. G., & Omar, H. (2003). Accumulation, depuration and distribution of cadmium and zinc in the green-lipped mussel *Perna viridis* (Linnaeus) under laboratory conditions. *Hydrobiologia*, *498*(1), 151-160.

Ye, X., Chen, X. F., Deng, C. L., Yang, L. T., Lai, N. W., Guo, J. X., & Chen, L. S. (2019). Magnesium-deficiency effects on pigments, photosynthesis and photosynthetic electron transport of leaves, and nutrients of leaf blades and veins in *Citrus sinensis* seedlings. *Plants*, *8*(10), 389.

Ye, Z., Shen, Y., Ye, X., Zhang, Z., Chen, S., & Shi, J. (2014). Phosphorus recovery from wastewater by struvite crystallization: property of aggregates. *Journal of Environmental Sciences*, *26*(5), 991-1000.

Yesiltas, B., García-Moreno, P. J., Gregersen, S., Olsen, T. H., Jones, N. C., Hoffmann, S. V., ... & Jacobsen, C. (2022). Antioxidant peptides derived from potato, seaweed, microbial and spinach proteins: Oxidative stability of 5% fish oil-in-water emulsions. *Food Chemistry*, *385*, 132699.

Yoon, H., Park, S., Lee, K., & Park, J. (2004). Oyster shell as substitute for aggregate in mortar. *Waste management & research*, *22*(3), 158-170.

Yu, C. S., Chen, Y. C., Lu, C. H., & Hwang, J. K. (2006). Prediction of protein subcellular localization. *Proteins: Structure, Function, and Bioinformatics*, *64*(3), 643-651.

Yu, J., Kan, Y., Rapp, M., Danner, E., Wei, W., Das, S., ... & Israelachvili, J. N. (2013). Adaptive hydrophobic and hydrophilic interactions of mussel foot proteins with organic thin films. *Proceedings of the National Academy of Sciences*, *110*(39), 15680-15685.

Yu, J., Wei, W., Danner, E., Ashley, R. K., Israelachvili, J. N., & Waite, J. H. (2011). Mussel protein adhesion depends on interprotein thiol-mediated redox modulation. *Nature chemical biology*, *7*(9), 588-590.

Yu, M. (1999). Role of L-3, 4-dihydroxyphenylalanine in mussel adhesive proteins. *J. Am. Chem. Soc.*, *121*, 5825-5826.

Yu, M., & Deming, T. J. (1998). Synthetic Polypeptide Mimics of Marine Adhesives. *Macromolecules*, *31*(15), 4739–4745.

Yuvaraj, D., Annushrie, A., Niranjana, M., Gnanasekaran, R., Gopinath, M., & Iyyappan, J. (2021). A review on process and characterization of mussels and cirripeds for adhesive properties and applications thereof. *Current Research in Green and Sustainable Chemistry*, *4*, 100092.

Zeng, H., Hwang, D. S., Israelachvili, J. N., & Waite, J. H. (2010). Strong reversible Fe^{3+}-mediated bridging between dopa-containing protein films in water. *Proceedings of the National Academy of Sciences*, *107*(29), 12850-12853.

Zentz, F., Hellio, C., Valla, A., De La Broise, D., Bremer, G., & Labia, R. (2002). Antifouling activities of N-substituted imides: antimicrobial activities and inhibition of *Mytilus edulis* phenoloxidase. *Marine Biotechnology*, *4*(4), 431-440.

Zewide, I., & Sherefu, A. (2021). Review paper on effect of micronutrients for crop production. *J. Nutrition and Food Processing*, *4*(7), 1-8.

Zhang, P., Wang, S., Wang, S., & Jiang, L. (2014). Superwetting surfaces under different media: effects of surface topography on wettability. *Small*, *11*(16), 1939–1946.

Zhang, T., Jiang, R., & Deng, Y. (2017). Phosphorus recovery by struvite crystallization from livestock wastewater and reuse as Fertilizer: A Review. *Physico-Chemical Wastewater Treatment and Resource Recovery*, 135-152.

Zhang, X., Huang, H., He, Y., Ruan, Z., You, X., Li, W., Wen, B., Lu, Z., Liu, B., Deng, X., & Shi, Q. (2019). High-throughput identification of heavy metal binding proteins from the byssus of chinese green mussel (*Perna viridis*) by combination of transcriptome and proteome sequencing. *PLOS ONE*, *14*(5), e0216605.

Zhang, X., Ruan, Z., You, X., Wang, J., Chen, J., Peng, C., & Shi, Q. (2017). De novo assembly and comparative transcriptome analysis of the foot from Chinese green mussel (*Perna viridis*) in response to cadmium stimulation. *PLOS ONE, 12*(5), e0176677.

Zhang, Y., Wu, H. L. S., & Liu, S. (2013). Analysis on the properties of calcined waste mussel shell. *Analytical Chemistry: An Indian Journal*, *13*, 167-171.

Zhao, H., & Waite, J. H. (2005). Coating proteins: structure and cross-linking in fp-1 from the green shell mussel *Perna canaliculus*. *Biochemistry*, *44*(48), 15915-15923.

Zhao, H., & Waite, J. H. (2006a). Proteins in load-bearing junctions: the histidine-rich metal-binding protein of mussel byssus. *Biochemistry*, *45*(47), 14223-14231.

Zhao, H., & Waite, J. H. (2006b). Linking adhesive and structural proteins in the attachment plaque of *Mytilus californianus*. *Journal of Biological Chemistry*, *281*(36), 26150-26158.

Zheng, L., Huang, F., Narsai, R., Wu, J., Giraud, E., He, F., ... & Shou, H. (2009). Physiological and transcriptome analysis of iron and phosphorus interaction in rice seedlings. *Plant Physiology*, *151*(1), 262-274.

Zhong, C., Gurry, T., Cheng, A. A., Downey, J., Deng, Z., Stultz, C. M., & Lu, T. K. (2014). Self-assembling multi-component nanofibers for strong bioinspired underwater adhesives. *Nature nanotechnology*, *9*(10), 858.

Zukri, N. I., Khamidun, M. H., Sapiren, M. S., Abdullah, S., & Rahman, M. A. A. (2018, April). Lake water quality improvement by using waste mussel shell powder as an adsorbent. In *IOP Conference Series: Earth and Environmental Science* (Vol. 140, No. 1, p. 012057). IOP Publishing, 1-8.